LBL-17953
c.2

# Lawrence Berkeley Laboratory
UNIVERSITY OF CALIFORNIA

## EARTH SCIENCES DIVISION

RECEIVED
LAWRENCE
BERKELEY LABORATORY
MAY 16 1985
LIBRARY AND
DOCUMENTS SECTION

ANALYSIS OF INJECTION TESTS IN LIQUID-DOMINATED GEOTHERMAL RESERVOIRS

S.M. Benson
(M.S. Thesis)

December 1984

TWO-WEEK LOAN COPY

*This is a Library Circulating Copy which may be borrowed for two weeks.*

Prepared for the U.S. Department of Energy under Contract DE-AC03-76SF00098

LBL-17953
c.2

# Analysis of Injection Tests in Liquid-Dominated Geothermal Reservoirs

Sally M. Benson

Masters Thesis

December 1984

This work was supported through U. S. Department of Energy Contract No. DE-AC03-76SF00098 by the Assistant Secretary for Conservation and Renewable Energy, Office of Renewable Technology, Division of Geothermal and Hydropower Technologies.

# TABLE OF CONTENTS

Page

Table of Contents . . . . . i

Nomenclature . . . . . ii

List of Tables . . . . . v

List of Figures . . . . . vi

INTRODUCTION . . . . . 1

BASIC PROBLEM . . . . . 4
Physical Description . . . . . 4
Related Research . . . . . 7

APPROACH . . . . . 10
Governing Equations . . . . . 11
Numerical Technique . . . . . 14
Numerical Simulation . . . . . 14

RESERVOIR RESPONSE TO NONISOTHERMAL INJECTION . . . . . 17
Pressure Buildup During Nonisothermal Injection . . . . . 17
Effect of a Pre-Existing Discontinuity . . . . . 20
Effect of Skin Factor . . . . . 23
Pressure Falloff . . . . . 27
Step-Rate Injection Tests . . . . . 31
Wellbore Effects . . . . . 38
Discussion . . . . . 45

FLUID SKIN FACTOR . . . . . 46
Derivation . . . . . 46
Application to Pressure Transient Analysis . . . . . 49
Application to Injection Test Analysis . . . . . 50
Front Tracking . . . . . 52

INJECTION TEST ANALYSIS . . . . . 57
Moving Front Dominated Tests . . . . . 57
Composite Reservoir Tests . . . . . 60
Pressure Falloff Analysis . . . . . 64
Step-Rate Analysis . . . . . 65
Front Tracking Method . . . . . 67

EXAMPLES OF NONISOTHERMAL INJECTION TEST ANALYSIS . . . . . 74
Example 1. Moving Front Analysis . . . . . 74
Example 2. Composite Reservoir Analysis . . . . . 79
Example 3. Pressure Falloff Analysis . . . . . 82
Example 4. Step-rate analysis and Front Tracking . . . . . 87
Example 5. Layered Reservoir Analysis . . . . . 94
Example 6. East Mesa Well 5-1: Pressure Buildup Analysis 101

CONCLUSION . . . . . 106

REFERENCES . . . . . 108

# NOMENCLATURE

| Symbol | Definition | Units (SI), field |
|---|---|---|
| $B_w$ | water formation volume factor, RB/STB | (-) |
| c | heat capacity | (J/kg/°C) |
| $c_p$ | pore volume compressibility | ($Pa^{-1}$), psi |
| $c_t$ | total compressibility ($c_p+c_w$) | ($Pa^{-1}$), psi |
| $c_w$ | compressibility of water | ($Pa^{-1}$), psi |
| C | cumulative injection | ($m^3$), STB |
| $C^*$ | wellbore storage coefficient | ($m^3$/Pa), BBL/psi |
| h | reservoir thickness | (m), ft |
| k | permeability | ($m^2$), md |
| $\bar{k}$ | average weighted permeability | ($m^2$), md |
| $k_s$ | permeability of the skin damaged zone | ($m^2$), md |
| m | slope of linear portion of semi-log plot of pressure transient data | (Pa/cy), psi |
| n | semi-log slope on a plot of $s_a$ vs. log (C) | (-) |
| p | pressure | (Pa), psi |
| $p_1$ | initial pressure | (Pa), psi |
| $\Delta p_o$ | offset of pressure curves for nonisothermal injection with a moving front | (Pa), psi |
| $p_D$ | dimensionless pressure $\left(\frac{4\pi kh}{Q\mu}\Delta p\right)$ | (-) |
| $p_e$ | pressure at the outer boundary of a steady-state flow region | (Pa), psi |
| $p_w$ | pressure at the injection well | (Pa), psi |
| $p_{wf}$ | bottom hole injection pressure prior to shut-in | (Pa), psi |

NOMENCLATURE (cont.)

| Symbol | Definition | Units (SI), field |
|---|---|---|
| $p_{1s}$ | extrapolated pressure at 1s on a pressure vs. log(time) graph | (Pa), psi |
| $p_{1s}^{*}$ | corrected injection pressure on the extrapolated semi-log straight line | (Pa), psi |
| $q$ | mass flowrate | (kg/s),lb/hr |
| $q_n$ | mass flowrate during step #n | (kg/s), lb/hr |
| $Q$ | volumetric flowrate | ($m^3$/s), STB/D |
| $r$ | radius to an observation point | (m), ft |
| $r_e$ | radius of the outer boundary of a steady-state flow region | (m), ft |
| $r_f$ | radial distance to the thermal front | (m), ft |
| $r_D$ | dimensionless radius ($r/r_w$) | (-) |
| $r_{Df}$ | dimensionless radial distance to the thermal front | (-) |
| $r_s$ | radius of the skin damaged region | (m), ft |
| $r_w$ | well radius | (m), ft |
| $s_a$ | apparent skin factor | (-) |
| $s_f$ | fluid skin factor | (-) |
| $s_m$ | mechanical skin factor | (-) |
| $s_{ma}$ | apparent mechanical skin factor | (-) |
| $t$ | time | (s), hr |
| $\Delta t$ | time increment since the last rate change | (s), hr |
| $t_o$ | transition time for moving-front dominated injection | (s), hr |
| $t_o'$ | intersection time of the two semi-log straight lines for final transition time for injection with a pre-existing discontinuity | (s), hr |
| $t_f$ | time when the drainage radius exceeds the size of the inner region | (s), hr |

NOMENCLATURE (cont.)

| Symbol | Definition | Units (SI), field |
|---|---|---|
| $t_D$ | dimensionless time ($kt/\phi\mu cr_w^2$) | (-) |
| T | temperature | (°C), °F |
| $T_r$ | reservoir temperature | (°C), °F |
| $\Delta T$ | temperature change | (°C), °F |
| u | fluid velocity | (m/s), ft/s |
| $u_r$ | radial fluid velocity | (m/s), ft/s |
| $u_z$ | vertical fluid velocity | (m/s), ft/s |
| $u_\theta$ | angular fluid velocity | (m/s), ft/s |
| | **Greek Letters** | |
| $\beta$ | water expansivity | $(°C^{-1})$, $°F^{-1}$ |
| $\Delta$ | difference | (-) |
| $\lambda$ | thermal conductivity | (J/s/°C/m), BTU/hr/°F/ft |
| $\mu$ | viscosity | (Pa.s), cp |
| $\phi$ | porosity | (-) |
| $\rho$ | density | $(kg/m^3)$, $lbm/ft^3$ |
| $\rho_a c_a$ | volumetric heat capacity of the reservoir | $(J/m^3/°C)$, BTU/ft /°F |
| $\rho_w c_w$ | volumetric heat capacity of water | $(J/m^3/°C)$, BTU/ft /°F |
| | **Subscripts** | |
| 1 | inner region | |
| o | outer region | |
| w | water | |

# LIST OF TABLES


| | | Page |
|---|---|---|
| Table 1. | Reservoir parameters used for the numerical simulations | 14 |
| Table 2. | Distances to the thermal front for several values of 1.151 $s_f/n$. | 55 |
| Table 3. | Reservoir properties used for the discussion of front tracking | 70 |
| Table 4. | Reservoir properties and well characteristics used for Example 1. | 75 |
| Table 5. | Calculated and apparent skin values for the pressure buildup data shown in Figure 6. | 78 |
| Table 6. | Reservoir properties, well characteristics and test parameters for Example 2. | 80 |
| Table 7. | Calculated and apparent skin values for the pressure buildup data shown in Figure 7. | 83 |
| Table 8. | Reservoir properties, well characteristics and test parameters for Example 3. | 85 |
| Table 9. | Apparent skin values for pressure falloff analyses after ,$10^2$, $10^3$, and $10^4$ $m^3$ of nonisothermal injection. | 88 |
| Table 10. | Reservoir properties, well dimensions and test parameters: Example 4. | 89 |
| Table 11. | Pertinent parameters for the step-rate test analysis: Example 4. | 91 |
| Table 12. | Summary of analyses for the step-rate test: Example 4. | 92 |
| Table 13. | Reservoir properties and well characteristics used for Example 5. | 95 |
| Table 14. | Injection test data summary: Example 6. | 102 |

# LIST OF FIGURES


| | | Page |
|---|---|---|
| Figure 1. | Viscosity and density of water as a function of temperature. | 2 |
| Figure 2. | Schematic of a 3-region composite reservoir. | 6 |
| Figure 3. | Pressure buildup during injection of 95°C water into a 250°C reservoir. | 19 |
| Figure 4. | Pressure buildup at the well due to injection of 50°C, 100°C and 150°C into a 250°C reservoir. | 21 |
| Figure 5. | Pressure buildup at the well for injection of 100°C water into a 250°C reservoir. Prior to injection the well is surrounded by 100°C cold spots with radii of 1-m, 5-m, and and 10-m. | 22 |
| Figure 6. | Pressure buildup at the well during 100°C injection into a 250°C reservoir for a well with several values of the skin factor. | 25 |
| Figure 7. | Pressure buildup at the well during 100°C injection into a 250°C reservoir with a 3-m cold spot around the well and several values of the skin factor. | 26 |
| Figure 8. | Temperature distribution in the reservoir after $10^5$ s (at 20 kg/s) and $10^7$ s (at 10 kg/s) of injection of 100°C water into a 250°C reservoir. | 28 |
| Figure 9. | Pressure falloff after $10^5$ s of injection int a 250°C reservoir. | 29 |
| Figure 10 | Pressure falloff after $10^7$ s of injection of 100°C water into a 250°C reservoir. | 30 |
| Figure 11. | Simulated step-rate injection test. | 32 |
| Figure 12. | Pressure transient data for Step 1 of the simulated step-rate test. | 33 |
| Figure 13. | Pressure transient data for Step 2 of the simulated step-rate test. | 34 |
| Figure 14. | Pressure transient data for Step 3 of the simulated step-rate test. | 35 |
| Figure 15. | Pressure transient data for the falloff after the simulated step-rate test. | 36 |

LIST OF FIGURES (cont.)


| | | Page |
|---|---|---|
| Figure 16. | Bottomhole pressure change vs. flowrate for the simulated step-rate test. | 39 |
| Figure 17. | Initial temperature profile for the simulated wellbore temperature transients. | 41 |
| Figure 18. | Calculated bottomhole temperature for injection of 20°C water at an injection rate of 20 kg/s. | 42 |
| Figure 19. | Schematic of the presure transient response during moving-front dominated injection tests. | 58 |
| Figure 20. | Schematic of the pressure transient response during composite-reservoir type injection tests. | 61 |
| Figure 21. | Apparent skin values vs. log (C) for four hypothetical cases. | 69 |
| Figure 22. | Pressure buildup at the well for Example 1 | 76 |
| Figure 23. | Pressure buildup at the well for Example 2 | 81 |
| Figure 24. | Pressure falloff after $10^5$ s of 100°C injection into a 250°C reservoir: Example 3. | 86 |
| Figure 25. | Apparent skin factors vs. cumulative injection for Example 4. | 93 |
| Figure 26. | Schematic of the layered reservoir used in Example 5. | 96 |
| Figure 27. | Pressure falloff data after $10^4$, $2.5 \times 10^4$ and $1 \times 10^5$ s of injection into a multilayered reservoir. | 98 |
| Figure 28. | Apparent skin factors vs. cumulative injection for Example 6. | 99 |
| Figure 29. | Distance to the thermal front after $10^4$, $2.5 \times 10^4$ and $10^5$ s of injection in a multilayered reservoir. | 100 |
| Figure 30. | Pressure buildup data from East Mesa well 5-1. | 104 |

# INTRODUCTION

Injection tests in geothermal wells are commonly performed for three specific purposes: (1) to obtain pressure transient data from which the reservoir transmissivity and skin factor of the well can be calculated, (2) to stimulate naturally fractured geothermal wells, and (3) to determine the cause of reinjection problems. Usually, the temperature of the injected fluid is different from that of the in situ reservoir fluid. In order to interpret the pressure transient data correctly from any type of injection test, the effect of nonisothermal reservoir conditions must be understood.

During injection of fluids at temperatures different from the in situ temperature, a thermal discontinuity is formed around the well. With increasing injection volumes, the distance to the radial discontinuity increases. Both the effect of this thermal radial-discontinuity and the effects of the movement of the thermal front on the pressure transient response must be considered to correctly interpret nonisothermal injection and falloff tests.

For the interpretation of well test data, the two most important temperature-dependent fluid properties of water are the dynamic viscosity and density. In Figure 1, the dynamic viscosity and density of water are plotted as a function of temperature. Between 20°C and 300°C the viscosity changes by an order of magnitude, the major change occurring between 20°C and 100°C. The fluid density decreases by approximately 30% between 20°C and 300°C. Because of the temperature sensitivity of these parameters, the mobility of the injected and in situ fluids can differ by an order of magnitude.

A similar problem, of interest to the petroleum industry, is the evaluation of waterflood injection wells. During injection, water

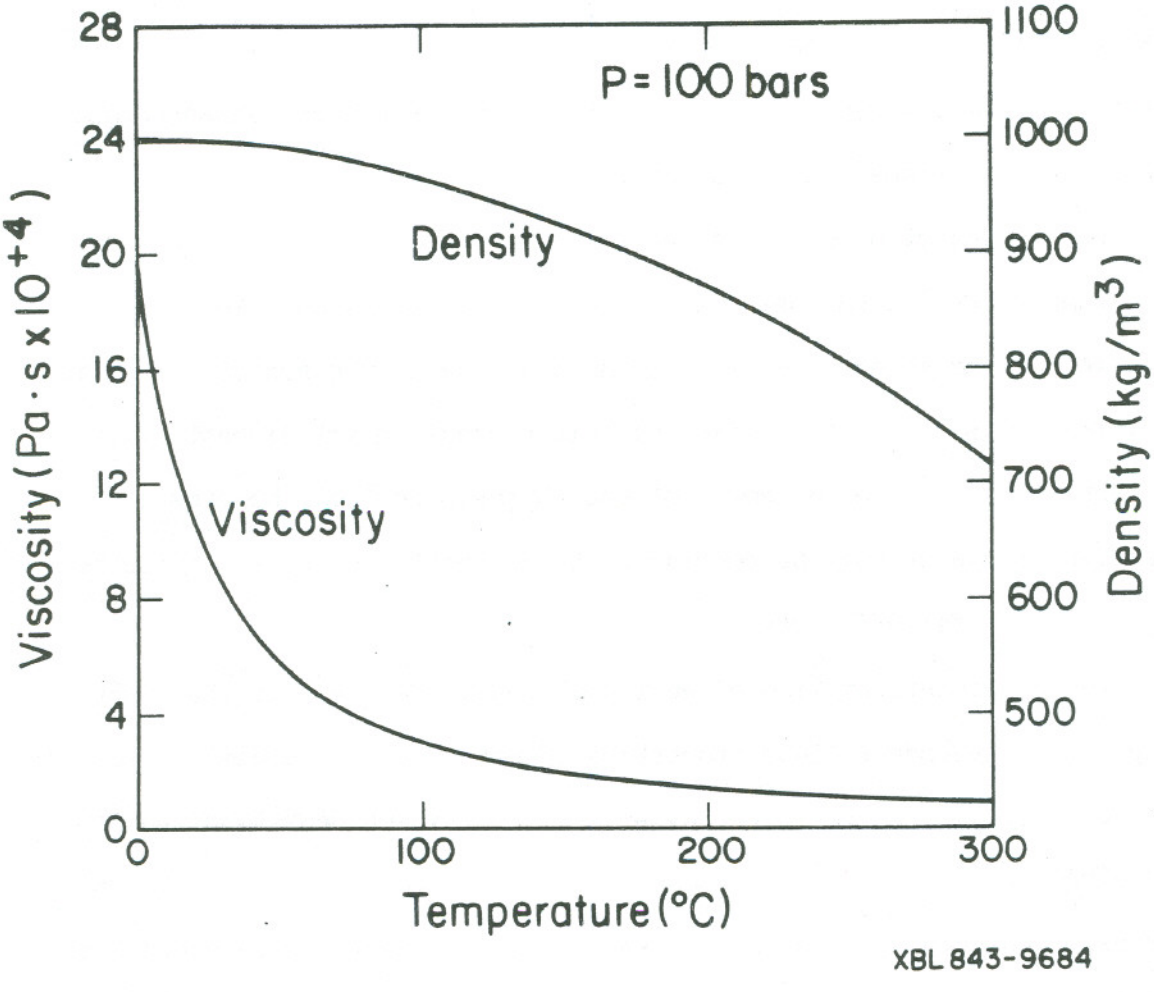


Figure 1. Viscosity and density of water as a function of temperature.

sweeps some of the oil from the rock pores and creates an oil bank ahead of the injected water. Around the injection well, the pore volume is filled mainly with water, which usually has a viscosity lower than the in situ oil. For evaluating pressure transients in such systems, the reservoir is treated as a composite system with an inner region mobility of $k_w/\mu_w$ and an outer region mobility of $k_o/\mu_o$. Using this approach, analysis methods have been developed for calculating the permeability of the formation, the skin factor of the well, and in some cases, the distance to the flood front. The major drawback of this approach is that the distance to the contact between the oil and water must be far enough from the well so that the presence of this inner region will be apparent in the pressure transient data.

Methods developed for evaluating composite systems are also applicable to nonisothermal injection in the sense that eventually the system is a composite one with an inner region at one temperature and an outer region at another. However, taking this approach has two drawbacks. First, it neglects the potential effects of the moving thermal front. Second, the methods are not applicable until the thermal front is very far from the injection well. This requires that large volumes of fluid be injected into the formation before pressure transient testing can be used to evaluate the injection process.

The objective of the current study is to develop procedures for analyzing nonisothermal injection test data during the early phases of injection. This will provide a means for detecting injection well plugging and predicting premature thermal breakthrough before the thermal front has moved very far from the well, thereby allowing remedial measures to be taken before the consequences of these problems become serious.

# BASIC PROBLEM

## Physical Description

When water is injected into a geothermal reservoir, numerous physical changes take place in the system. These changes can be grouped according to one of the following categories;

1) Pressure increases in the pore spaces of the rock.
2) Movement of both the injectate and in situ pore fluid away from the well.
3) Temperature changes in both the rock and pore fluid resulting from temperature differences between the injectate and reservoir fluid.
4) Porosity and permeability changes resulting from chemical interactions between the injectate, pore fluid and reservoir rock.
5) Porosity and permeability changes resulting from mechanical changes in the near-wellbore region (e.g., hydraulic fracturing, fracture dilation, thermal stress cracking, and particulate plugging)

Fortunately, for the purposes of this study, these can be classified into the even broader groups: very-near wellbore efects; near-wellbore effects; and reservoir-scale effects.

Changes in porosity and permeability resulting from both mechanical and chemical changes are concentrated in a region very-near the wellbore. Such changes can be treated as a skin effect around the well (van Everdingen, 1953). Initially, temperature changes are also limited to the very-near wellbore region. However, with increasing injection, the thermal front moves away from the well. Temperature changes are better classified as a near-well effect. For typical values of the reservoir

properties, large volumes of the reservoir quickly experience a pressure increase which results in fluid movement. Therefore, these are classified as reservoir-scale effects.

This division of the reservoir suggests that the three-region composite reservoir, depicted in Figure 2, is a suitable framework for evaluating pressure transients during nonisothermal injection. Immediately surrounding the well is a skin region where the permeability may be different from that of the reservoir. In general the size of this region is small and mathematically is treated as infinitesimally thin. The second region in the reservoir extends from the outer radius of the skin region to the thermal front. It has the same permeability as the reservoir but is the temperature of the injected fluid. Although in actuality the thermal front is not sharp, for the time being, it is considered to be so. The properties of the outer region which extends from the thermal front to an unspecified distance from the well, are those of the undisturbed reservoir.

Numerous researchers in the field of petroleum engineering, have used this framework for developing mathematical models for calculating pressure transients in waterflood injection wells and composite reservoirs. Major results of these studies are presented in the next section. They have been successful at describing pressure transients and developing techniques for analyzing pressure transients in such systems. However, as mentioned previously, there are two major limitations to the applicability of existing analysis techniques. First, the majority of previous studies assume that the distance to the "flood front" does not change during the time period of interest. Second, in general, methods of analysis are applicable only after large volumes have been injected.

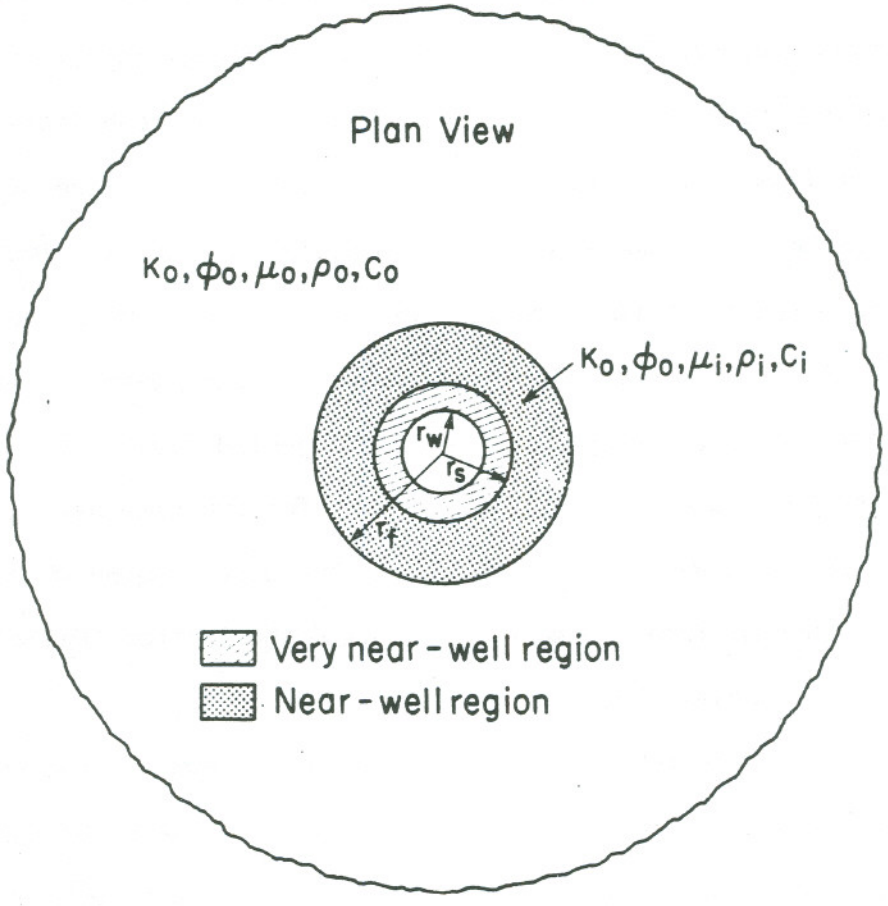


Figure 2. Schematic of a 3-region composite reservoir.

## Related Research

Numerous studies have been published on the analysis of well test data in composite reservoirs. One of the earliest of these, published by Hazebroek et al., (1958) proposed a method for analyzing pressure falloff tests in water injection wells. They show that by using a trial and error procedure in which the late-time pressure transient data are adjusted in such a way as to make them linear on a pressure vs. log (time) plot, the correct average reservoir pressure, permeability-thickness of the reservoir, and skin factor of the well can be determined. Several other authors have reported on the development of analytic solutions or approximate analytic solutions for calculating pressure transients in composite reservoir systems with a stationary boundary separating the reservoir regions of different fluid or rock properties (Larkin, 1963; Kazemi, 1966; Odeh, 1969; and Ramey, 1970). These studies show that two semi-log straight lines, the first corresponding to the properties of the inner region, and the second to the properties of the outer region, should be apparent in the pressure buildup and falloff data. The permeability-thickness product of the two reservoir regions can be calculated from the slopes of the semi-log straight lines. The skin factor for the well can be calculated using conventional methods and the first semi-log straight line. The radial distance to the discontinuity can be evaluated from the time at which the two semi-log straight lines intersect (van Poollen, 1965).

The problem has also been investigated by using numerical methods to simulate the pressure falloff in systems with radial discontinuities (Bixel and van Poollen, 1967; Kazemi et a., 1972; and Merrill et al., 1974). These authors have investigated the effects of different mobility

ratios, storage coefficient ratios, afterflow, and the presence of reservoir boundaries on the pressure transient data. They indicated that unless storage capacity is approximately equal on both sides of the discontinuity, the slope of the second semi-log straight line cannot be used to calculate the permeability-thickness of the outer region. Furthermore, they showed that if wellbore storage masks the early-time data, it may not be possible to determine the properties of the inner region, and the calculated distance to the front may be erroneous.

More recently, several papers discuss the interpretation of pressure buildup and falloff tests in geothermal injection wells. Tsang and Tsang (1978) developed a semi-analytic solution for calculating the pressure buildup during nonisothermal injection in an idealized well/reservoir system. They demonstrated that under special conditions, the physical properties of the injected fluid control the pressure response. Tsang et al., (1978) and Bodvarsson and Tsang (1980) used a numerical simulator to study the pressure buildup in response to cold water injection into a hot water reservoir. They illustrated the effects of the temperature dependent fluid properties (viscosity and density) and elaborated on the effect of a moving thermal boundary on the pressure response. Mangold et al., 1980, used a numerical model to study the effects of nonisothermal reservoir conditions on both production and injection pressure transients. They showed that the effects of thermal discontinuities may be erroneously interpreted as reservoir boundaries. O'Sullivan and Pruess (1980) and Garg and Pritchett (1981) investigated the pressure buildup and falloff in response to cold water injection

into a two-phase geothermal reservoir. The above studies confirmed that, under certain circumstances, the permeability-thickness product of the reservoir can be calculated from pressure buildup or falloff data by using conventional analysis methods.

## APPROACH

The description of the reservoir/well model used for this study is as follows:

1) With the exception of an annular region around the well, (skin region) the reservoir is of constant porosity, compressibility, permeability, heat capacity, and thermal conductivity.

2) The reservoir is horizontal, infinite, of constant thickness, and bounded above and below by impermeable rock.

3) Thermal conduction to the caprock and bedrock is neglected.

4) The reservoir is fully saturated with slightly compressible liquid water.

5) The effects of gravity on the shape of the thermal front are neglected.

6) The well has a finite radius and fully penetrates the reservoir.

Several of the constraints on the present study warrant discussion. First, during nonisothermal injection it is well known that the density contrast between the fluids creates a tilting of the thermal front. The degree of tilting depends on a number of factors including the vertical permeability of the rock and the duration of injection (Hellstrom et al., 1979). As many porous media formations consist of inter-bedded sands and shales, the vertical permeability is lower than the horizontal permeability. This tends to inhibit tilting of the front (Hellstrom et al., 1979). Also, since the present study is concerned primarily with injection testing when the thermal front has not advanced very far from the well, the importance of front tilting is minimal (Hellstrom et al., 1979). A second constraint on the present study is the assumption that the absolute permeability of the rock is independent of the temperature.

In general, laboratory studies support this assumption, however, several studies suggest that the rock permeability may be temperature sensitive (Gobran et al., 1980; Grant, 1983; Bodvarsson et al., 1982). Since the primary objective of this study is to evaluate the system while the thermal front remains relatively close to the well, temperature dependent rock properties should be reflected by changes in the skin factor of the well, rather than the overall permeability of the system. Therefore, this constraint does not limit the generality of the approach.

## Governing Equations

The governing equations that describe the hydrodynamics of fluid injection into a porous medium are developed by considering the mass and energy conservation requirements. In cylindrical coordinates the mass conservation equation is expressed as

$$\frac{\partial(\rho u_r)}{\partial r} + \frac{\rho u_r}{r} + \frac{1}{r}\frac{\partial(\rho u_\theta)}{\partial \theta} + \frac{\partial(\rho u_z)}{\partial z} = \frac{-\partial(\phi\rho)}{\partial t} \qquad (1)$$

For the system described above, that is, one in which the gravity term is neglected and the medium is assumed to be homogeneous and isotropic, Equation (1) can be simplified to

$$\frac{\partial(\rho u_r)}{\partial r} + \frac{\rho u_r}{r} = \frac{-\partial(\phi\rho)}{\partial t} \qquad (2)$$

In order to evaluate this expression, an equation of motion and an equation of state for the fluid are required. Assuming Darcy flow, the equation of motion is expressed as

$$u_r = -\frac{k}{\mu}\frac{\partial p}{\partial r} \qquad (3)$$

There is no simple expression for the equation of state that includes both the temperature and pressure dependence of the fluid density. Therefore, for the time being let it suffice to define

$$\beta = -\frac{1}{\rho}\frac{\partial \rho}{\partial T}\bigg|_p \tag{4}$$

and

$$c_w = \frac{1}{\rho}\frac{\partial \rho}{\partial p}\bigg|_T \tag{5}$$

By substituting equations (3)-(5) into Equation (2), the governing equation for the pressure distribution in the system can be expressed as

$$\frac{\partial^2 p}{\partial r^2} + \frac{1}{r}\frac{\partial p}{\partial r} - \frac{\beta \partial p}{\partial r}\frac{\partial T}{\partial r} + c_w\left(\frac{\partial p}{\partial r}\right)^2 - \frac{\partial \ln \mu}{\partial T}\frac{\partial T}{\partial r}\frac{\partial p}{\partial r} = \frac{\phi \mu c_t}{k}\left[\frac{\partial p}{\partial t} + \frac{\beta}{c_t}\frac{\partial T}{\partial t}\right] \tag{6}$$

The propagation of the thermal front into the reservoir is governed by the energy balance equation

$$\int_0^t Q\rho_w c_w \Delta T\, dt = \int_V \rho_a c_a \Delta T dV \tag{7}$$

where $\rho_a c_a$ is the volumetric heat capacity of the reservoir. Bodvarsson (1969) showed that if the conduction to the confining strata is neglected, the distance to the thermal front is given by

$$r_f = \sqrt{\frac{Qt}{\pi h}\frac{\rho_w c_w}{\rho_a c_a}} \tag{8}$$

This expression, however, does not provide information about the distribution of temperatures around the thermal front. Evaluation of this is more complex and has been done by Avdonin (1964).

Analytically evaluating Equation 6 is a formidable task. Tsang and Tsang (1978) evaluated a similar expression that 1) neglected the

dependence of fluid density on temperature and ii) assumed that the distribution of temperature about the front could be expressed by the Fermi-Dirac function. Although this approach provides insight into the hydrodynamics of nonisothermal fluid injection it neither allows rigorous evaluation of the problem nor the flexibility to incorporate the effects of complications such as variable flowrates or reservoir heterogeneity.

For this study, a numerical simulator is used to generate the pressure transients in response to nonisothermal injection. This approach is taken for several reasons, the most important one being the flexibility inherent in a numerical simulator. It can be argued that development of an analytic solution provides general results from which the physical significance of groups of parameters is readily apparent. It can also be argued that the inaccuracies inherent in numerical methods shed doubt on the results of such a study. However, unless the physical system is very simple, the analytic solution (if one exists) becomes extremely complicated, as demonstrated by the governing equations. Since the authors mentioned previously have already studied many idealized systems using a variety of techniques, to repeat this work would be unnecessary duplication. It is the purpose of this study to consider the effects of some of the common problems encountered in geothermal injection well testing that do not apriori lend themselves to analytic treatment (e.g., variable flowrates, a diffuse front, finite of skin damage, a layered reservoir, etc.). Numerical simulators are a tool that can aid us in moving intuitively from a physical observation (simulated result) to a general rule without requiring the intervention of cumbersome mathematics. As for the question of the accuracy of the

results, the numerical simulator used for this study has been verified both analytical and experimental results.

## Numerical Technique

The numerical simulator PT (pressure-temperature), developed by Bodvarsson (1982) is used for this study. The code is 3-dimensional and solves the coupled mass and energy transport equations for a liquid-saturated, heterogeneous, porous and/or fractured media. It employs the "integrated finite difference method " (IFDM) for discretizing the medium and formulating the governing equations (Narasimhan and Witherspoon, 1976; Edwards, 1972). The set of linear equations is solved at each timestep by direct means using an efficient sparse matrix solver (Duff, 1977).

The simulator allows for temperature- and/or pressure-dependent fluid and rock properties. The fluid density is calculated as a function of pressure and temperature, using a polynomial approximation, accurate to within 1%. Fluid viscosity is calculated as a function of temperature using an accurate (within 1%) exponential expression. The simulator has been validated against many analytical solutions as well as in field experiments (Bodvarsson, 1982; and Doughty et al., 1983). A detailed description of the simulator is given by Bodvarsson (1982).

## Numerical Simulation

Numerous numerical simulations were perormed in order to determine the characteristic pressure response during nonisothermal injection. Most of the simulations were performed assuming a set of "typical" physical parameters for a geothermal system (for instance, see Table 1).

| | |
|---|---|
| $k$ | $1.0 \times 10^{-14}$ $m^2$ (10 md) |
| $h$ | 100.0 m |
| $\phi$ | 0.2 |
| $\rho_a c_a$ | $2.57 \times 10^6$ $J/m^3°C$ |
| $\lambda$ | 2.0 J/m/°C/s |
| $r_w$ | 0.1 m |
| $c_t$ | $1 \times 10^{-9}$ $Pa^{-1}$ ($6.9 \times 10^{-6}$ $psi^{-1}$) |
| $T_r$ | 250 °C |

Table 1. Reservoir parameters used for the numerical simulations.

However, values of parameters were varied in order to determine the appropriate dimensionless groupings of these parameters.

For most of the simulations a single-layer radial mesh (concentric circles) with a realistic wellbore radius of 0.1 m is used. Close to the well, very fine elements are used for accurate modeling of temperature variations during injection. Farther away from the well, the mesh spacing increases logarithmically for accurate modeling of the pressure response. For most computer runs, a mesh with approximately 100 elements is used. The grid is chosen to optimize accurate modeling of the movement of the thermal front and the propagation of the pressure pulse. As such, different grids are used depending on the specific problem being investigated.

The time steps are automatically selected by the numerical code, based upon user specified criteria for the maximum allowable pressure and temperature changes during a time step (Bodvarsson, 1982). For most runs the maximum allowable pressure and temperature changes are $10^5$ Pa and 1°C, respectively.

## RESERVOIR RESPONSE TO NONISOTHERMAL INJECTION

In the following sections, the pressure transients that occur in response to nonisothermal injection are demonstrated. Pressure transients during both hot water injection into a cold reservoir and cold water injection into a hot reservoir were investigated. However, because cold water injection is more common and of greater interest, the examples cited are limited to this case. The results are just as applicable to the other problem. Because the intention of the work is to develop methods of analysis for injection tests, the results of these simulations are presented in such a way as to facilitate understanding of how they may be used to analyze injection tests. As such, they are graphed according to the Miller-Dyes-Hutchinson, Horner, or variable rate technique, depending on the method most appropriate for the specific problem (Matthews and Russell, 1967; Earlougher, 1977).

### Pressure Buildup During Nonisothermal Injection

The pressure buildup during cold water injection (95°C), into a hot reservoir (250°C) is illustrated in Figure 3.* The pressure transients at the well and several other radii are plotted. Note that all of the data points fall on the same curve when plotted in terms of $t/r_D^2$. At early times, the pressure transients are identical to those for 250°C injection (see 250°C Theis line in Figure 3). After a period of time, the slope of the semi-log straight line changes and becomes identical to the slope for isothermal 95°C injection (see 95°C Theis line in Figure 3). This type of pressure transient behavior is consistent with the numerically

*The reservoir properties used for this simulation are listed in Table 1.

simulated results of Bodvarsson and Tsang, 1980, and the analytical model of Tsang and Tsang, 1978. Also plotted in the top of Figure 3 are the temperature data at several distances from the injection well. Note that in each case (with the exception of the well), the change in slope of the semi-log straight line occurs when the thermal front passes. This observation can be used to develop a general expression for the time when the slope of the semi-log straight line changes.

The relationship between the time at which the slope of semi-log straight line changes and the passage of the thermal front can be derived as follows. Recalling Equation (8), we know that the thermal front reaches a radius, $r_f$, when

$$t = \frac{\rho_a c_a}{\rho_w c_w} \frac{\pi h}{Q} r_f^2 \qquad (9)$$

If Equation (9) is divided by the dimensionless radial distance to the front ($r_{Df} = r_f/r_w$), the movement of the front can be expressed as

$$t/r_{Df} = \frac{\rho_a c_a}{\rho_w c_w} \frac{\pi h}{Q} r_w^2 \qquad (10)$$

Evaluating Equation (10) at $r_w$, we see that the slope on the semi-log straight line changes when

$$t_o = \frac{\rho_a c_a}{\rho_w c_w} \frac{\pi h}{Q} r_w^2 \qquad (11)$$

For the reservoir properties and well dimensions listed in Table 1 and an injection rate of 10 kg/s (5,660 STB/D), $t_o$ occurs at approximately 200 seconds.

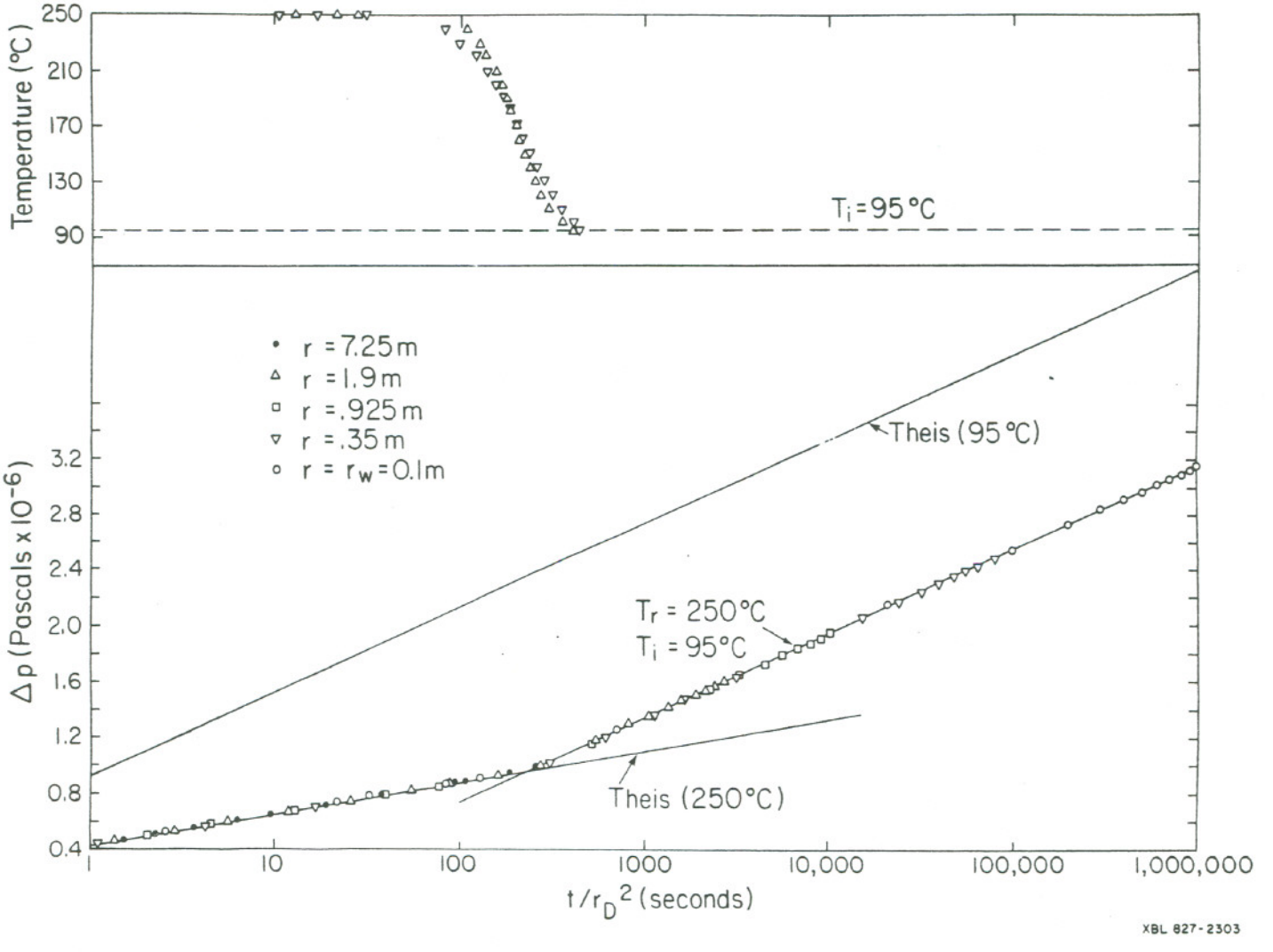


Figure 3. Pressure buildup during injection of 95°C water into a 250°C reservoir.

Numerous simulations were conducted to determine the dependence of $t_o$ on the rock permeability, porosity, compressibility, injection temperature, reservoir temperature and flowrate. These studies verify that Equation (11) gives a reasonable approximation for the intersection of the two semi-log straight lines. For example, Figure 4 shows the pressure transient behavior due to injecting fluids at 50°C, 100°C, and 150°C into a 250°C reservoir. In each case the pressure data fall first on the slope corresponding to the 250°C reservoir fluid, and then on the corresponding cold slope. Note that the intersection of the two semi-log straight lines is nearly identical for each case.

This type of pressure transient response is henceforth referred to as moving-front dominated behavior. The characteristics of this response are 1) an initial period during which the pressure response is governed by the reservoir fluid properties and 2) a second period during which the fluid properties of the injectate govern the response.

Effect of a Pre-Existing Discontinuity

Injection tests are often conducted after the well has been cooled by drilling, or after an extended period of injection. Therefore, the effect of a "cold spot" around the injection well must be considered. In this case the pressure response at the well is as follows (see Figure 5). Initially, the pressure behavior is governed by the fluid properties of the cold spot. After a period of time (depending on the size of the cold spot) the data depart from this curve and fall on a second semi-log straight line with a slope corresponding to the properties of the reservoir fluids. The slope changes to that of the hot outer region

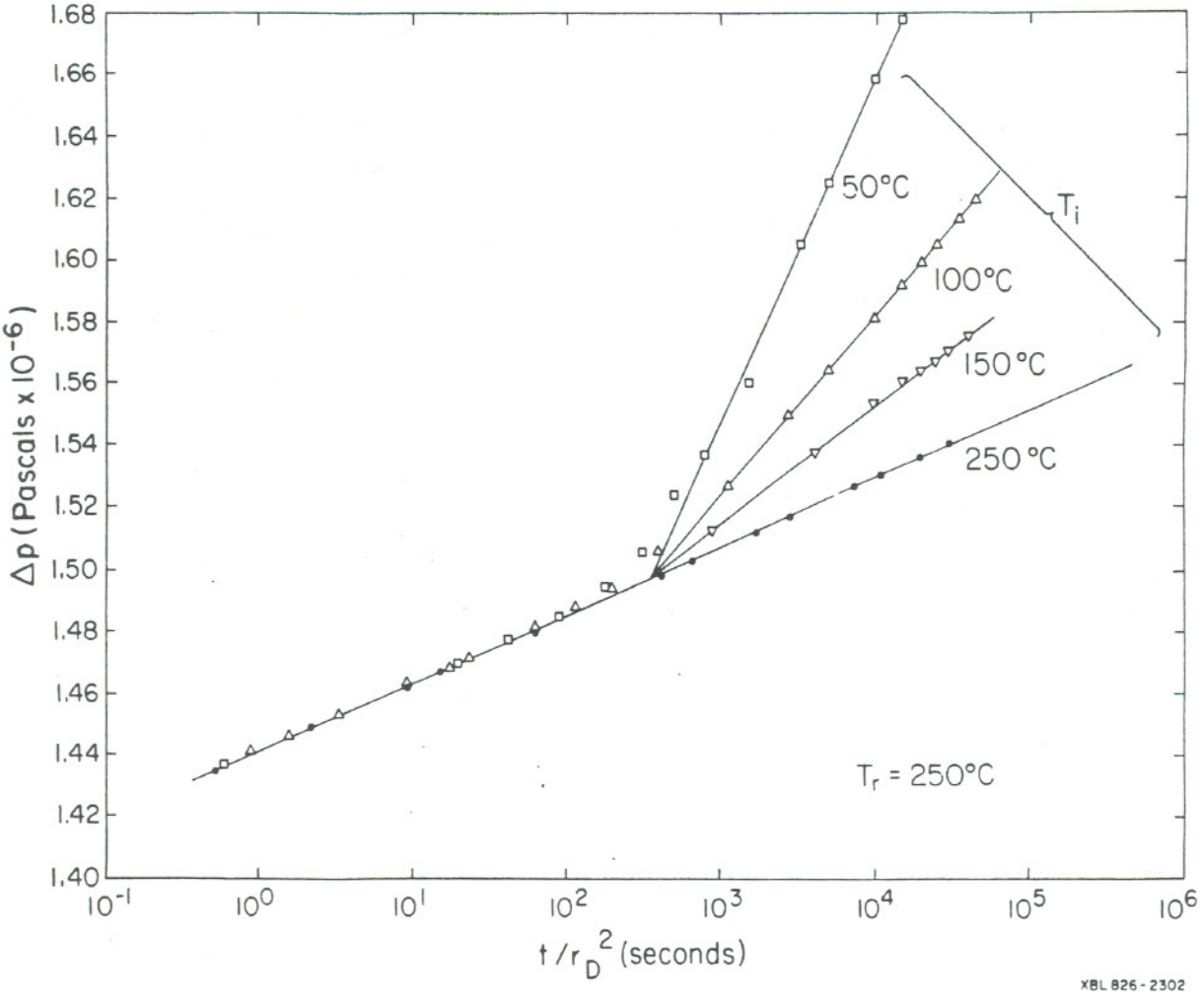


Figure 4. Pressure buildup at the well due to injection of 50°C, 100°C and 150°C into a 250°C reservoir.

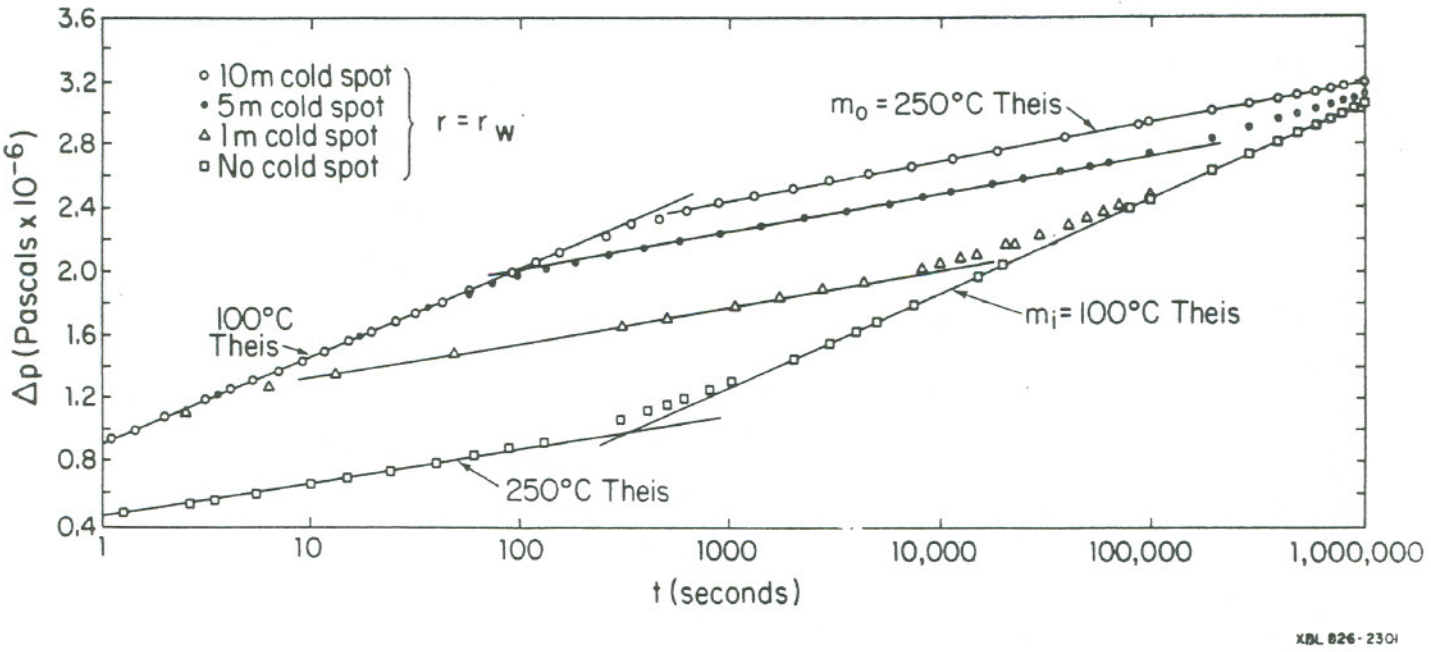


Figure 5. Pressure buildup at the well for injection of 100°C water into a 250°C reservoir. Prior to injection the well is surrounded by 100°C cold spots with radii of 1-m, 5-m, and 10-m.

when the drainage radius exceeds the size of the cold spot. This time ($t_f$) is approximated by (Earlougher, 1977)

$$t_f = \frac{\phi \mu_1 c_t}{4k} r_f^2 \qquad (12)$$

For the reservoir properties listed in Table 1, $t_f$ is approximately 140 s for a 10-m cold spot, a 35 s for a 5-m cold spot and 1 s for a 1-m cold spot.

With continued injection, the slope eventually changes again (see Figure 5) and the pressure response is nearly identical to the no-cold-spot pressure transient. The second transition ($t_o'$) occurs when

$$t_o' = \frac{\rho_a c_a}{\rho_w c_w} \frac{\pi h}{Q} r_f^2 \qquad (13)$$

For a flowrate of 10 kg/s (5,600 STB/D) and the reservoir properties listed in Table 1, $t_o'$ is approximately 20 days for a 10-m cold spot, 5 days for a 5-m cold spot, and 5 hours for a 1-m cold spot.

This type of response, up until the final change in slope, are henceforth referred to as the composite reservoir behavior. The characteristics of this response are 1) an initial period during which the pressure response is governed by the properties of the injected fluid and 2) a second period during which the properties of the reservoir fluid govern the pressure response. Note that this is the opposite of the moving-front dominated response.

## Effect of Skin Factor

Wells are typically surrounded by an annular region with a permeability different from that of the reservoir. This region is usually treated mathematically in terms of an infinitesimally thin skin that

influences the capacity of the well (Hurst, 1953; Van Everdingen, 1955). The influence of this region on the magnitude of the pressure buildup and the times at which the slope transitions occur must be determined in order to develop a general theory for injection test data analysis. The skin factor is incorporated in the simulations by modeling it as an annular region of reduced or enhanced permeability around the well. The corresponding skin factor is given by (Hawkins, 1956)

$$s = \left( \frac{k}{k_s} - 1 \right) \ln \left( \frac{r_s}{r_w} \right) \qquad (14)$$

The influence of the skin factor on the moving-front dominated behavior is demonstrated in Figure 6, which shows the pressure buildup at the well for several values of the skin factor. In this case the skin factor displaces the absolute pressure change and shifts $t_o$ the factor of $e^{-2s}$. Therefore,

$$t_o = \frac{\rho_a c_a}{\rho_w c_w} \frac{\pi h}{Q} \left( r_w e^{-s} \right)^2 \qquad (15)$$

The problem is more complex if there is a cold spot around the well. The system is described by three regions: the skin region with a mobility of $k_s/\mu_1$; a cold spot with a mobility of $k/\mu_i$; and the hot reservoir with a mobility of $k/\mu_o$. Figure 7 shows the pressure transients for 100°C injection into a 250°C reservoir with a 3-m cold spot for several values of the skin factor. The figure shows that the skin factor only displaces the curves, without changing their slopes or the transition times.

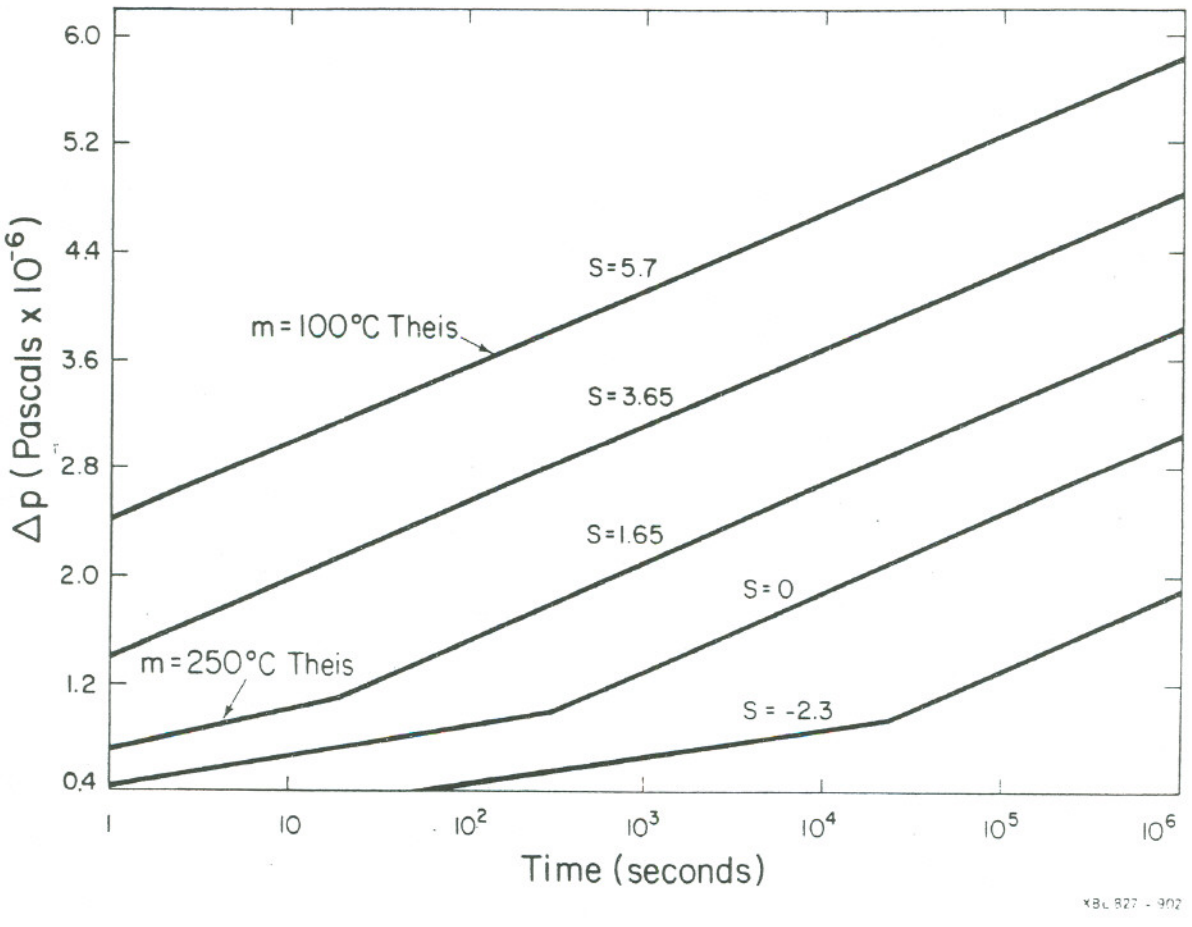


Figure 6. Pressure buildup at the well during 100°C injection into a 250°C reservoir for a well with several values of the skin factor.

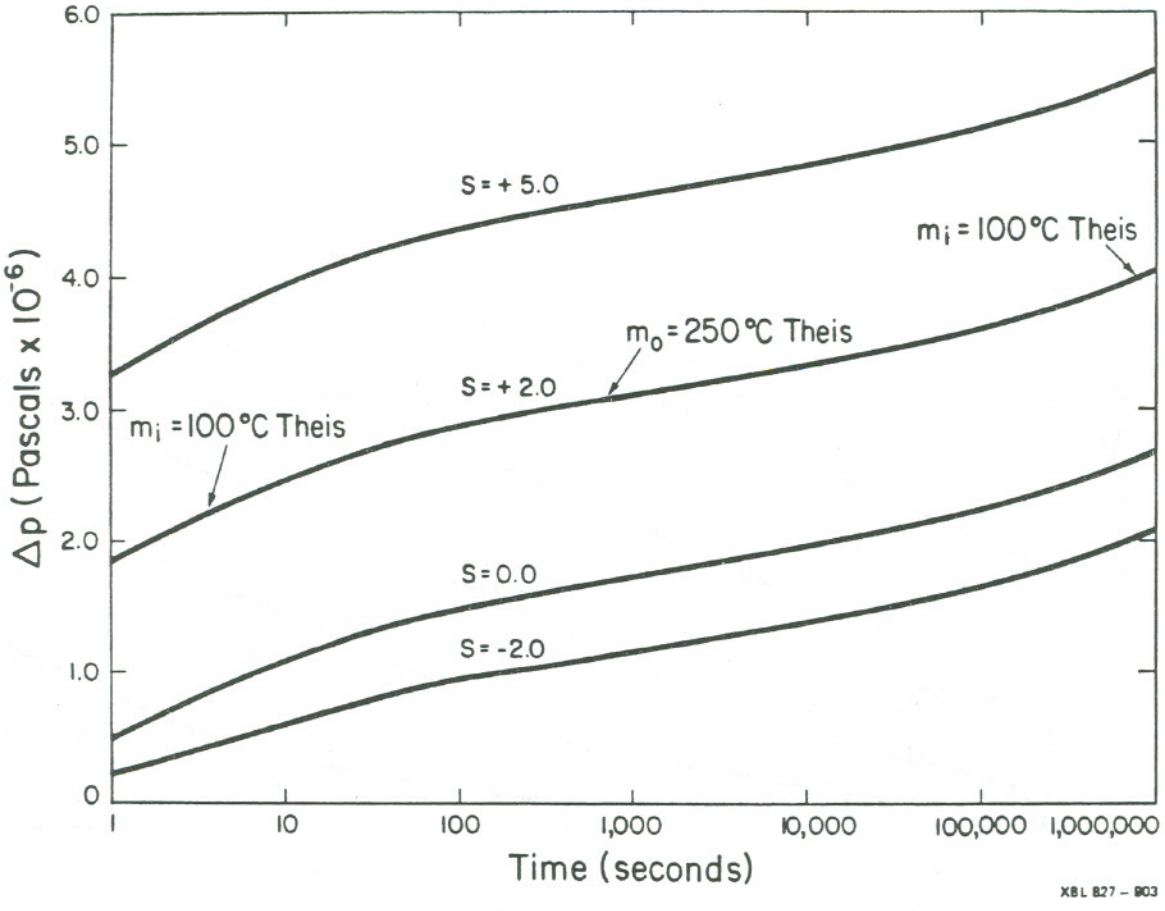


Figure 7. Pressure buildup at the well during 100°C injection into a 250°C reservoir with a 3-m cold spot around the well and several values of the skin factor.

Pressure Falloff

After shut-in, immediately following nonisothermal injection, the reservoir is essentially a composite system with an inner region of mobility $k/\mu_1$, a transition region with mobility ranging from $k/\mu_1$ to $k/\mu_o$, and an outer region of mobility $k/\mu_o$. For example, Figure 8 shows the temperature distribution in the reservoir for two cases: i) after $10^5$ s of injection at 0.2 kg/s/m (11,320 STB/D); and ii) a second after $10^7$ s of injection at 0.1 kg/s/m (5660 STB/D). As seen in the figure, the width of the transition region is significant with respect to the distance to the thermal front for both cases.

The pressure falloff data from these two cases are plotted in Figures 9 and 10. As anticipated, the pressure falloff initially reflects the presence of the inner region. After a period of time, the properties of the reservoir fluid begin to affect the response and the data fall on a second semi-log straight line that corresponds to the properties of the in situ reservoir fluid. The time at which the data depart from the first slope can be calculated from Equation 12 if the radius to the front is evaluated at the median temperature between injected and in situ fluids. Interpretation of numerous simulations show that for purposes of injection test analysis, there is a negligible difference between the pressure transient response for a system with a diffuse thermal front and a system in which the front is infinitesimally thin. Therefore the system can be treated in terms of a two-fluid composite system, where the radius of the inner region is assumed to coincide with the thermal front.

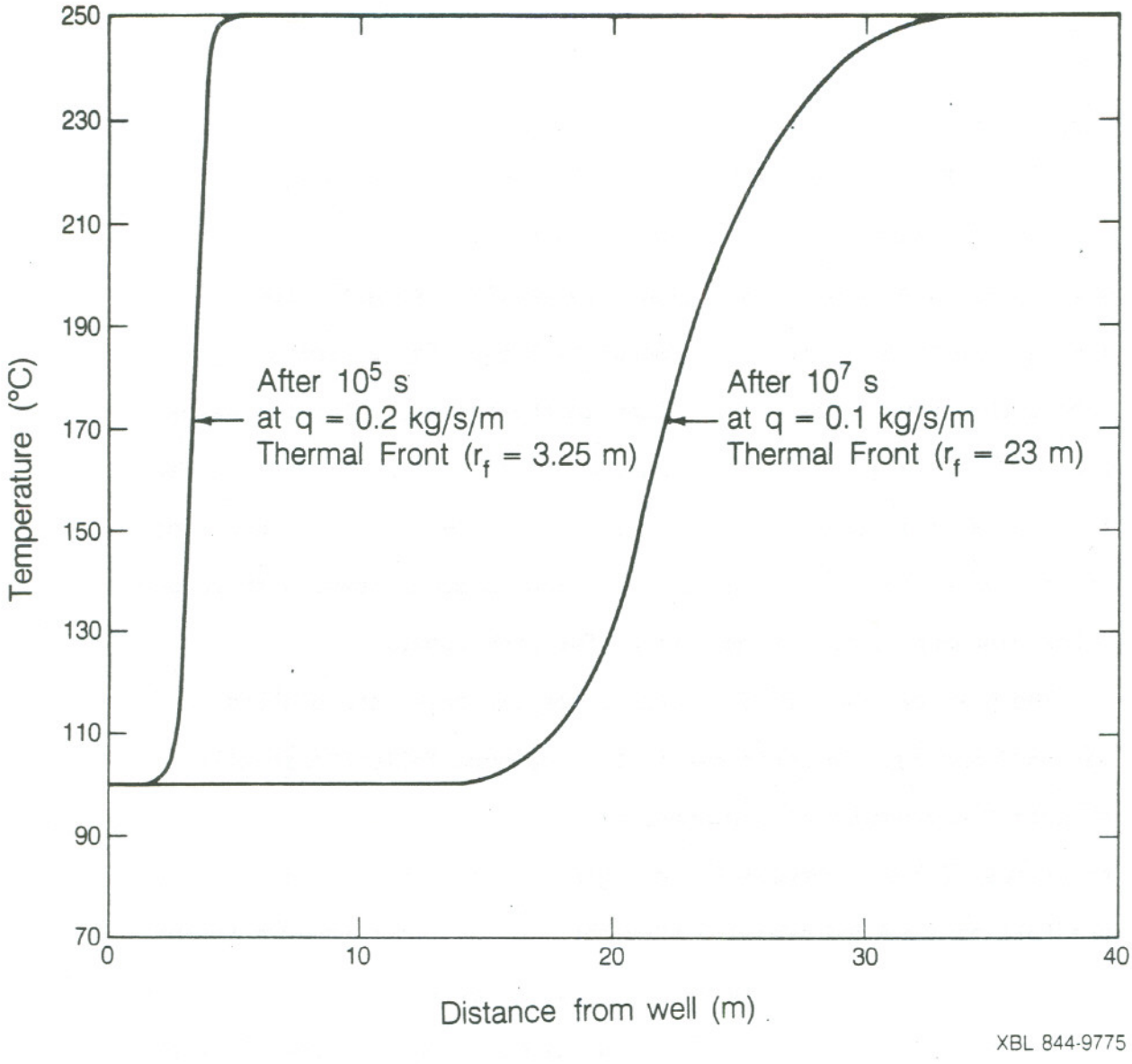


Figure 8. Temperature distribution in the reservoir after $10^5$ s (at 20 kg/s) and $10^7$ s (at 10 kg/s) of injection of 100°C water into a 250°C reservoir.

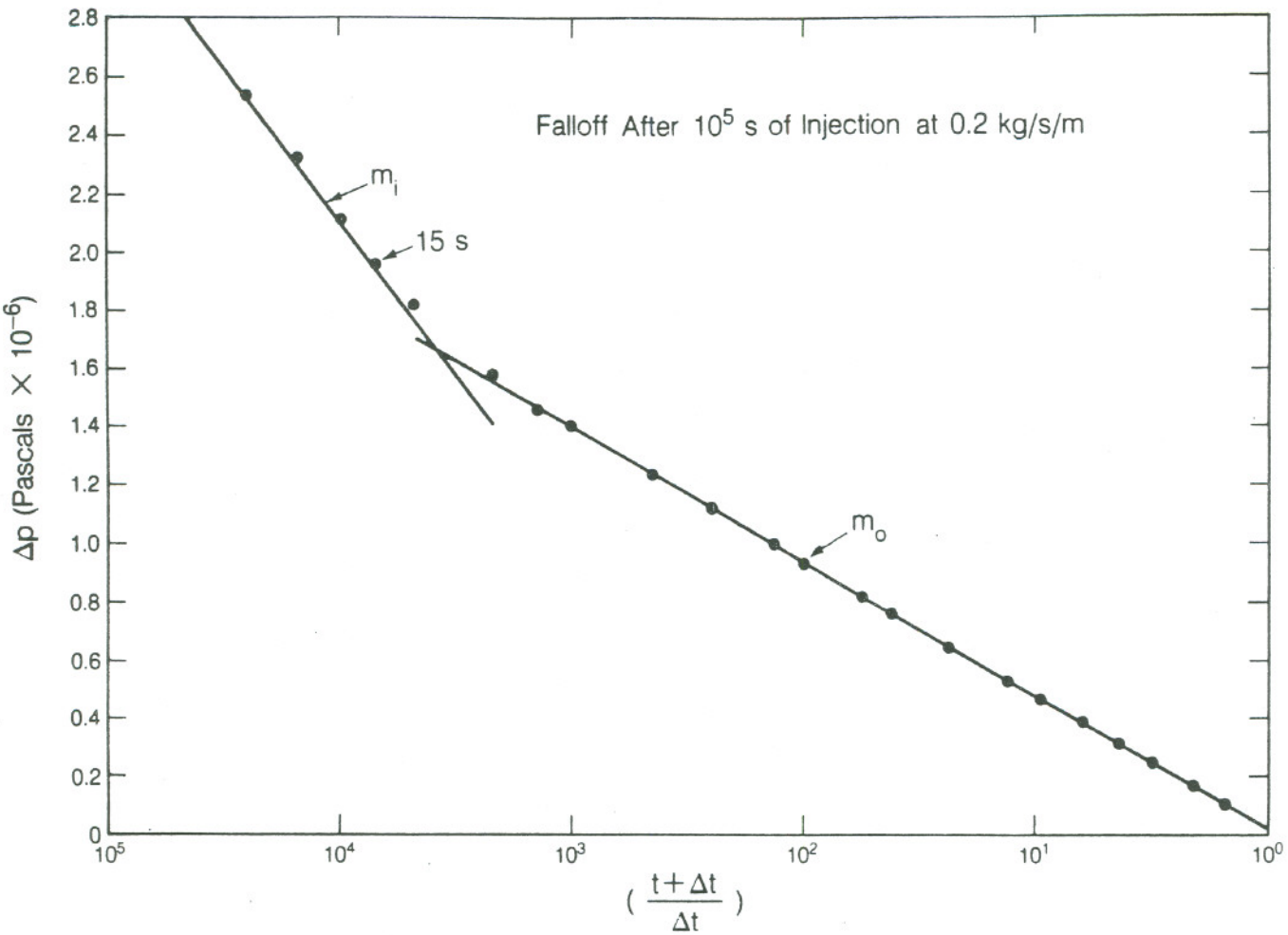


XBL 844-9777

Figure 9. Pressure falloff after $10^5$ s of injection int a 250°C reservoir.

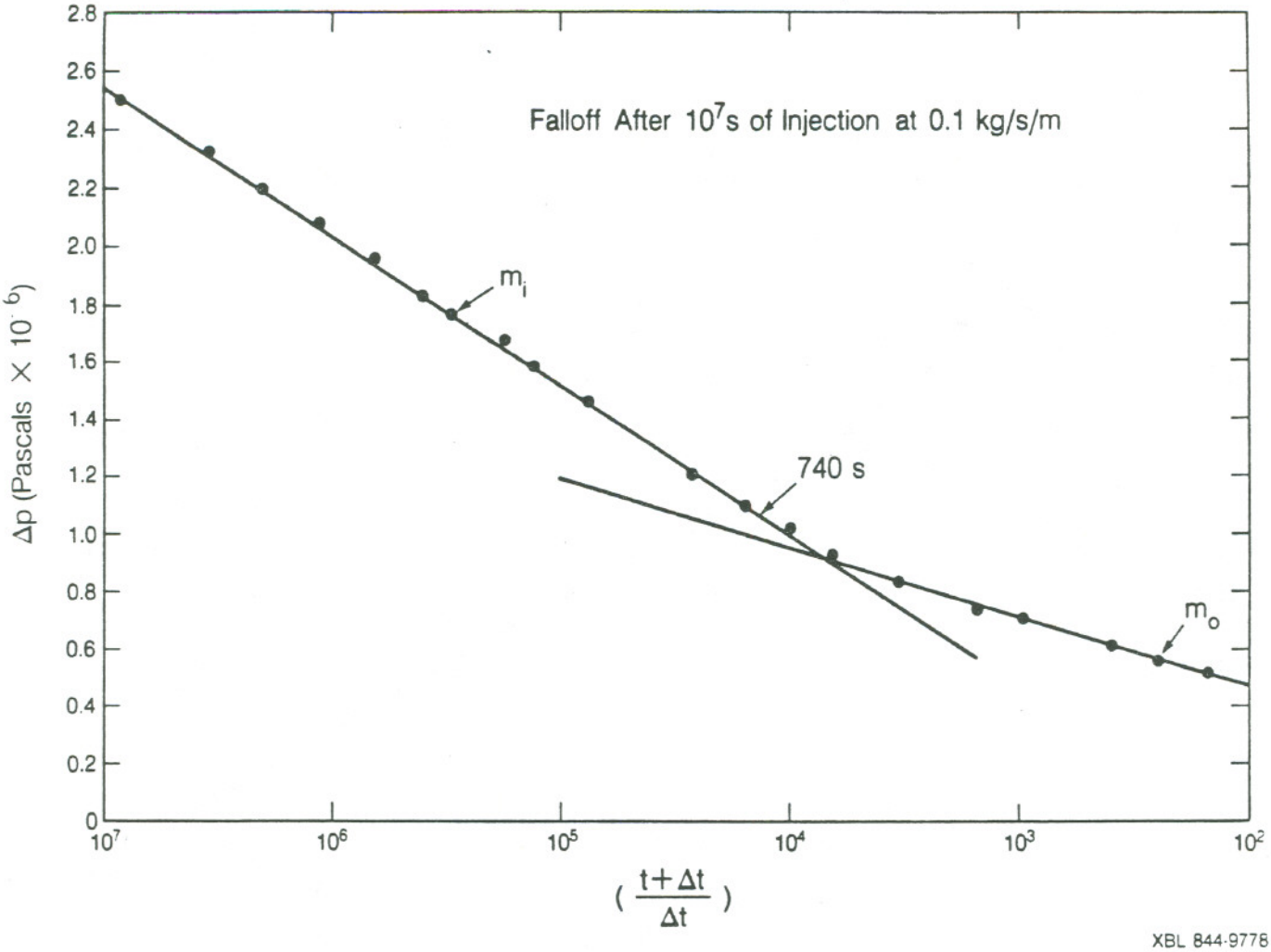


Figure 10 Pressure falloff after $10^7$ s of injection of 100°C water into a 250°C reservoir.

Step-Rate Injection Tests

Typically, injection tests are not conducted at a single flowrate. Instead, they are conducted in a series of step-rates followed or preceded by a complete shut-in (Howard et al., 1978; Allen and Baza, 1980; and Bodvarsson, et al., 1984). Therefore, the effect of flowrate variations on the pressure transient response must be determined.

The following simulation illustrates the key aspects of nonisothermal step-rate injection tests. Three 6-hour steps with injection rates of 10, 20, and 15 kg/s of 20°C fluid into a 250°C reservoir are followed by a complete shut-in. Table 1 summarizes the properties of the reservoir used for this simulation. The simulated pressure data are shown in Figure 11. For comparison, simulated results for 20°C and 250°C isothermal injection are also plotted. The pressure transients during each step are plotted in Figures 12 through 15. Note that pressures are graphed as a function of

$$\sum_{i=1}^{n} \frac{q_i}{q_n} \log \frac{t_i + \ldots. t_n + \Delta t}{t_{i+1} + \ldots. + t_n + \Delta t} \qquad (15)$$

in accordance with conventional multi-rate theory (Earlougher, 1977).

The pressure transient resonse during each step is as follows. Step 1 is a typical moving-front dominated case, as is shown in Figure 12. Initially, the data are identical to the 250°C isothermal pressure transients (also shown in Figure 12). At approximately 300 s, the data depart from the initial curve and fall on a second semi-log straight line with a slope that corresponds to the properties of the injectate.

The second step, shown in Figure 13, first displays the composite reservoir behavior, and then the moving-front dominated behavior. The

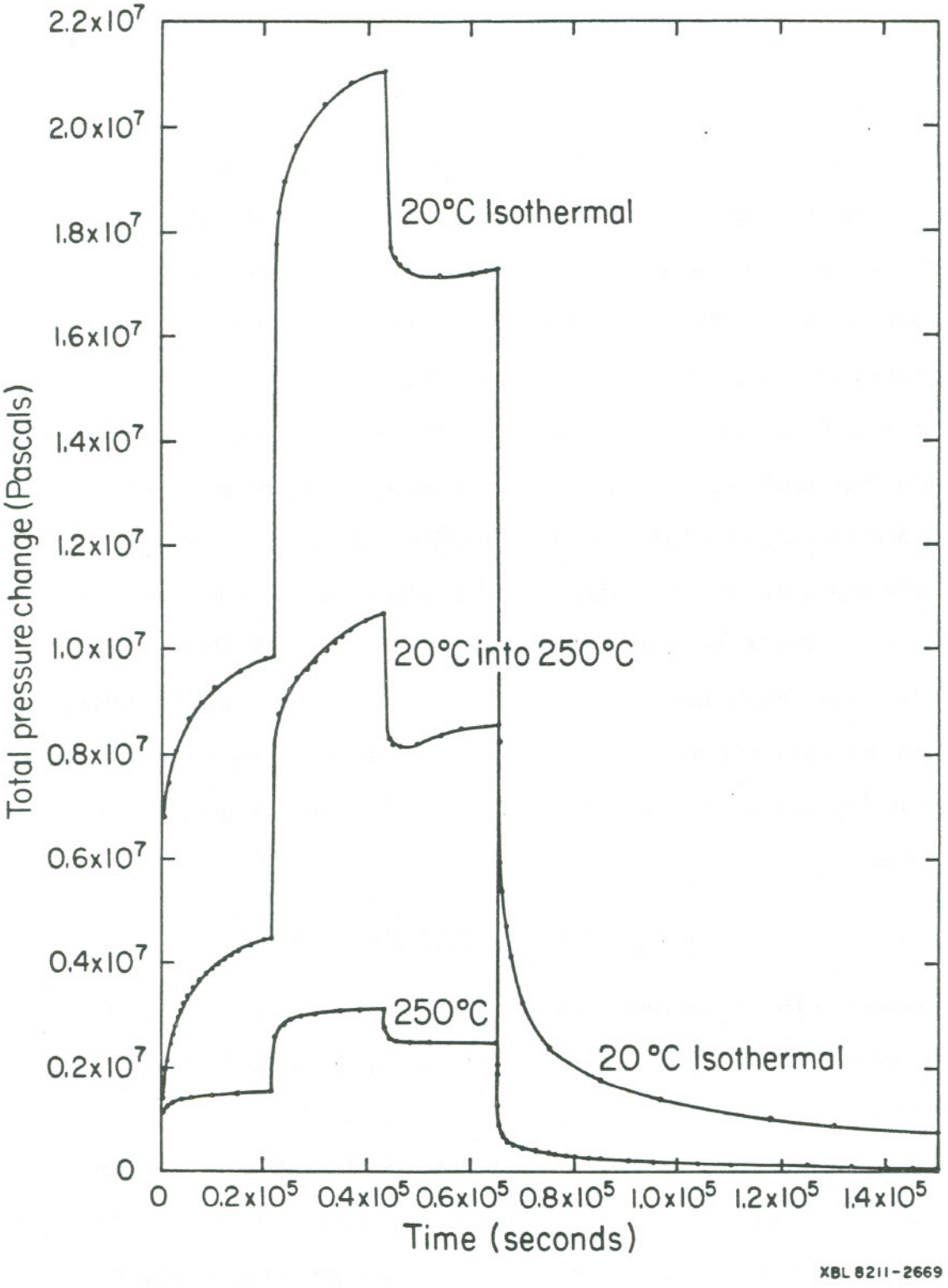


Figure 11. Simulated step-rate injection test.

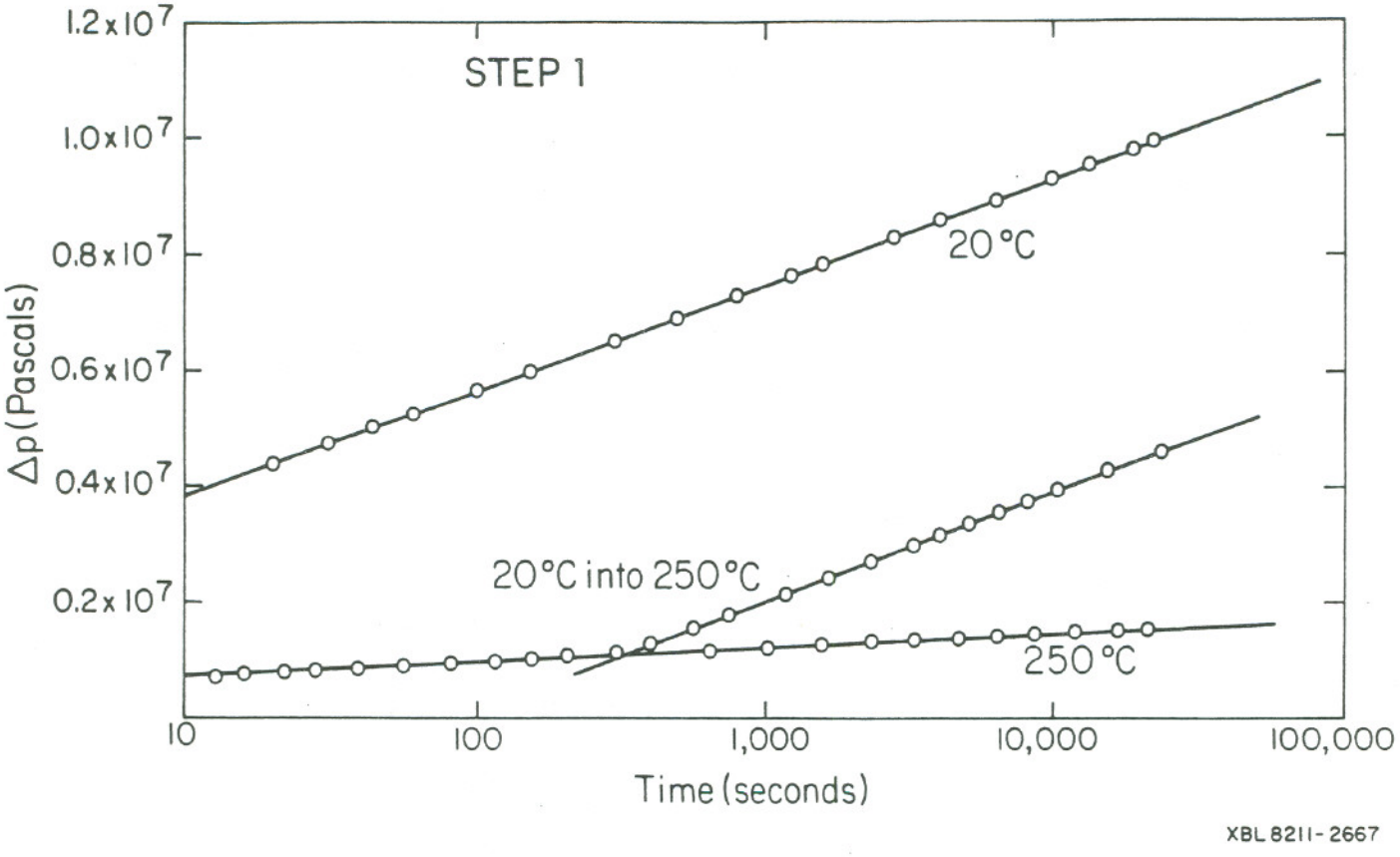


Figure 12. Pressure transient data for Step 1 of the simulated step-rate test.

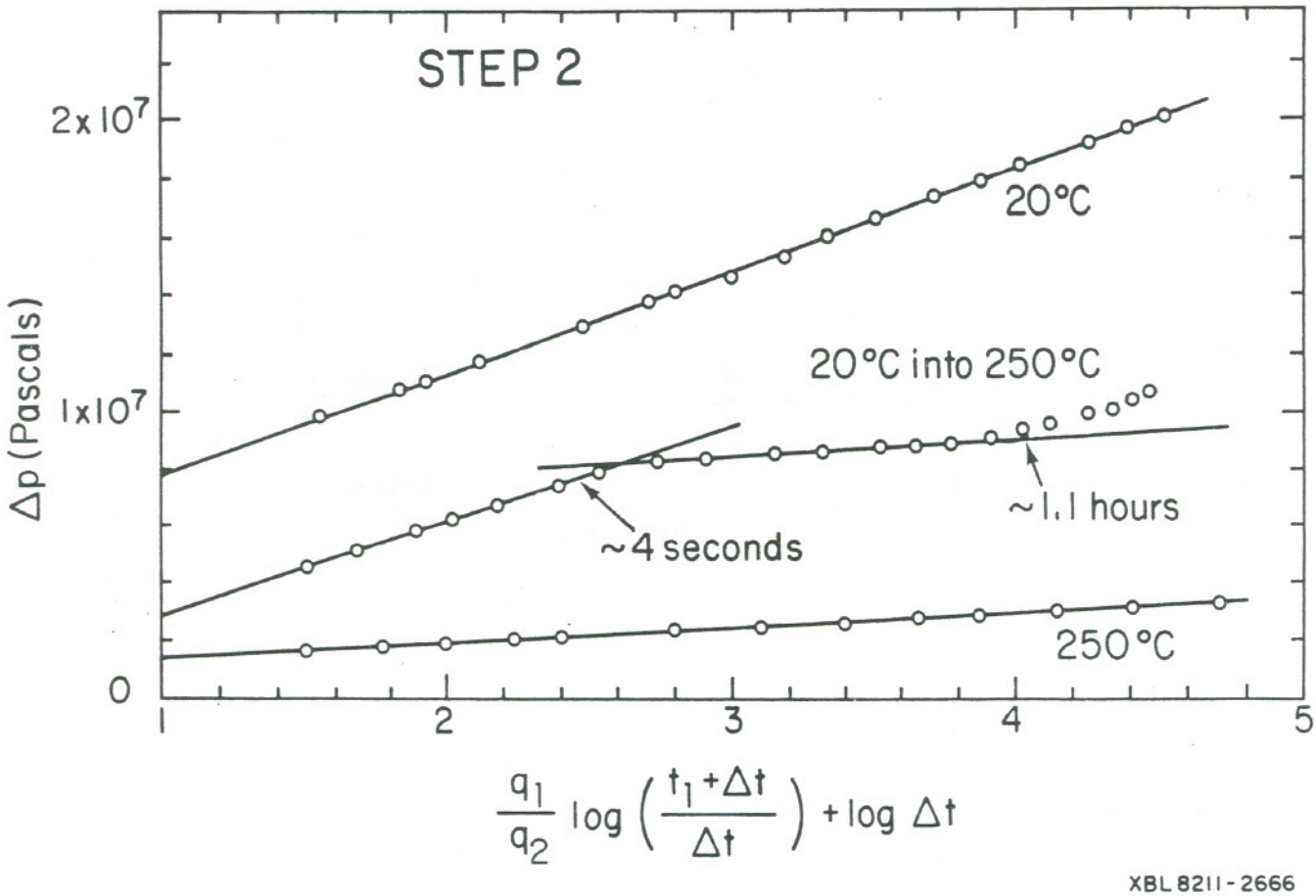


Figure 13. Pressure transient data for Step 2 of the simulated step-rate test.

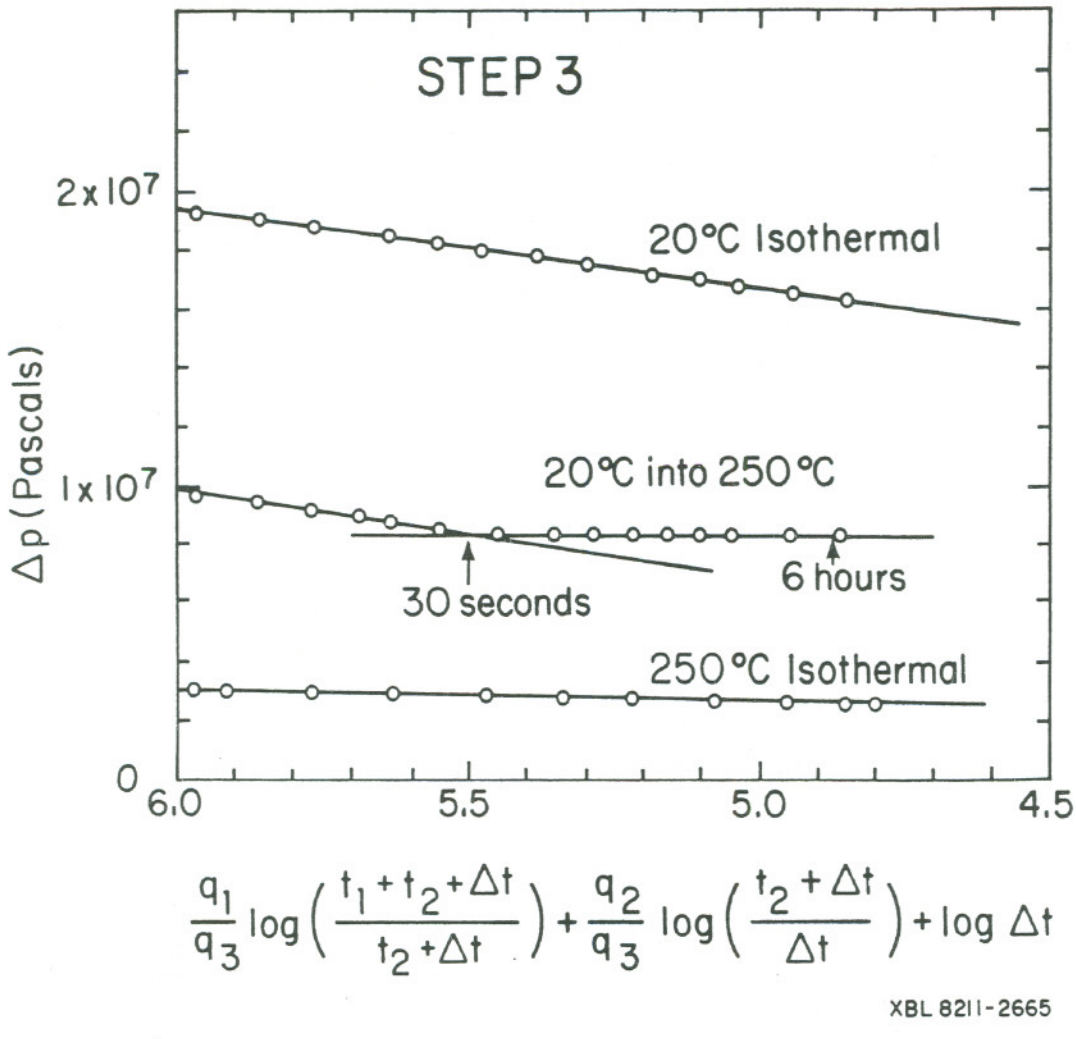


Figure 14. Pressure transient data for Step 3 of the simulated step-rate test.

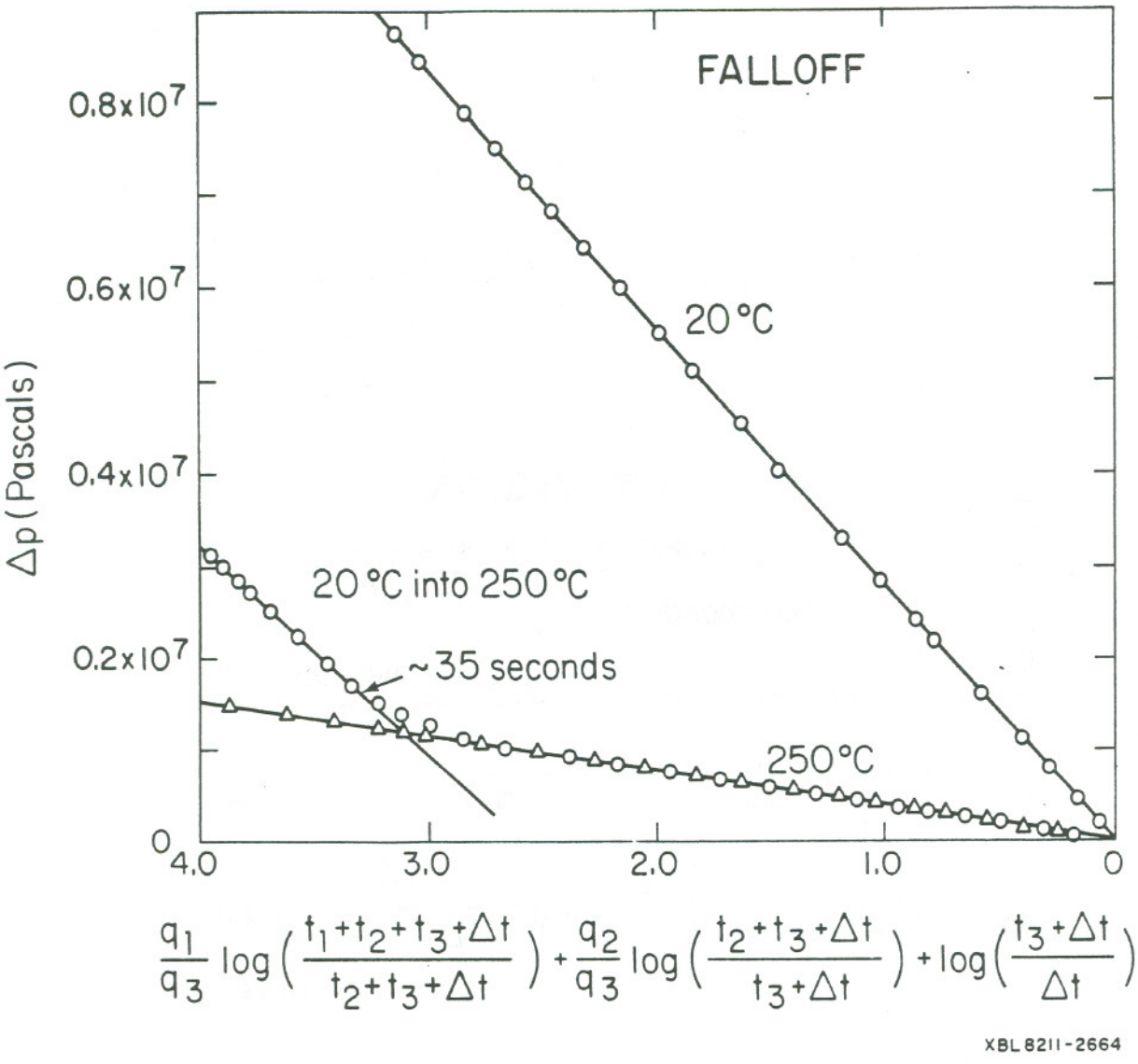


Figure 15. Pressure transient data for the falloff after the simulated step-rate test.

early transients are governed by the 1.1-m cold spot formed during Step 1. At approximately 4 s the pressure data depart from the first slope and fall on a second slope which corresponds to the properties of the reservoir fluid. At approximately 1.1 hours the data depart from the second slope and the moving thermal front begins to control the pressure response. The transition times ($t_f$ and $t'_o$) are in reasonable agreement with those calculated from Equations (12) and (13), or 5 s and 2.7 hours, respectively. Note that the transition time ($t'_o$) is not evaluated from the plot because the test did not run long enough to develop the final semi-log straight line.

The third step begins at 12 hours into the test. By this time the thermal front has advanced 1.9 m into the formation. Equation (13) indicates that the reservoir will behave as a composite system until 16 hours after the rate change. Therefore, the entire 6-hour step will only reflect the composite reservoir behavior. This is clearly shown in Figure 14, where only two slopes are apparent, the first corresponding to the fluid properties of the cold spot, and the second, to the reservoir fluid.

The pressure falloff data following the step test are plotted in Figure 15. As expected, the data initially follow a slope corresponding to the properties of the cold spot and then become identical to the pressure falloff for 250°C isothermal injection.

It is apparent that superposition is an acceptable way to treat this problem and that the equations developed for single-rate tests are valid if the effects of the growing cold spot and variable injection rates are taken into consideration.

It is interesting to note that the well injectivity, shown in Figure 16, is of little value for the inference of downhole well productivity. This results from the lack of a simple relationship between the nonisothermal injectivity (middle curve) and the two isothermal cases (from which, theoretically, productivity could be inferred).

Wellbore Effects

In the preceding discussions the influence of wellbore effects have been neglected. Both thermal transients in the wellbore and the effects of wellbore storage must be considered. If a free liquid level is present in the wellbore, wellbore-storage effects will be large and may mask much of the early time pressure data.

The duration of wellbore storage effects can be estimated by constructing a plot of log ($\Delta p$) vs. log (t). If a one-to-one slope is apparent, the beginning of the correct semi-log straight line will begin 1 to 1-1/2 log cycles after the end of the one-to-one slope (Earlougher, 1977). If the one-to-one slope is not apparent, the beginning of the semi-log straight line can be estimated (in field units) by (Earlougher, 1977)

$$t > \frac{(200{,}000 + 12{,}000s)\ C^*}{(kh/\mu)} \qquad (16)$$

For a falloff test, the beginning of the semi-log straight line is estimated using the same log-log procedure, or (in field units) by (Chen and Brigham, 1974)

$$t > \frac{170{,}000\ C^*\ e^{0.14s}}{(kh/\mu)} \qquad (17)$$

Earlougher et al., (1973) and Earlougher (1977) give a more complete discussion of wellbore storage effects.

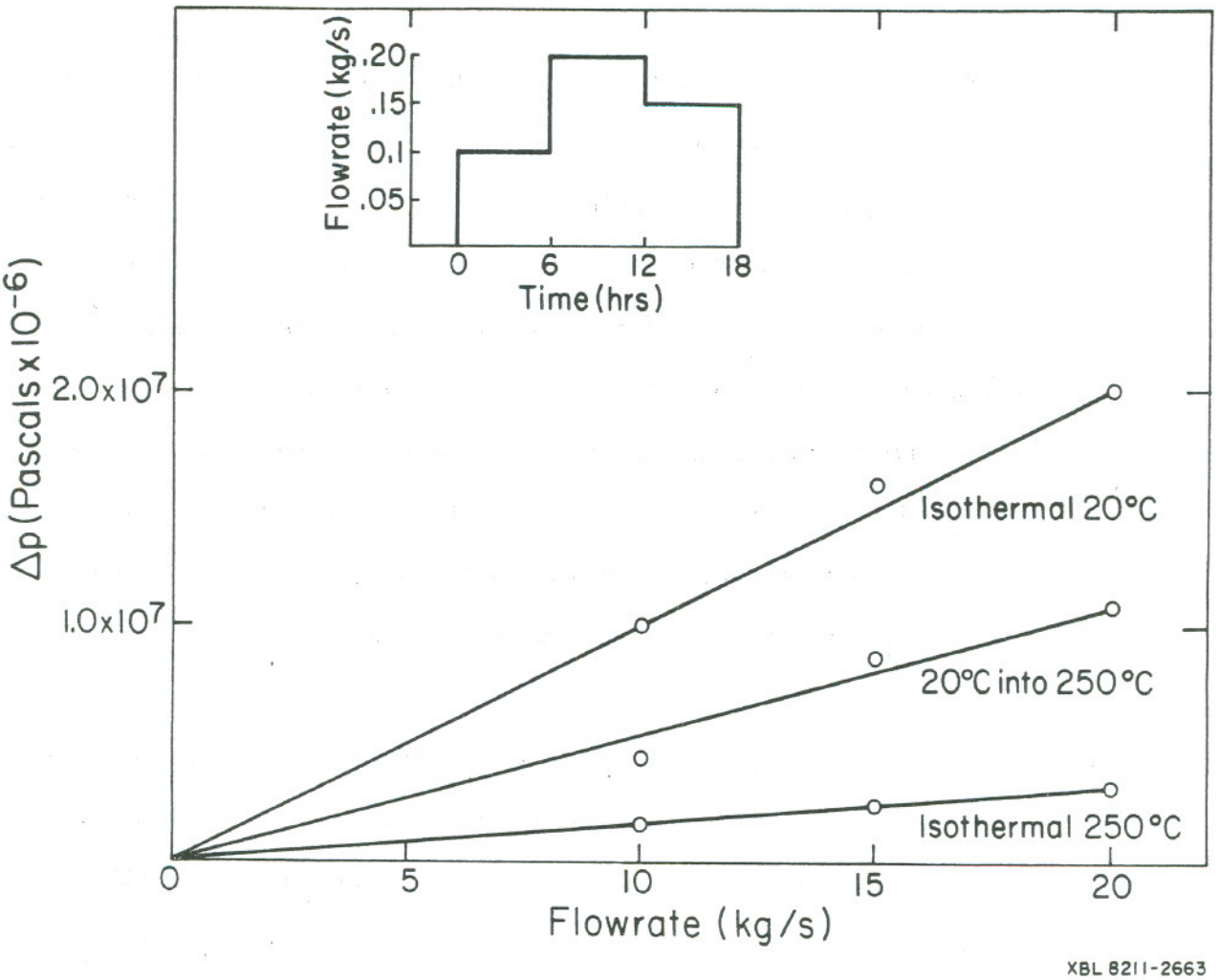


Figure 16. Bottomhole pressure change vs. flowrate for the simulated step-rate test.

Thermal transients may also influence the early time pressure response. If the well is deep or the casing diameter large, it takes a significant period of time before the bottomhole injection temperature stabilizes. The importance of this depends primarily on the pre-injection temperature profile in the well, the injection rate, the depth of interval being tested, and the pre-test well history. In order to demonstrate the significance of thermal transients, the wellbore simulator HEATLOS (Miller, 1980) is used to calculate sandface injection temperature during injection of 20°C water into a 250°C reservoir. The pre-injection temperature profile of the 2000 m deep well is shown in Figure 17. A wellbore radius of 0.1 m, and an injection rate of 20 kg/s are used for the simulation. Figure 18 shows the calculated sandface temperature as a function of time. Note that injection of more than two wellbore volumes is required before the injection temperature is within 10% of its steady-state value (approximately 70°C). This does not occur until 1.7 hours after injection begins.

Clearly the effects of the temperature changes in the bore must be considered to accurately evaluate injection test data. Figure 18 also clearly demonstrates that the downhole injection temperature may be very different from the wellhead temperature. Therefore, all calculations must be based on the sandface fluid temperature instead of the wellhead temperature. Because the pre-test temperature profile and the well configuration are site-specific, it is not possible to develop a general rule for these effects. However, $t_o$ will be delayed until the bottom-hole temperature stabilizes. If thermal transients are significant, $t_o$ must be evaluated with a well/reservoir simulator.

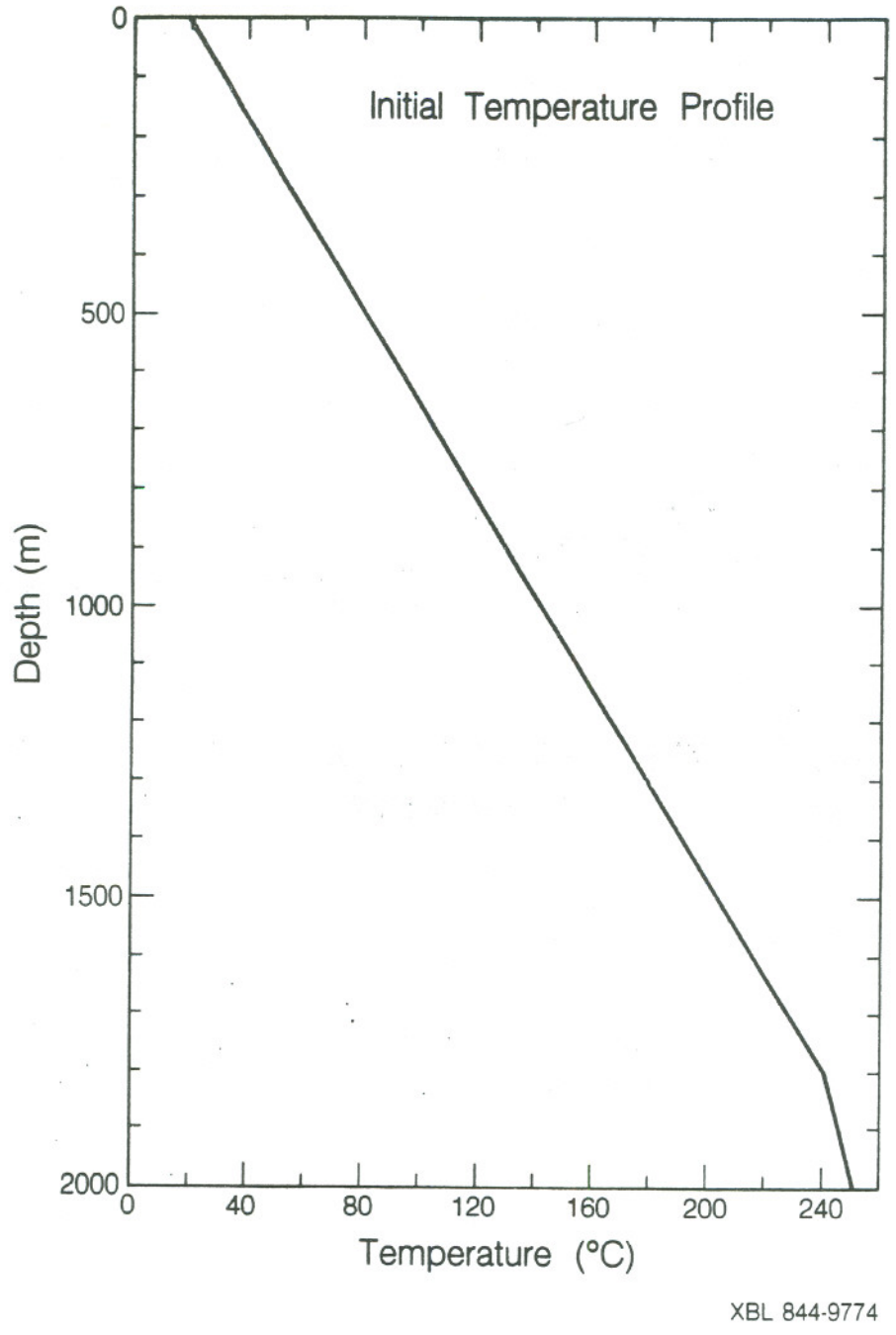


Figure 17. Initial temperature profile for the simulated wellbore-temperature transients.

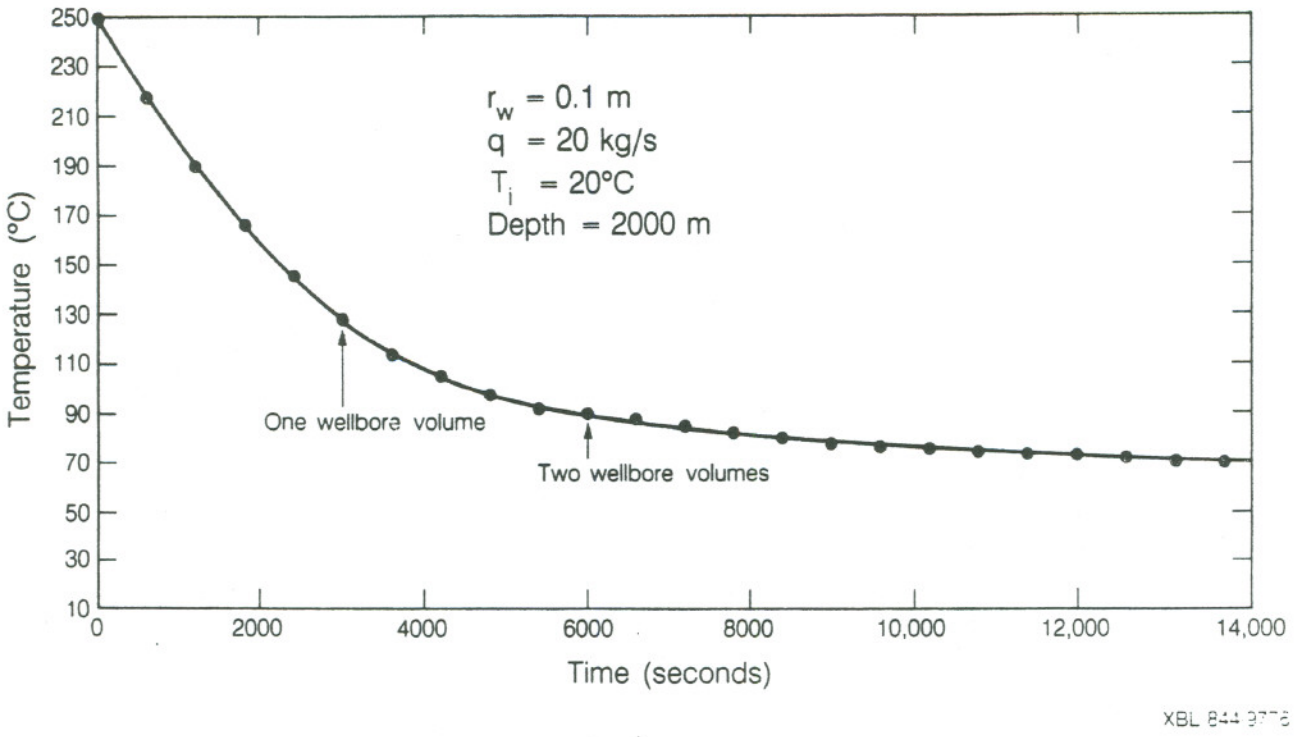


XBL 844 9778

Figure 18. Calculated bottomhole temperature for injection of 20°C water at an injection rate of 20 kg/s.

Careful test planning can be used to avoid the effects of thermal transients on the data. For instance, pressure buildup tests in wells already surrounded by a thermal discontinuity are the least affected by thermal wellbore transients. Also, pressure falloff tests are unaffected by thermal wellbore transients if downhole pressures are measured. It is important to realize that even small changes in the wellbore fluid temperature can result in significant changes in the water level of the well. Therefore, as a general rule, water level data are not suitable for pressure transient injection test analysis.

Discussion

The discussions in the previous sections have shown that pressure transients during nonisothermal injection can be characterized by one of two types of behavior: moving front dominated or composite reservoir behavior. Moving front dominated behavior occurs if the well has not been used for injection prior to the test. Composite reservoir behavior occurs if the well is surrounded by a thermal discontinuity created by previous injection.

In the absence of wellbore effects, pressure transients in the moving-front dominated case are described by two semi-log straight lines; the first corresponds to the properties of the in situ reservoir fluid and the second to the properties of the injected fluid. The intersection of these two semi-log straight lines can be estimated by Equation (11) if the effects of thermal wellbore transients and wellbore storage are negligible. If thermal wellbore transients are significant, as is almost always the case, the transition can only be evaluated with a wellbore and/or reservoir simulator.

The composite reservoir behavior is also characterized by two semi-log straight lines. However, in this case the first slope corresponds to the properties of the inner region and the second to the reservoir fluids. The time at which the data depart from the first slope can be estimated by Equation (12). This expression is approximately correct even if the temperature distribution around the thermal front is relatively diffuse (i.e., pressure falloff or step-rate tests). During injection, the pressure transients eventually fall on a third semi-log straight line (in the case of composite reservoir behavior) having that

has a slope corresponding to the properties of the injected fluid. The intersection of the last two semi-log straight lines can be approximated by Equation (13). From this time onwards, the pressure transients are characterized by the moving-front dominated behavior.

For many practical cases, the composite reservoir model is applicable for injection test data analysis. However, until the distance to the thermal front is far enough from the well, the semi-log straight line corresponding to the properties of the inner region will not be apparent (i.e., it will be masked by wellbore storage effects or measurement inaccuracy). Therefore, only the second semi-log straight line is available for analysis. Clearly, the permeability thickness (kh) of the reservoir can be evaluated from this slope. However, if the skin factor is evaluated using this line, the calculated value will reflect the presence of the inner region. This problem can be resolved by using the concept of a "fluid skin factor", which accounts for steady-state pressure buildup due to the cold region around the well. In the next section, this term is derived and applied to injection test analysis.

## FLUID SKIN FACTOR

From the discussion of the pressure transients in a system with a pre-existing thermal discontinuity, it is clear that until the effects of the moving thermal front control the pressure response, the system behaves like a composite system. The mobilities of the inner and outer regions are $k/\mu_1$, and $k/\mu_o$, respectively. Until the radius of the inner region is sufficiently large, the semi-log straight line corresponding to the properties of the inner region will not be observed in the measured pressure data. Therefore, an alternative approach is required in order to account for the effects of the inner region. To improve the understanding of this type of system, a steady-state analysis of the two-fluid composite reservoir can be performed. Based on the steady-state analysis, a fluid skin factor, which is analogous to the mechanical skin factor, can be defined. The fluid skin factor ($s_f$) can be used in the same manner as the mechanical skin factor ($s_m$) to calculate an additional component of pressure buildup due to an annular region of cold water around the well. It will also be shown that the concept of the fluid skin factor can also be used as the basis for a method of monitoring the penetration of cold water into the reservoir (Benson, 1982).

### Derivation

The steady-state pressure buildup in a two-fluid composite system with a stationary boundary separating the two regions can be calculated by the following procedure. From Darcy's Law

$$Q = \frac{-kA}{\mu} \frac{dp}{dr} \tag{18}$$

Rearranging, substituting $Q = q/\rho$ into Equation (18), and integrating; we see that at steady state

$$\int_{r_w}^{r_e} \frac{q\mu \, dr}{2\pi kh \, r} = -\int_{p_w}^{p_e} dp \tag{19}$$

Recognizing that the steady-state mass flowrate is constant, and assuming that the fluid properties within each of the two regions are uniform, this integral can be evaluated

$$\frac{q\mu_i}{2\pi kh\rho_i} \ln\left(\frac{r_f}{r_w}\right) + \frac{q\mu_o}{2\pi kh\rho_o} \ln\left(\frac{r_e}{r_f}\right) = p_w - p_e \tag{20}$$

where $r_f$ is the radius of the inner region. Equation 20 can be rearranged as

$$\Delta p = \frac{Q_o\mu_o}{2\pi kh}\left[\frac{\mu_i\rho_o}{\mu_o\rho_i} \ln\left(\frac{r_f}{r_w}\right) + \ln\left(\frac{r_e}{r_f}\right)\right] \tag{21}$$

If the term $\ln(r_f/r_w)$ is added and subtracted from the right-hand side of the equation,

$$\Delta p = \frac{Q_o\mu_o}{2\pi kh}\left[\left(\frac{\mu_i\rho_o}{\mu_o\rho_i} - 1\right) \ln\left(\frac{r_f}{r_w}\right) + \ln\left(\frac{r_e}{r_w}\right)\right] \tag{22}$$

The second term in the equation, when multiplied by the expression outside of the parenthesis, is just the pressure buildup in a homogeneous reservoir with the properties of the initial in situ fluid. Therefore, the steady state pressure buildup at the well can be written as the sum of two terms

$$\Delta p = \frac{Q_o\mu_o}{2\pi kh}\left[\ln\left(\frac{r_e}{r_w}\right) + s_f\right] \tag{23}$$

where $s_f$ is the fluid skin factor and is defined as

$$s_f = \left[\frac{\mu_i}{\mu_o}\frac{\rho_o}{\rho_i} - 1\right] \ln\left(\frac{r_f}{r_w}\right) \tag{24}$$

Comparing Equation (24) to Equation (14), we see that the fluid skin factor and mechanical skin factor have nearly the same form. Therefore, establishing the validity of a fluid skin factor, to account for the pressure buildup due to the cold spot during unsteady conditions, is analogous to establishing the validity of using a conventional skin factor to account for the pressure buildup due to a region of permeability of degradation or enhancement around the wellbore. Essentially, it must be shown that it is reasonable to assume pseudo-steady conditions within the fluid skin region.

Wattenbarger and Ramey (1970) performed a finite difference analysis of an annular region of permeability degradation or enhancement around a well in in order to determine the validity of the thin skin concept (van Everdingen, 1953; Hurst, 1953). Their criterion for determining the validity of the concept is based on whether or not the semi-log straight line corresponding to the permeability of the inner region will be observed in the pressure transient data. If observed, they determine that the concept is not valid. They conclude that for large values of the wellbore storage coefficient (i.e., the early time data is masked), the concept is valid for $r_s<100\times r_w$. However, recall that the duration of the first semi-log straight line is not governed simply by the ratio of $r_s/r_w$ or the wellbore storage coefficient, but primarily by the diffusivity $(k/\phi\mu_1 c_t)$ of the inner region.

Since the skin factor and the fluid skin factor are calculated only as a function of the ratios of the permeabilities or fluid properties of the inner and outer regions, the criterion that $r_s< r_w\times 100$ is not generally applicable. Although it is certainly useful as a general

rule, especially when it is not possible to evaluate $r_f$ or $r_s$, it may be overly conservative. A more general approach is to estimate the duration of the first semi-log straight line using Equation (12). However, use of Equation (12) requires an estimate of $r_f$. If records of cumulative injection into the well are available, $r_f$ can be evaluated with Equation (8). Therefore, Equation (12) can be evaluated.

In summary, use of the fluid skin factor to account for the pressure buildup due to the presence of the cold spot is valid for times greater than $t_f$, which can be calculated from Equation (12). However, for large cold spots, the correct second semi-log log straight line may not develop until relatively long times (Ramey, 1970). Therefore, if the cold spot is large, the analysis should be approached cautiously to ensure that the correct semi-log straight line has been identified.

Application to Pressure Transient Analysis

Outside the cold region the transient response is identical to that for a homogeneous system with properties of the in situ fluid. Therefore, the transient response at the well can be approximated by

$$\Delta p = \frac{Q_o \mu_o}{4\pi kh} \left( p_D + 2s_f \right) \tag{25}$$

where

$$p_D = - Ei \left(\frac{-1}{4t_D}\right) \tag{26}$$

and $t_D$ is defined according to the conventional definition

$$t_D = \frac{kt}{\phi \mu_o c_t r_w^2} \tag{27}$$

If the well has a mechanical skin factor, the pressure buildup has three components, one due to the mechanical skin, a second due to the region inside the thermal front, and the third due to the reservoir. A steady-state analysis, similar to the one above, shows that

$$\Delta p = \frac{Q_o \mu_o}{2\pi kh} \left[ \left( \frac{k}{k_s} \frac{\mu_i}{\mu_o} \frac{\rho_o}{\rho_i} - 1 \right) \ln \left( \frac{r_s}{r_w} \right) + \left( \frac{\mu_i \rho_o}{\mu_o \rho_i} - 1 \right) \ln \left( \frac{r_f}{r_s} \right) + \ln \left( \frac{r_e}{r_w} \right) \right] \tag{28}$$

If the radius of the skin damaged region is small in comparison to the radius to the front then $\ln(r_f/r_s) \approx \ln(r_f/r_w)$. Therefore, the fluid skin factor can again be used to express the steady-state pressure buildup as

$$\Delta p = \frac{Q_o \mu_o}{2\pi kh} \left[ \ln \left( \frac{r_e}{r_w} \right) + s_f + s_{ma} \right]; \tag{29}$$

where the mechanical skin factor of the well combines with fluid related components to give an apparent mechanical skin factor ($s_{ma}$), defined as

$$s_{ma} = \left( \frac{k}{k_s} \frac{\mu_i}{\mu_o} \frac{\rho_o}{\rho_i} - 1 \right) \ln \left( \frac{r_s}{r_w} \right) \tag{30}$$

Application to Injection Test Analysis

In the previous section it was shown that, in general, the pressure buildup at the injection well has three components, one due to the apparent mechanical skin factor ($s_{ma}$), a second due to the fluid skin factor ($s_f$), and third due to the reservoir. If a pressure buildup or falloff test is analyzed using the semi-log straight line that corresponds to the properties of the reservoir fluids, then the total apparent skin factor ($s_a$) will be given by

$$s_a = s_{ma} + s_f \tag{31}$$

If the radius to the cold front and the properties of the injected and in situ fluids are known, the value of the fluid skin factor can be calculated from Equation (24). The apparent mechanical skin factor ($s_{ma}$) is calculated from the difference between $s_a$ and $s_f$.

In order to determine the relation between $s_m$ and $s_{ma}$, it is useful to re-examine the definition of the mechanical skin factor for a finite region of permeability degradation or enhancement (Hawkins, 1956):

$$s_m = \left( \frac{k}{k_s} - 1 \right) \ln \left( \frac{r_s}{r_w} \right) \tag{32}$$

Also, recall that

$$s_{ma} = \left( \frac{\mu_i \rho_o}{\mu_o \rho_i} \frac{k}{k_s} - 1 \right) \ln \left( \frac{r_s}{r_w} \right) \tag{33}$$

From the two equations it can be seen that in general there is no direct means to evaluate the mechanical skin factor from apparent mechanical skin factor because both $k_s$ and $r_s$ are unknown. However, in two important cases it is possible to approximate the value of the mechanical skin factor. First, if $k_s << k$, Equation (32) can be approximated by

$$s_m = \frac{k}{k_s} \ln \left( \frac{r_s}{r_w} \right) \qquad \text{for } k_s << k \tag{34}$$

similarly for Equation 33

$$s_{ma} = \frac{\mu_i \rho_o}{\mu_o \rho_i} \frac{k}{k_s} \ln \left( \frac{r_s}{r_w} \right) \qquad \text{for } k_s << k \tag{35}$$

Equating these two expressions indicates that

$$s_m = \frac{\mu_o \rho_1}{\mu_1 \rho_o} s_{ma} \qquad \text{for } k_s << k \tag{36}$$

Therefore, for positive skin factors it is possible to approximate $s_m$ from the calculated value of $s_{ma}$. A second important case arises when $k_s >> k$. In this case

$$s_m = -\ln \frac{r_s}{r_w} \qquad \text{for } k_s >> k \qquad (37)$$

and

$$s_{ma} \simeq s_m \qquad \text{for } k_s >> k \qquad (38)$$

Therefore, $s_m$ can be evaluated simply from the difference between $s_a$ and $s_f$.

From the above discussion it is clear that if the apparent skin factor ($s_a$) can be calculated from a standard pressure transient injection test, and if the radius to the inner region is known, it is possible to estimate the mechanical skin factor of the well. However, if the distance to the front is not known, evaluation of $s_f$ is not possible. In order to avoid this difficulty, an alternative method of analysis has been developed. This method gives both the ability to track the movement of the front into the reservoir and estimate the mechanical skin factor of the well. Development of this procedure, discussed in the next section, is based on the relationship between the growth of the fluid skin factor and the increasing distance to the thermal front.

## Front Tracking

In order to use the fluid skin factor as a front tracking tool, a test and analysis procedure must be developed that allows differentiation between the mechanical and fluid skin factors of a well. In cases where the front between the injected and reservoir fluid moves as a function of $t/r^2$, which is the case for many injection processes considered in

a porous medium, such a procedure is developed as follows. From Equation (8), the radial position of the front can be expressed as

$$r_f = \sqrt{a \frac{Qt}{\pi h}} \tag{39}$$

where a is a constant of proportionality that depends on the mass- and energy-balance equations governing the displacement process. For example

$$a = \frac{\rho_w c_w}{\rho_a c_a} \tag{40}$$

for nonisothermal injection. Noting that the term Qt can be replaced by the cumulative injection (C) and substituting Equation (39) into Equation (24), we see that

$$s_f = 1.151 \left( \frac{\mu_1 \rho_o}{\mu_o \rho_1} - 1 \right) \left[ \log (C) + \log \left( \frac{a}{\pi h r_w^2} \right) \right] \tag{41}$$

Since the second logarithmic term is a constant, it is clear that a plot of the logarithm of the cumulative injection vs. the fluid skin factor will result in a semi-log straight line with a slope of

$$n = 1.151 \left( \frac{\mu_1 \rho_o}{\mu_o \rho_1} - 1 \right) \tag{42}$$

If $s_f$ is evaluated at $C = \pi h r_w^2$,

$$s_f (\pi h r_w^2) = n \log (a) \tag{43}$$

Since the value of a is simply the ratio of the volumetric heat capacities of the injected water and the reservoir fluid, $s_f (\pi h r_w^2)$ is easily evaluated.

For a well with a mechanical skin factor, the extrapolation of the semi-log line to a value of $C = \pi h r_w^2$ yields

$$s_a(\pi h r_w^2) = s_{ma} + n\log(a) \tag{44}$$

and

$$s_{ma} = s_a(\pi h r_w^2) - n\log(a) \tag{44a}$$

Therefore, the mechanical skin factor can be estimated using Equation (36) or (38), depending upon which is appropriate.

The fluid skin factor for any value of the cumulative injection is evaluated by

$$s_f(C) = s_a(C) - s_{ma} \tag{45}$$

Since $s_{ma}$ is calculated by Equation (44a), we see that

$$s_f(C) = s_a(C) - s_a(\pi h r_w^2) + n\log a \tag{46}$$

Once $s_f(C)$ is known, the distance to the thermal front can be estimated by

$$r_f(C) = r_w \exp\left[\frac{1.151 s_f(C)}{n}\right] \tag{47}$$

In Table 2, the radial distance to the front is given as a function of $1.151\ s_f/n$. For small values of this term, resolution of the radial distance to the front is good. However, at large values of $1.151\ (s_f/n)$, small errors in the calculated fluid skin factor result in large errors in the computed radial distance to the front. Therefore, this method of front tracking is most useful during the early stages of injection.

| $1.151s_f/n$ | $r_f$ |
|---|---|
| .1 | 0.11 m |
| .2 | 0.12 m |
| .3 | 0.13 m |
| .4 | 0.15 m |
| .5 | 0.16 m |
| 1.0 | 0.27 m |
| 2.0 | 0.74 m |
| 3.0 | 2.00 m |
| 4.0 | 5.46 m |
| 5.0 | 14.84 m |
| 6.0 | 40.34 m |

Table 2. Distances to the thermal front for several values of $1.151s_f/n$.

## INJECTION TEST ANALYSIS

Methods for analyzing injection data fall into two categories, based on whether there has been no injection prior to the test (moving front dominated tests), or the well has been used for injection prior to the test (composite reservoir tests); (Benson and Bodvarsson, 1982). The first case occurs when an injection test is being used to determine the reservoir characteristics or when injection is being carried out in an attempt to stimulate the well. An injection well being tested for diagnostic purposes will fit into the latter case. The analysis method for each case is developed separately.

### Moving Front Dominated Tests

In the previous discussions, pressure buildup due to nonisothermal injection with a moving thermal front has been demonstrated. Clearly, the pressure transient data can be used to calculate the mobility-thickness product, $kh/\mu$, from one of the semi-log straight lines on the pressure vs. log (time) plot. If the fluid properties to which the slope corresponds can be determined, then kh can be determined. Furthermore, if the first slope is apparent, either in the case of a cold spot or a moving thermal front, then the correct skin value can be calculated using conventional methods of analysis.

In practice, however, the first slope and the first break in slope are masked by wellbore storage. Therefore, it is important to be able to determine independently the fluid properties to which the analyzed portion of the data correspond. In the following section, techniques are developed to determine the appropriate method of analysis and to identify the fluid properties to which the data correspond. Also, methods

for calculating the mechanical skin factor of the well in the absence of the first slope are developed.

The pressure buildup in response to nonisothermal injection without a pre-existing thermal discontinuity is demonstrated in Figure 19. Initially as shown by case 2, the pressure buildup is controlled by the in situ fluid temperature. At $t_o$ the slope changes and the data fall on a second semi-log straight line, indicating that the pressure buildup is thereafter governed by the temperature of the injected fluid. Comparing this to Case 1 in Figure 19, it can be seen that the pressure buildup is identical to that of isothermal injection at the temperature of the injected fluid, except for a short period during which the pressure changes correspond to the reservoir fluid properties. The pressure offset ($\Delta p_o$) created between the two curves is a function of $\mu_i$, $\mu_o$, $t_o$ and the density contrast of the fluids.

The pressure offset, $\Delta p_o$, can be calculated if kh and $\phi c_t h$ are known. Since kh can be determined from the pressure vs. log (time) graph and $\phi c_t h$ can be estimated from well log data, the offset between the curves is calculated as follows:

$$\Delta p_o = \frac{q}{4\pi kh} \left[ \frac{\mu_1}{\rho_1} P_D(t_{Do})_1 - \frac{\mu_o}{\rho_o} P_D(t_{Do})_o \right] \qquad (48)$$

where

$$(t_{Do})_1 = \frac{kt_o}{\phi \mu_1 c_t r_w^2} \quad ; \text{ and } \quad (t_{Do})_o = \frac{kt_o}{\phi \mu_o c_t r_w^2} \qquad (48a,b)$$

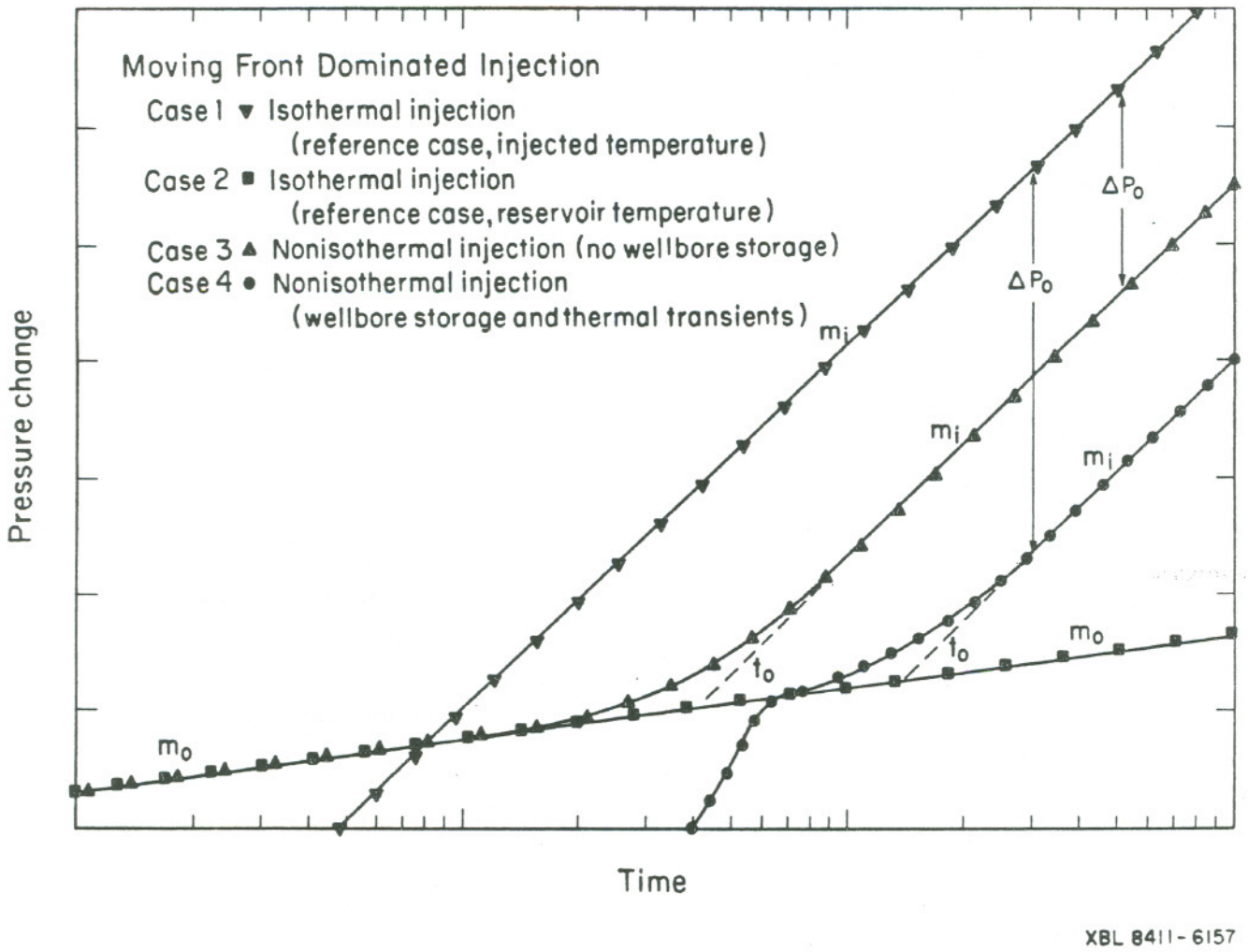


Figure 19. Apparent skin values vs. log (C) for four hypothetical cases.

Note that the skin factor of the well does not affect the magnitude of $\Delta p_o$ because dimensionless time is shifted by a factor of $e^{-2s}$ for both isothermal and nonisothermal injection (see Equation (15)).

The time, $t_o$, is extremely site-specific because it is a function of the well configuration, pre-test well history, initial geothermal gradient and flow-rate. As discussed earlier it is not possible to develop a general rule for calculating $t_o$ under these circumstances. However, the time at which this transition occurs can be calculated if a simulator such as PT is available (Bodvarsson, 1982). Case 4 in Figure 19 shows a typical pressure buildup curve where both wellbore storage and thermal wellbore transients are significant. The effects of these factors is to increase $t_o$ (hence $\Delta p_o$) and mask the initial semilog straight line coresponding to the properties of the in situ reservoir fluid.

In general, since $t_o$ may be time consuming to evaluate, it is recommended that injection tests be designed to avoid evaluating this term. This is accomplished by conducting pressure falloff tests or step-rate tests in which the front is sufficiently far from the well so that composite reservoir behavior prevails. However, if these conditions cannot be satisfied, the data can be analyzed by the following procedure.

1) Use Equation (11) or a numerical simulator to estimate the time at which the slope of the pressure transient changes to that corresponding to the injected fluid.

2) Estimate the duration of wellbore storage by conventional methods.

3) On a plot of pressure vs. log (time), find the straight line from which kh can be calculated, making sure that the data being analyzed are for times greater than $t_o$ and that wellbore storage effects have ceased. Then, calculate

$$kh = 0.183 \frac{q\mu_1}{\rho_1 m_1} \tag{49}$$

4) Use Equation (48) to calculate the pressure offset between the isothermal and nonisothermal injection.

5) Extrapolate the semi-log straight line ($m_i$) to 1 second and determine $p_{1s}$. Calculate

$$p_{1s}^* = p_{1s} + \Delta p_o \tag{50}$$

6) Calculate the skin factor

$$s = 1.151 \left[ \frac{p_{1s}^* - p_i}{m_i} - \log \frac{k}{\phi \mu_i c_t r_w^2} - 0.351 \right] \tag{51}$$

7) Re-evaluate $t_o$ with Equation 15 to ensure that the data used to calculate the slope of the semi-log straight line corresponds to the properties of the injected fluid. Repeat the above procedure if the incorrect data were used.

Analysis of Composite Reservoir Injection Tests

The pressure response to nonisothermal injection into a reservoir with a pre-existing thermal discontinuity around the well can be described in terms of three periods. The first corresponds to the pressure transient associated with the fluid properties of the inner region of radius ($r_f$), the second to the in situ reservoir fluid, and the third to the injected fluid. The first two periods correspond to the composite reservoir behavior. Typical pressure transients, characteristic of this type of system, are shown in Figure 20. As shown by Case 2 in Figure 20, for a sufficiently large inner region, the first semi-log straight line may be apparent; if so, it can be used to calculate kh and the skin factor (Odeh, 1969; Bixel and Van Poollen, 1967; Merrill et al, 1974;

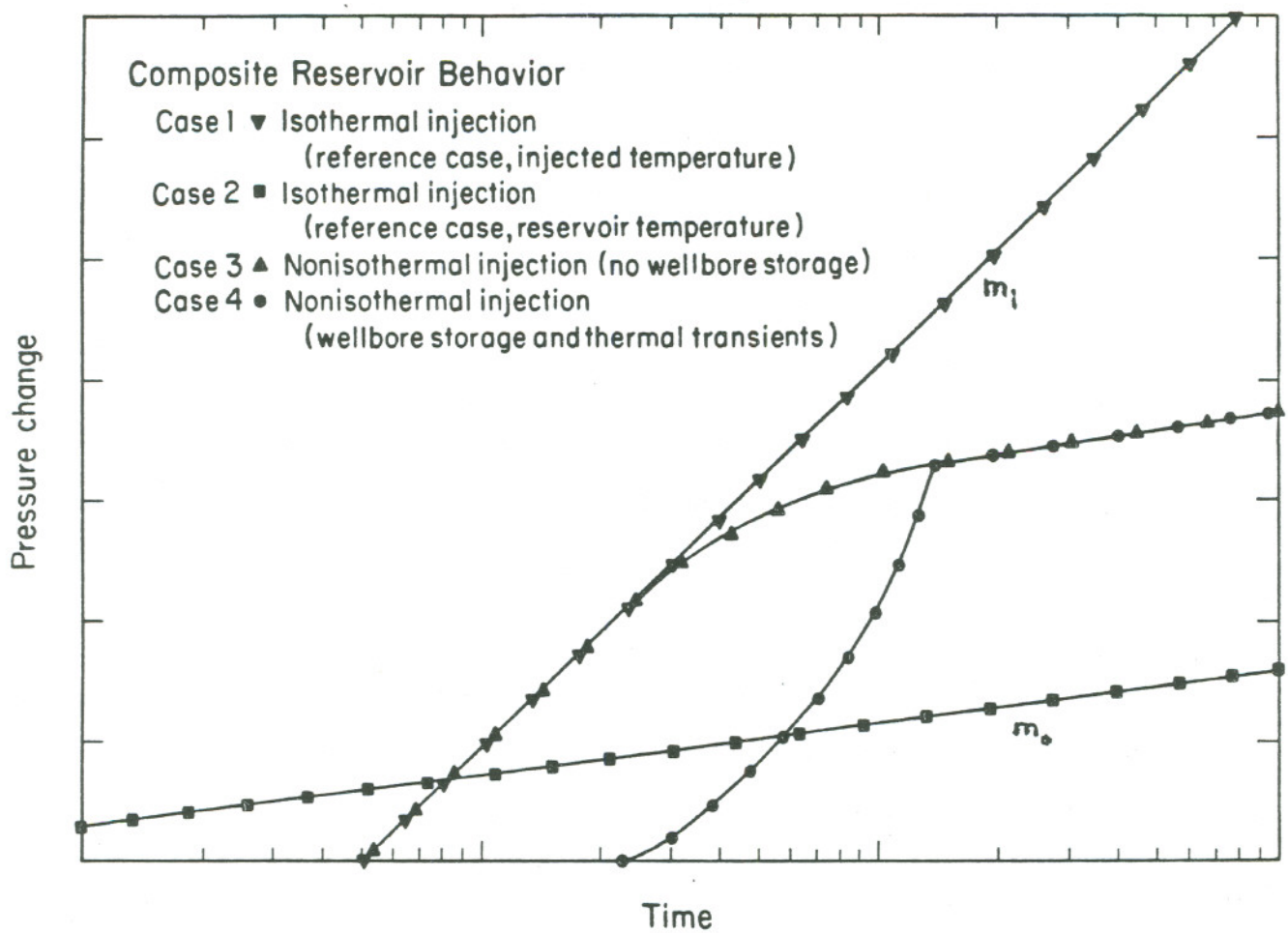


Figure 20. Schematic of the presure transient response during moving-front dominated injection tests.

Earlougher, 1977). However, if the first slope is masked by the effects of wellbore storage, another method of analysis is needed.

The analysis procedure developed below is based on using the semi-log straight line that corresponds to the properties of the in situ reservoir fluid. From the slope of this line, kh and the apparent skin factor can be calculated.

It is important to have a reasonably accurate estimate of the cumulative injection into the well prior to the test. Of course, if the temperature of the fluid around the well has re-equilibriated to the in situ reservoir temperature, the pressure buildup will not resemble that of a composite reservoir. In this case, moving front analysis is appropriate. Lack of proper planning and incorrect information about the pre-test well history may result in extremely erroneous interpretation of injection test data.

If an estimate of the cumulative injection is available, the following analysis procedure is used to calculate kh and the mechanical skin factor of the well.

1) Estimate the distance to the front from

$$r_f = \sqrt{\frac{\rho_w c_w}{\rho_a c_a} \frac{C}{\pi h}} \qquad (52)$$

2) Use Equation (12) to estimate the time at which the data will depart from the first semi-log straight line,

$$t_f = \frac{\phi \mu_i c_t}{4k} r_f^2 \qquad (12)$$

and Equation (13) to estimate the time at which the data will depart from the second semi-log straight line

$$t_o' = \frac{\rho_a c_a}{\rho_w c_w} \frac{\pi h}{Q} r_f^2 \qquad (13)$$

3) Estimate the duration of wellbore storage by conventional methods.

4) From the slope ($m_o$) on a plot of pressure vs. log (time) calculate

$$kh = 0.183 \frac{q\mu_o}{\rho_o m_o} \qquad (53)$$

5) Determine $p_{1s}$ by extrapolating $m_o$ to 1 second.

6) Calculate the apparent skin factor

$$s_a = 1.151 \left( \frac{p_{1s} - p_i}{m_o} - \log \frac{k}{\phi \mu_o c_t r_w^2} - 0.351 \right) \qquad (54)$$

7) Calculate the fluid skin factor from Equation (24) and the estimate of $r_f$ obtained from step 1

$$s_f = 1.151 \left( \frac{\mu_1}{\mu_o} \frac{\rho_o}{\rho_1} - 1 \right) \ln \left( \frac{r_f}{r_w} \right) \qquad (24)$$

8) Calculate the apparent mechanical skin factor

$$s_{ma} = s_a - s_f \qquad (55)$$

9) Estimate the apparent mechanical skin factor

$$s_m \approx \frac{\mu_o}{\mu_1} \frac{\rho_1}{\rho_o} s_{ma} \quad \text{where} \quad s_{ma} \gg 0 \quad \text{or} \qquad (36)$$

$$s_m \approx s_{ma} \quad \text{where} \quad s_{ma} \ll 0 \qquad (38)$$

If $S_{ma}$ is close to zero, the conditions under which Equations (36) and (38) are valid are not satisfied. In this case, it can only be determined that the mechanical skin factor lies somewhere between the predicted values by these two equations.

10) If Equation (16) is used to estimate the duration of wellbore storage effects, the expression should be reevaluated to ensure that the correct data are used for the analysis. Equation (16) must be modified to account for nonisothermal injection effects. Therefore, the start of the semi-log straight line can be estimated by (in field units)

$$t > \frac{(200{,}000 + 12{,}000s_a)C^*}{kh/\mu_o} \qquad (56)$$

This modification is necessary because the apparent skin factor, rather than just the mechanical skin factor, provides the resistance to flow near the wellbore.

Pressure Falloff Analysis

When a well is shut-in after nonisothermal injection it behaves like a two-fluid composite system. Therefore, the analysis procedure closely parallels that developed for composite-reservoir analysis. Pressure falloff analysis is subject to the least uncertainty because eventually, the properties of the reservoir fluid will govern the pressure transient response. In the case the the distance to the thermal front is sufficiently large, the first slope will be apparent in the pressure transient data. The early time data can be analyzed to evaluate the well skin factor, the permeability of the formation and to estimate the distance to the front (Bixel and van Poollen, 1967; Kazemi et al., 1972; Merrill et al., 1975; Satman et al., 1980; van Poollen et al., 1965). However, if the inner region is relatively small, the semi-log straight line corresponding to its fluid properties will not be apparent. Therefore, only the second semi-log straight line, corresponding to the properties of the reservoir fluid, will be available for analysis. In this case the following analysis procedure is used.

1) Prepare a Horner graph of the pressure buildup data (Horner, 1951) (e.g., p vs log $(t + \Delta t/\Delta t)$).

2) Estimate the distance to the thermal front from Equation (52).

3) Estimate the time at which the pressure falloff data depart from the first semi-log straight line using Equation (12).

4) Estimate the duration of wellbore storage effects from Equation (17).

5) Calculate the kh of the reservoir using the slope of the semi-log straight line on the Horner graph and Equation (53). Make sure that the semi-lop straight line used for the analysis begins after the times indicated by steps 3 and 4.

6) Calculate the fluid skin factor of the well by Equation (24).

7) Evaluate $p_{1s}$ by extrapolating the semi-log straight line on the Horner graph to the value of $(t + \Delta t)/\Delta t)$ where $\Delta t = 1$ s.

8) Evaluate the apparent skin factor of the well:

$$s_a = 1.151 \left( \frac{p_{1s} - p_{wf}}{m_o} - \log \frac{k}{\phi \mu_o c_t r_w^2} - 0.351 \right) \qquad (57)$$

9) Evaluate the apparent mechanical skin factor from Equation (55).

10) Estimate the mechanical skin factor from Equation (36) or (38).

11) Re-evaluate the duration of the effects of wellbore storage using a modification of the Chen and Brigham (1974) equation (in field units):

$$t > \frac{170{,}000 \; e^{0.14 s_a} \; C^*}{kh/\mu_o} \qquad (58)$$

Repeat the above procedure if the incorrect semi-log straight line was used.

Step-Rate Analysis

A discussion of the behavior of the pressure buildup during nonisothermal step-rate tests was presented previously. It was shown

that the pressure transients behave in a composite or moving-front-dominated manner depending upon the size of the thermal discontinuity surrounding the well. If the step-rate test is conducted in a well never before used for injection, the transients initially correspond to the moving front behavior. During the second and all subsequent steps, the data behave for a period of time like those in a composite system. If the distance to the thermal discontinuity is relatively small, both the composite and moving front may be observed in a single step (see Figure 13). In this case, the data are difficult to analyze accurately. The test must be designed so that the observed pressure transients clearly correspond to either the composite-reservoir or moving-front behavior. However, since composite reservoir behavior is easier to analyze, tests should be designed so that this procedure is applicable. Equations (8), (12), and (13) can be used to calculate the times at which the pressure data will change from one behavior to another Hence, the test can be designed to achieve the required results.

Assuming that the test is designed so that all of the pressure transients after the first step behave according to the composite-reservoir model, the following analysis procedure can be applied (Benson, 1982).

1) Prepare a plot of

$$\text{pressure vs. } \sum_{i=1}^{n} \frac{q_i}{q_n} \log \frac{t_1 + \ldots t_n + \Delta t}{t_{i+1} + \ldots t_n + \Delta t} \qquad (59)$$

2) Estimate the duration of the effects of wellbore storage using the methods outlined previously, depending on which is appropriate.

3) Calculate kh from the slope of the correct semi-log straight line on the prepared graph:

$$kh = 0.183 \frac{q_n \mu_o}{\rho_o m_o} \tag{60}$$

4) Calculate the apparent skin factor:

$$s_a = 1.151 \left( \frac{q_n}{q_n - q_{n-1}} \frac{p_{1s} - p_{wf}}{m_o} - \log \frac{k}{\phi \mu_o c_t r_w^2} - 0.351 \right) \tag{61}$$

5) Estimate the distance to the thermal front from Equation (52).

6) Calculate the fluid skin factor using Equation (24).

7) Calculate the apparent mechanical skin factor from Equation (55).

8) Estimate the mechanical skin factor of the well using Equation (36) or (38).

9) Re-evaluate the duration of wellbore storage using Equation (56) or (58). If the correct semi-log straight line was not used for the analysis, repeat the above procedure using the correct semi-log straight line.

Step-rate tests can be valuable tools for monitoring the injection process. Not only can the data be used to evaluate the near wellbore formation changes resulting from injection, but they can be used also to track the advancement of the thermal front into the reservoir (Benson and Bodvarsson, 1983). In the following section a procedure for thermal front tracking is developed.

Front Tracking Method

During cold water injection the thermal front advances into the reservoir. In the previous discussion of the fluid skin factor, the relationship between the advancement of the front and the growth of the fluid skin factor was developed. It was found that

$$s_f = n \left( \log(C) + \log \frac{a}{\pi h r_w^2} \right) \tag{62}$$

and the apparent skin factor, when evaluated at $C = \pi h r_w^2$, is given by

$$s_a(\pi h r_w^2) = n\log(a) + s_{ma} \tag{63}$$

The constant n is a function of the ratio of the fluid properties of the inner and outer regions and is expressed as

$$n = 1.151 \left( \frac{\mu_i}{\mu_o} \frac{\rho_o}{\rho_i} - 1 \right) \tag{64}$$

If the fluid skin factor is known, the radius to the thermal front can be calculated by

$$r_f = r_w e^{1.151\, s_f/n} \tag{65}$$

These four equations provide the theoretical basis of the following procedure for front tracking.

The method consists of conducting a series of injection and/or falloff tests after increasing periods of injection. Each of these tests is analyzed using the methods outlined previously, depending upon which method is appropriate. (Note that this method is not valid until the pressure transients are characteristic of the composite-reservoir behavior.) Once two values of the apparent skin factor are available the following procedure can be used. Refer to Figure 21 for a graphical explanation of the text. (Table 3 summarizes the well and reservoir parameters used for this example.)

1) Prepare a plot of $s_a$ vs. log(C). For example, Case 1 in Figure 21 shows that at $C = 10\ m^3$, $s_a = 2.6$ and at $C = 100\ m^3$, $s_a = 6.3$.

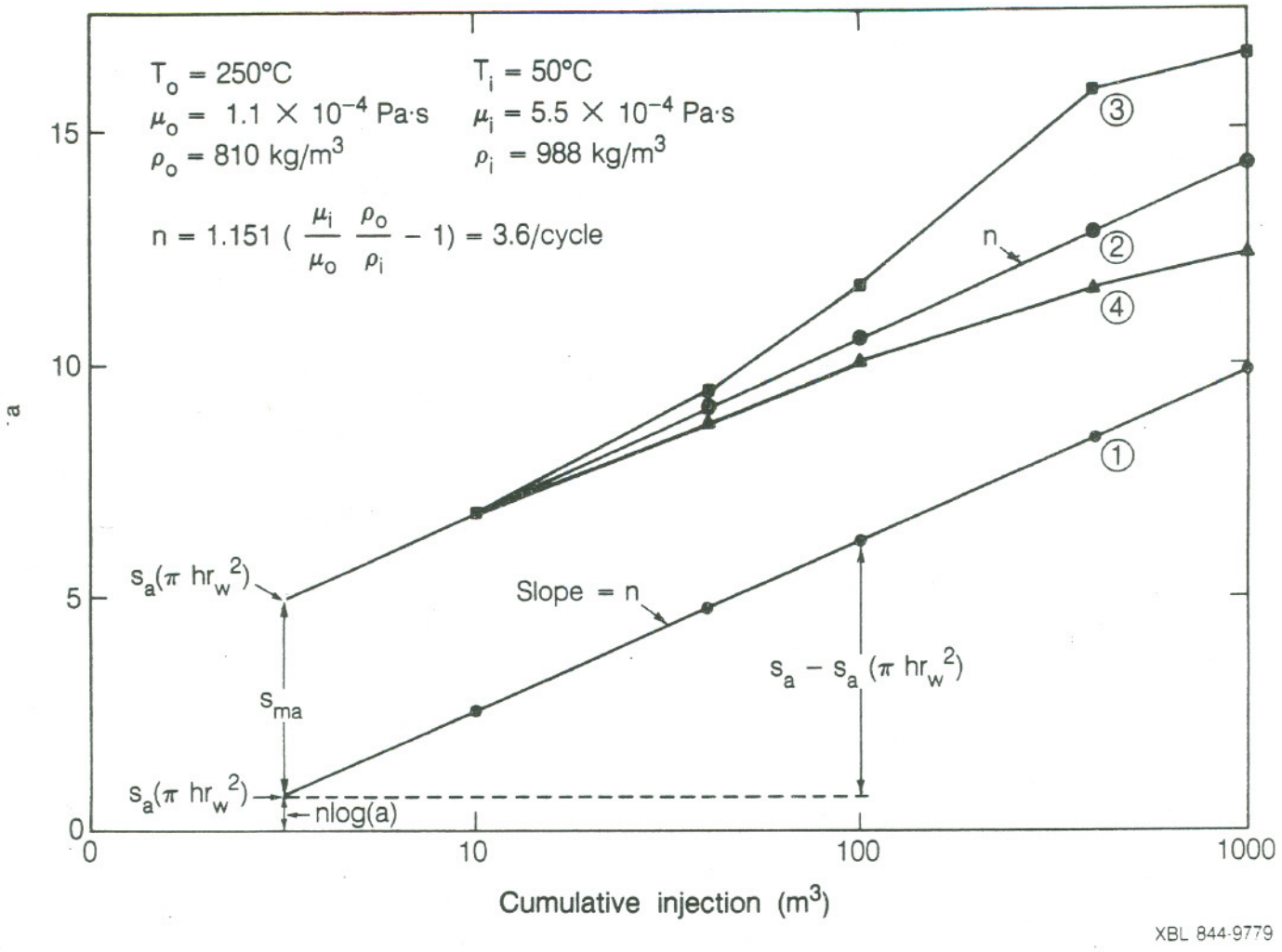


Figure 21. Schematic of the pressure transient response during composite-reservoir type injection tests.

| | |
|---|---|
| $\rho_a c_a$ | $2.46 \times 10^6$ J/m$^3$/°C |
| $T_r$ | 250°C |
| $T_i$ | 50°C |
| $\mu_o$ | $1.1 \times 10^{-4}$ Pa.s (0.11 cp) |
| $\mu_i$ | $5.5 \times 10^{-4}$ Pa.s (0.55 cp) |
| $\rho_o$ | 810 kg/m$^3$ |
| $\rho_i$ | 988 kg/m$^3$ |
| h | 100 m |
| $r_w$ | 0.1 m |
| $s_m$(case 1) | 0 |
| $s_m$(case 2) | 1 |
| $s_m$(case 3) | 1 |
| $s_m$(case 4) | 1 |

Table 3. Reservoir properties used for the discussion of front tracking.

2) Draw a straight line connecting the points, or the best straight line through a set of points.

3) Calculate the slope of the semi-log straight line, n (i.e., the change in $s_a$ for one log cycle of C). For both Cases 1 and 2, n = 3.6.

4) Compare the slope, n, to the value of n calculated by Equation (64). If they are in good agreement with one another this indicates that the method is applicable. If the slope does not agree with that calculated by Equation (64), either the skin factor of the well is changing or the thermal front is moving away from the well at a rate different than expected. This will be discussed later. For the time being, assume that the slope is close to its anticipated value.

5) Extrapolate n back to $C = \pi h r_w^2$ and evaluate $s_a$. For example, in Figure 21, $C = 3.14\ m^3$.

6) Calculate the apparent mechanical skin factor:

$$s_{ma} = s_a(\pi h r_w^2) - n\log(a) \qquad (66)$$

For both Cases 1 and 2, nlog(a) = 0.87. Therefore, from Figure 21 we see that $s_{ma} = 0$ for Case 1 and $s_{ma} = 4.1$ for Case 2.

7) Calculate the fluid skin factor for the test of interest (i.e., at a specific value of C)

$$s_f(C) = s_a(C) - s_{ma}, \qquad (67)$$

i.e., Case 1 $\quad s_f(100\ m^3) = 6.3-0=6.3$

Case 2 $\quad s_f(100\ m^3) = 10.4-4.1=6.3$

8) Calculate the radius to the thermal front from Equation (65). For Cases 1 and 2:

$$r_f = 0.1e^{\,1.15(6.3/3.6)} = 0.75\ m$$

This value agrees very well with the value of 0.73 m calculated from Equation (39).

Note that the mechanical skin factor of the well can also be estimated because this procedure provides a direct method of evaluating $s_{ma}$.

For Cases 1 and 2, calculated values of $s_m$ are equal to 0 and 1, respectively, which agree well with the input values.

The procedure outlined above assumes that the front is displacing the in situ fluids in a piston-like manner and that the mechanical skin factor of the well remains constant. If these conditions are not satisfied then the slope of the semi-log straight line will be different from the anticipated value. In fact, the line might not be straight. Two scenarios are demonstrated by Cases 3 and 4 in Figure 21. In Case 3, the well is progressively damaged by injection, hence the skin factor is increasing with time. This is reflected in plot of the apparent skin factor vs. log(C) by the calculated values of $s_a$ rising above the anticipated values (Case 2). The slope of the line between the points is greater than that calculated by Equation (64). If the slope is greater than that calculated by Equation (64) it can be assumed the well is being damaged during injection or the thermal front is advancing into the formation more rapidly than expected. If the slope of the semi-log straight line is significantly greater than anticipated, this front tracking procedure may not be applicable. However, it does provide a means of detecting injection well plugging or rapid advancement of the thermal front. Unfortunately, it may not be possible to differentiate between these two cases.

A second set of circumstances is shown by Case 4 in Figure 21. Here, the effects of conduction to the confining strata are influencing the rate at which the thermal front moves into the formation. Therefore, the growth of the apparent skin factor is not as rapid as expected. In this case it may be possible to apply the front tracking method if

another means of evaluating $s_{ma}$ is available. For instance, if apparent skin factors are calculated for relatively small injection volumes, then the effects of conduction to the confining strata may be negligible. The factor $s_{ma}$ can then be evaluated by the procedure outlined here if only the early data are considered. For example, in Figure 21 the data points up to C = 100 $m^3$ (Case 4) fall on the correct slope. Therefore, the line through these data points can be extrapolated back to $C = \pi h r_w^2$ in order to evaluate $s_{ma}$. The fluid skin factor and distance to the thermal front can be determined for any value of C by Equations (67) and (65) if n is calculated from the known fluid properties and $s_{ma}$ is assumed to be unchanged from its earlier value.

## EXAMPLES OF NONISOTHERMAL INJECTION TEST ANALYSIS

The analysis methods developed in this paper are demonstrated by application to several simulated data sets (Examples 1-5) and one field data set (Examples 6). As the equations for this are presented in the previous section, they are not repeated here. However, the calculations is demonstrated, thereby allowing a clear description of the procedure.

### Example 1. Moving Front Analysis

The following example demonstrates the analysis procedure used for an injection test conducted in a well that has not been used previously for injection. Knowing this, it is assumed that the pressure transients will behave like those dominated by a moving thermal front. Therefore, the moving-front dominated analysis procedure is appropriate.

The reservoir properties and test parameters for this simulation are given in Table 4. Both thermal wellbore transients and wellbore storage are neglected. However, the data are analyzed with the assumption that the early time data (i.e., the data showing the slope that corresponds to the properties of the reservoir fluid) are not available for analysis. A plot of $\Delta p$ vs. log(t) for this example is shown in Figure 22. In general, semi-log plots are prepared using the absolute pressure instead of pressure changes. The data here are plotted in terms of $\Delta p$ for convenience, rather than out of necessity.

The pressure data follow the slope corresponding to the reservoir fluid properties initially ($m_0$). At approximately 250 s the data fall on a second straight line with a slope $m_1$. The permeability-thickness of the reservoir is calculated using Equation (49). For this case,

| | |
|---|---|
| $k$ | $1.0 \times 10^{-14}$ $m^2$ (10 md) |
| $h$ | 100 m |
| $\phi$ | 0.2 |
| $\rho_a c_a$ | $2.57 \times 10^6$ $J/m^3/°C$ |
| $\lambda$ | 2.0 J/m/°C/s |
| $c_t$ | $1.0 \times 10^{-9}$ $Pa^{-1}$ ($6.9 \times 10^{-6}$ $psi^{-1}$) |
| $r_w$ | 0.1 m |
| $T_r$ | 250°C |
| $T_i$ | 100°C |
| $q$ | 10 kg/s (5660 STB/D) |
| $s_m$ | 0 |

Table 4. Reservoir properties and well characteristics used for Example 1.

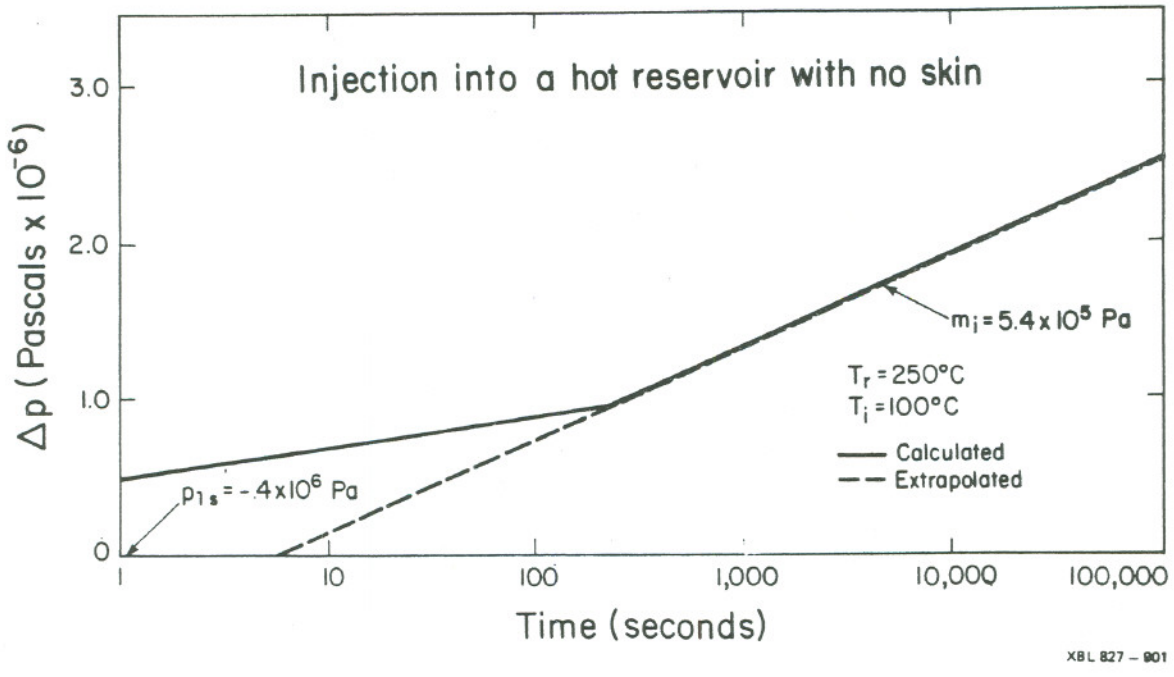


Figure 22. Pressure buildup at the well for Example 1.

$$kh = 0.183 \frac{(10)\ (2.8 \times 10^{-4})}{(960)\ (5.4 \times 10^{5})} = 9.9 \times 10^{-13} m^3 \ (990 \text{ md-m})$$

which compares well with the input data. The flowing pressure at 1s is obtained by extrapolating $m_i$ to 1s and evaluating the pressure:

$$p_{1s} = -0.4 \times 10^{6} \text{ Pa}$$

The offset between isothermal and nonisothermal injection is calculated by Equation (48):

$$p_o = 1.3 \times 10^{6} \text{ Pa}$$

The corrected flowing pressure is evaluated from Equation (50):

$$p^*_{1s} = -0.4 \times 10^{6} + 1.3 \times 10^{6} = 0.9 \times 10^{6} \text{ Pa}$$

The skin factor is calculated with Equation (51):

$$s_m = 1.151 \left[\frac{0.9\times10^{6}}{5.4\times10^{5}} - \log\left(\frac{1\times10^{-14}}{(0.2)(2.8\times10^{-4})(1\times10^{-9})(0.1)^2}\right) - 0.351\right]$$

$$\approx 0.1$$

This is in good agreement with the value input to the simulator, $s_m = 0$. If $p_{1s}$ is not corrected to account for the nonisothermal behavior, a skin value of -2.7 is calculated. Table 5 summarizes the skin factors, calculated skin factors, and apparent skin factors for the pressure transient data plotted in Figure 6.

The effect of ignoring nonisothermal pressure transients during cold water injection dominated by a moving front is that the skin factor is underestimated. In fact, even a well with a positive skin may appear to have a negative skin. The larger the viscosity constrast between the injected and in situ fluids, the more the skin factor is underestimated.

| Input $s_m$ | Calculated $s_m$ | $s_a$ |
|---|---|---|
| 5.7 | 5.6 | 3.0 |
| 3.6 | 3.6 | 0.9 |
| 1.6 | 1.6 | -1.1 |
| 0.0 | 0.1 | -2.7 |
| -2.3 | -2.3 | -4.9 |

Table 5. Calculated and apparent skin values for the pressure buildup data shown in Figure 6.

Example 2. Composite Reservoir Analysis

Composite analysis procedure is used when the well has been used for injection prior to the test. For this example, injection into a well surrounded by a 3-m cold spot is simulated. The method described here is applicable if a well has been used for injection and then left idle for a period sufficient for the pressure gradients in the reservoir to dissipate, but not long enough for the cold spot to re-equilibrate with the reservoir temperature. The reservoir properties, well characteristics and test parameters for this example are listed in Table 6. Once again, the effects of wellbore storage are neglected but it is assumed that the early time data, when the pressure transients correspond to the properties of the cold spot, are not available for analysis. A semi-log plot of the pressure buildup is shown in Figure 23.

The data initially follow a slope that corresponds to the fluid properties of the cold spot. After approximately 20 s, the data fall on the slope corresponding to the fluid properties of the hot reservoir. At approximately $1.5 \times 10^5$ s (approximately 42 hours), the data again change to the cold slope. This change corresponds to the time when the moving thermal front begins to dominate the pressure response. The pressure buildup is analyzed using only the data during the time when the semi-log straight line corresponds to the properties of the reservoir fluid.

First, calculate kh using Equation (53) and the slope of the semi-log straight line $m_o$:

$$kh = 0.183 \frac{(15.0)(1.1\times10^{-4})}{(810)(2.4\times10^{5})} = 1.0\times10^{-12}\ m^3\ (1000\ md\text{-}m)$$

| | |
|---|---|
| $k$ | $1.0 \times 10^{-14}$ $m^2$ (10 md) |
| $h$ | 150 m |
| $\phi$ | 0.2 |
| $\rho_a c_a$ | $2.57 \times 10^6$ $J/m^3/°C$ |
| $\lambda$ | 2.0 J/m/°C/s |
| $c_t$ | $1.0 \times 10^{-9}$ $Pa^{-1}$ ($6.9 \times 10^{-6}$ $psi^{-1}$) |
| $r_w$ | 0.1 m |
| $r_f$ | 3.0 m |
| $T_r$ | 250°C |
| $T_i$ | 100°C |
| $q$ | 15 kg/s (8490 STB/D) |
| $s$ | 2 |

Table 6. Reservoir properties, well characteristics and test parameters for Example 2.

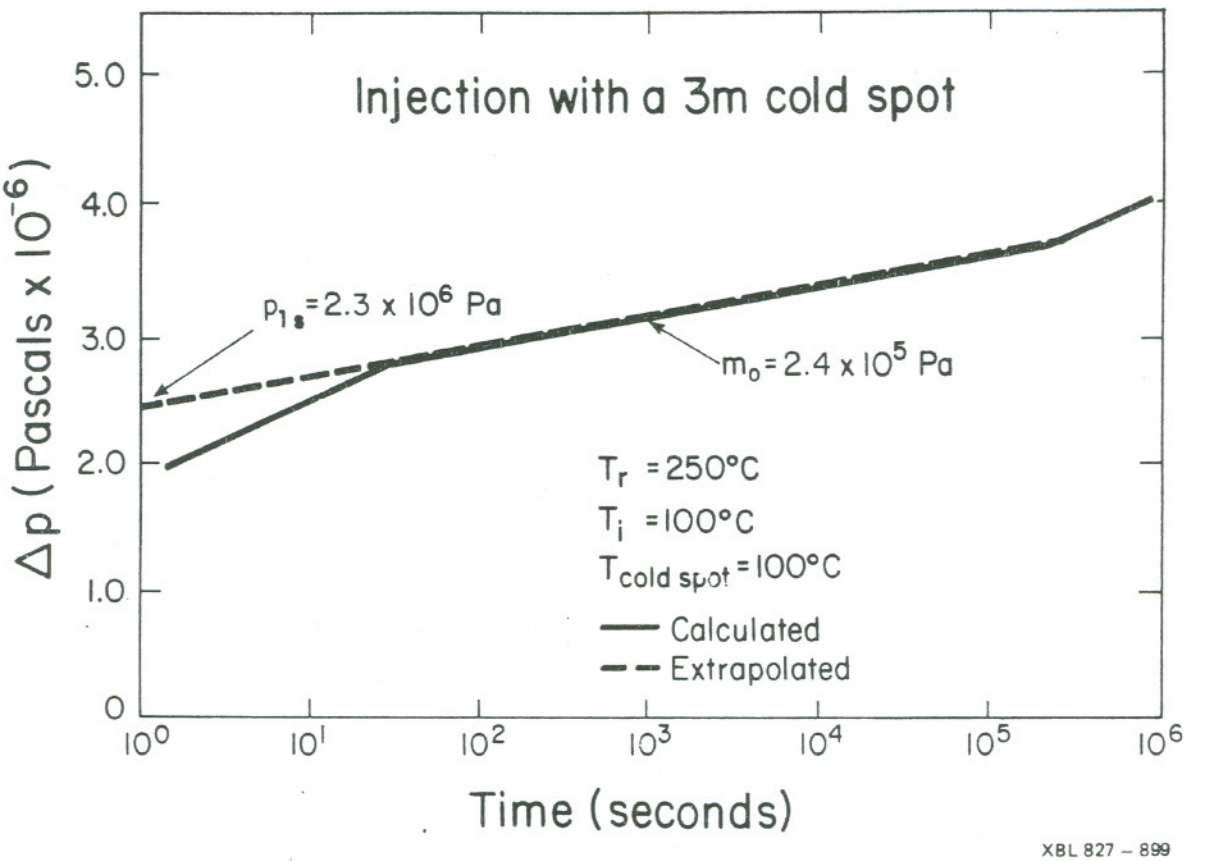


Figure 23. Pressure buildup at the well for Example 2.

Extrapolate $m_o$ to 1s and evaluate $p_{1s}$:

$$\Delta p_{1s} = 2.3\times10^{6} \text{ Pa}$$

Calculate the apparent skin factor using Equation (54):

$$s_a = 1.151 \left(\frac{2.3\times10^{6}}{2.4\times10^{5}} - \log\left(\frac{1\times10^{-14}}{(0.2)(1.1\times10^{-4})(1\times10^{-9})(0.1)^2}\right) - 0.351\right)$$

$$s_a \approx 8.7$$

The fluid skin factor is calculated using Equation (24):

$$s_f = \left(\frac{2.8\times10^{-4}}{1.1\times10^{-4}}\frac{810}{960} - 1\right) \ln\left(\frac{3}{0.1}\right) = 3.9$$

The apparent mechanical skin factor is evaluated using Equation (55):

$$s_{ma} = 8.7 - 3.9 = 4.8$$

Equation 36 can be used to estimate the mechanical skin factor

$$s_m = \frac{(1.1\times10^{-4})\ (960)}{(2.8\times10^{-1})\ (810)}\ 4.8 = 2.2$$

which is in good agreement with the input data, s = 2.

If the nonisothermal behavior is neglected, a skin value of +8.7 is calculated by conventional methods. The values of the input skin factor, nonisothermally calculated skin factor, and the apparent skin factor for the pressure transient data shown in Figure 7 are summarized in Table 7. For cold water injection into a hot reservoir with a cold spot surrounding the well, a failure to account for nonisothermal behavior results in a very large overestimation of the skin factor.

Example 3. Pressure Falloff Analysis

In this example, a pressure falloff after $10^5$ s (approximately one day) of injection is analyzed. The reservoir properties, well

| Input $s_m$ | Calculated $s_m$ | $s_a$ |
|---|---|---|
| 5.0 | 5.0 | 18.3 |
| 2.0 | 2.1 | 8.7 |
| 0.0 | -0.2 | 3.6 |
| -2.0 | -2.0 | 0.2 |

Table 7. Calculated and apparent skin factors for the pressure buildup data shown in Figure 7.

dimensions and test parameters used in this example are given in Table 8. A Horner plot of the pressure falloff is shown in Figure 24. Note that in this case time increases to the left. In this example, as in the previous ones, wellbore storage is neglected. However, the early time data are not required for the analysis; hence, the procedure is equally applicable if significant wellbore effects are present.

After $10^5$ s of injection at 10 kg/s, the thermal front has penetrated 2.2 m into the formation (based on Equation 8). Therefore, the falloff data reflect the presence of this region until approximately 4s (calculated from Equation 12). After ~ 10 seconds, the pressure data correspond to the properties of the in-situ reservoir fluid.

From the slope of the semi-log straight line, $m_o$, and Equation (53), the kh of the reservoir is calculated:

$$kh = 0.183 \frac{(10.0)\ (1.1 \times 10^{-4})}{(1000)\ (2.0 \times 10^{5})}$$

$$= 1.0 \times 10^{-12} m^2\ (1000\ \text{md-m})$$

The shut-in pressure at 1s is evaluated by extrapolating $m_o$ to 1s.

From Figure 24

$$p_{1s} = 1.05 \times 10^{6}\ \text{Pa}$$

The apparent skin factor is calculated from Equation (57):

$$s_a = 1.151 \left( \frac{2.26\times10^{6} - 1.05\times10^{6}}{2.0\times10^{5}} - \log \frac{1\times10^{-14}}{(0.1)(1.1\times10^{-4})(1\times10^{-9})(0.1)^2} - 0.351 \right)$$

$$= 4.3$$

The fluid skin factor is calculated by Equation (24):

$$s_f = \left( \frac{2.8\times10^{-4}\ (1000)}{1.1\times10^{-4}\ (1000)} - 1 \right) \ln \frac{2.2}{0.1} = 4.8$$

| | |
|---|---|
| $k$ | $1.0 \times 10^{-14}$ $m^2$ (10 md) |
| $h$ | 100 m |
| $\varphi$ | 0.1 |
| $\rho_a c_a$ | $2.57 \times 10^6$ $J/m^3/°C$ |
| $\rho_i$ | 1000 $kg/m^3$ |
| $\rho_o$ | 1000 $kg/m^3$ |
| $\lambda$ | 2.0 J/m/°C/s |
| $r_w$ | 0.1 m |
| $c_t$ | $1.0 \times 10^{-9}$ $Pa^{-1}$ ($6.9 \times 10^{-6}$ $psi^{-1}$) |
| $T_r$ | 250°C |
| $T_i$ | 100°C |
| $q$ | 10 kg/s (5430 STB/D) |
| $s$ | 0 |

Table 8. Reservoir properties, well characteristics and test parameters for Example 3.

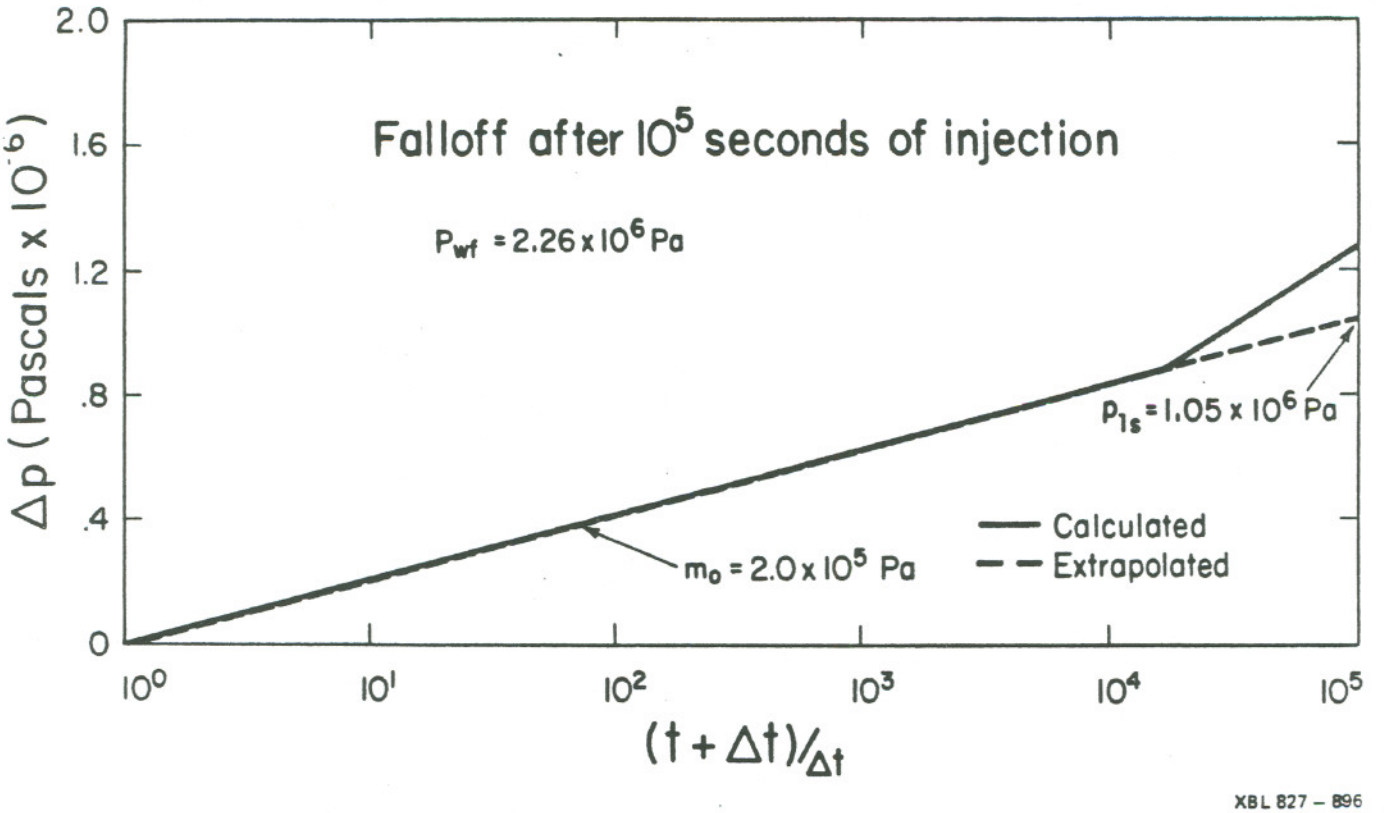


Figure 24. Pressure falloff after $10^5$ s of 100°C injection into a 250°C reservoir: Example 3.

The apparent mechanical skin factor is calculated from Equation (55):

$$s_{ma} = 4.3 - 4.8 = -0.5$$

The small negative skin is the result of approximation that the distance to the cold spot is equal to the distance to the thermal front. This is also a good example of the difficulty of evaluating the mechanical skin factor from the apparent mechanical skin. The appropriate form of the equation (i.e., 36 or 38) is uncertain. Clearly, using (36) will result in a better approximation of the true skin factor in this case. Therefore,

$$s_a = \left(\frac{1.1\times10^{-4}\ (1000)}{2.8\times10^{-4}\ (1000)}\right)(-0.5) = -0.2$$

This is in good agreement with the input value of s = 0. If the skin value is calculated by ignoring the effects of the nonisothermal pressure transients, a value of s = 4.4 is obtained. Large positive skin values are often reported for geothermal injection wells. One such example is reported by Saltuklaroglu and Rodriguez (1978).

Table 9 summarizes the apparent skin factors for falloff tests after $10^4$, $10^5$, and $10^6$ s of injection at an injection rate of 10 kg/s (for the reservoir properties used in the previous example). The correctly calculated skin values are also included in Table 9 for comparison.

Example 4. Step-Rate Analysis and Front Tracking

In this example the simulated data step rate test data discussed before are analyzed. Recall that this test consisted of three flowrates, each with a duration of 6 hours. The reservoir properties and well characteristics used for this simulation are given in Table 10.

| Cumulative Injection (kg) | $r_f$ (m) | Input $s_m$ | Calculated $s_m$ | $s_a$ |
|---|---|---|---|---|
| $1 \times 10^3$ | 0.7 | 0.0 | -0.2 | 2.5 |
| $1 \times 10^4$ | 2.2 | 0.0 | -0.2 | 4.4 |
| $1 \times 10^5$ | 7.0 | 0.0 | 0.0 | 6.0 |

Table 9. Skin values for pressure falloff analyses after $10^2$, $10^3$, and $10^4$ seconds of injection at a rate of 10 kg/s.

| | |
|---|---|
| $k$ | $1 \times 10^{-14}$ $m^2$ (10 md) |
| $h$ | 100 m |
| $\phi$ | 0.2 |
| $\rho_a c_a$ | $2.57 \times 10^6$ $J/m^3/°C$ |
| $\lambda$ | 2.0 J/m/°C/s |
| $r_w$ | 0.1 m |
| $c_t$ | $1 \times 10^{-9}$ $Pa^{-1}$ ($6.9 \times 10^{-6}$ $psi^{-1}$) |
| $T_r$ | 250°C |
| $T_i$ | 20°C |
| $q$ | Step 1. 10 kg/s (5430 STB/D)<br>Step 2. 20 kg/s (10,865 STB/D)<br>Step 3. 15 kg/s (8,150 STB/D) |
| $s$ | 0.0, 2.0, 5.0 |

Table 10. Reservoir properties, well dimensions and test parameters for Example 4.

During each step the pressure transients are somewhat different. Therefore, the analysis method must be chosen by evaluating the correct set of fluid properties to which the data correspond. Table 11 summarizes the key quantities for each of the steps. The table indicates that Step 1 should be analyzed with the moving-front-dominated procedure. Step 2 may be difficult to analyze because the early time data will most likely be masked by wellbore storage and the remaining data display both the composite reservoir behavior and the moving front behavior. Steps 3 and 4 both exhibit only the composite reservoir behavior. Methods for analyzing these data are given in detail in previous sections. As they are very similar to the procedures described in Examples 1 through 3, they are not discussed in detail here. The values of apparent skin factors for Steps 2, 3, and 4 are listed in Table 12. These data are used to demonstrate the front tracking procedure.

In Figure 25 the apparent skin factors are plotted as a function of the volume of water injected into the formation. The results of the analysis of two similar data sets are also shown (i.e., for wells with mechanical skin factors of 2 and 5, respectively). Note that in each case the data points fall on a straight line with the same slope. The slope of this line, (7.2) agrees well with the value calculated by Equation (64):

$$n = 1.151 \left( \frac{1.0 \times 10^{-3}}{1.1 \times 10^{-4}} \frac{(810)}{(1000)} - 1 \right) = 7.3$$

By extrapolating this line back to the value where $C = \pi h r_w^2 = 3.4\ m^3$, the value $s_a\ (\pi h r_w^2)$ is obtained:

$$s_a\ (3.14 m^3) = 1.5$$

| Step | $r_f$(m) | $t_o$(s) | $t_f$(s) | $t_o'$(s) | Analysis Method |
|---|---|---|---|---|---|
| 1 | 0.0 | 185 | - | - | Moving Front |
| 2 | 1.1 | - | 6 | $1.1 \times 10^4$ | Both |
| 3 | 1.9 | - | 18 | $4.4 \times 10^4$ | Composite Reservoir |
| 4 (falloff) | 2.3 | - | 26 | - | Composite Reservoir |

Table 11. Pertinent parameters for the step-rate test analysis: Example 4.

| Step | $r_f$(m) | Cumulative Injection ($m^3$) | $s_a$ $s_m = 0$ | $r_f$ (m) (calculated) | |
|---|---|---|---|---|---|
| 2 | 1.1 | 32.4 | 14.0 | 0.9 | 0.0 |
| 3 | 1.9 | 64.8 | 18.9 | 2.0 | 2.0 |
| 4 (falloff) | 2.3 | 97.2 | 19.8 | 2.3 | 5.2 |

Table 12. Summary of analyses for the step-rate test: Example 4.

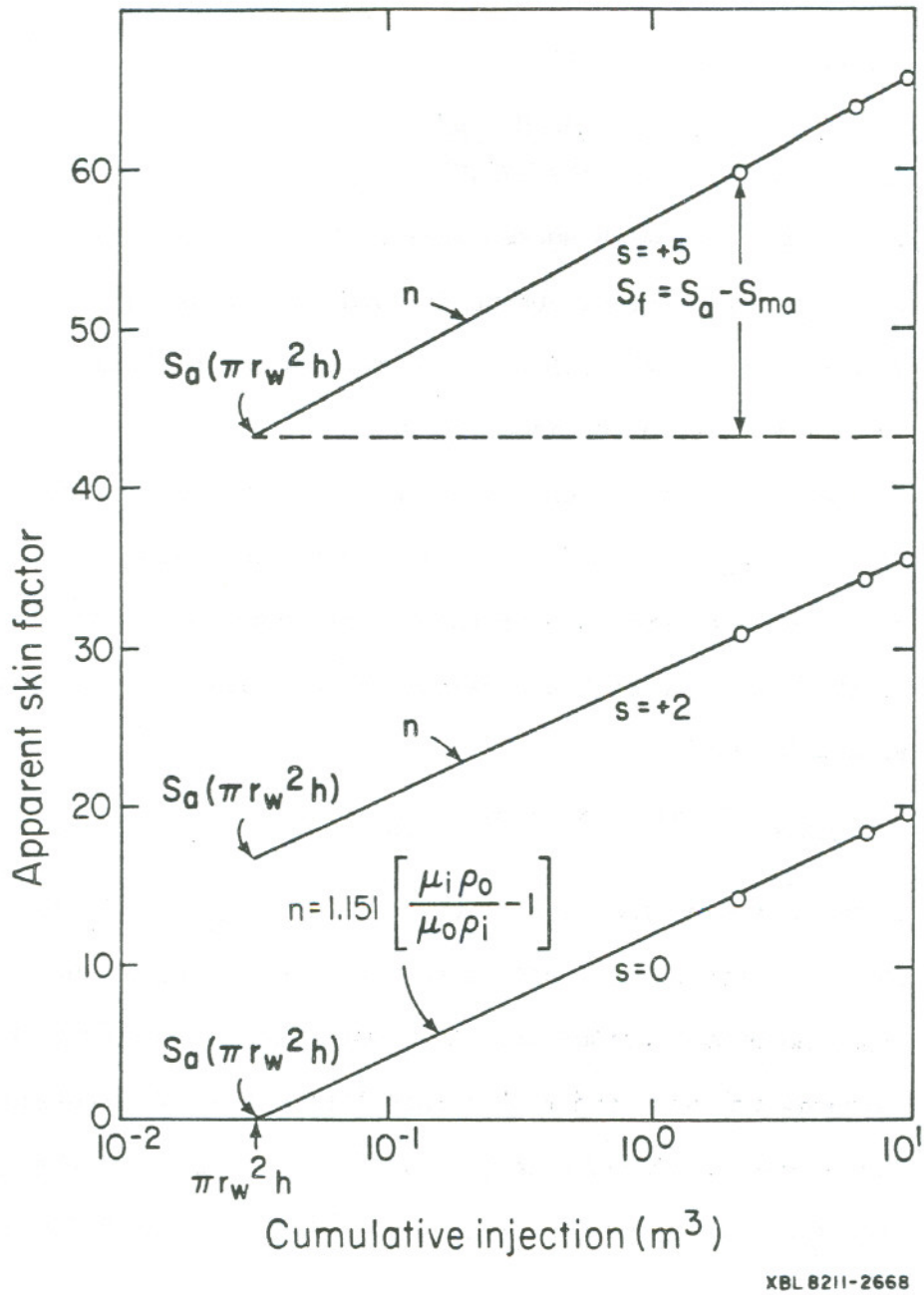


Figure 25. Apparent skin factors vs. cumulative injection for Example 4.

$s_{ma}$ is calculated by Equation (66):

$$s_{ma} = 1.5 - 7.3 \log \frac{(4200)(1000)}{(2.57 \times 10^6)} = 0.0$$

This implies that $s_m = 0$, which agrees well with the value input to the simulator. Similar analyses can be applied for the other two cases with the result that $s_m$ equals 2.0 and 5.2, respectively. Both of these values agree well with the input data.

The fluid skin factors for each value of C are calculated by Equation (67). Since $s_{ma}$ is zero for Case 1, the fluid skin factors are identical to the apparent skin factors. The distances to the thermal front at each value of C are calculated by Equation (65). For example, when C = 64.8 $m^3$

$$r_f = 0.1\ e^{(1.151(18.9)/7.3)} = 2.0 \text{ m}$$

The same procedure is used for each of the values of $s_a$. Table 12 summarizes the values of $r_f$ for each of the steps. The agreement between the calculated and actual values is very good. Note that the calculated value of the slope n is used rather than the value obtained from the graph. If the value obtained from the graph is used, the distance to the front is only changed slightly, from 1.97 to 2.05 m.

Example 5. Layered Reservoir Analysis

In order to determine the applicability of these methods of analysis to a layered reservoir, the pressure falloff following injection of 50°C water into a 250°C three-layer reservoir was simulated. The reservoir and fluid properties used are listed in Table 13. A schematic of the reservoir is shown in Figure 26.

| | |
|---|---|
| $k_1$ | $5.0 \times 10^{-14}/m^2$ (50 md) |
| $k_2$ | $1.0 \times 10^{-13}/m^2$ (100 md) |
| $k_3$ | $5.0 \times 10^{-14}/m^2$ (50 md) |
| $h_1$ | 10 m |
| $h_2$ | 10 m |
| $h_3$ | 10 m |
| $\phi$ | 0.2 |
| $c_r$ | 1000 J/kg/°C |
| $\rho_r$ | $2200\ kg/m^3$ |
| $\lambda$ | 2.0 J/m/°C/s |
| $c_t$ | $1.0 \times 10^{-9}\ Pa^{-1}$ ($6.9 \times 10^{-6}\ psi^{-1}$) |
| $r_w$ | 0.1 m |
| s | 0.0 |
| $T_i$ | 50°C |
| $T_r$ | 250°C |

Table 13. Reservoir properties and well characteristics used for Example 5.

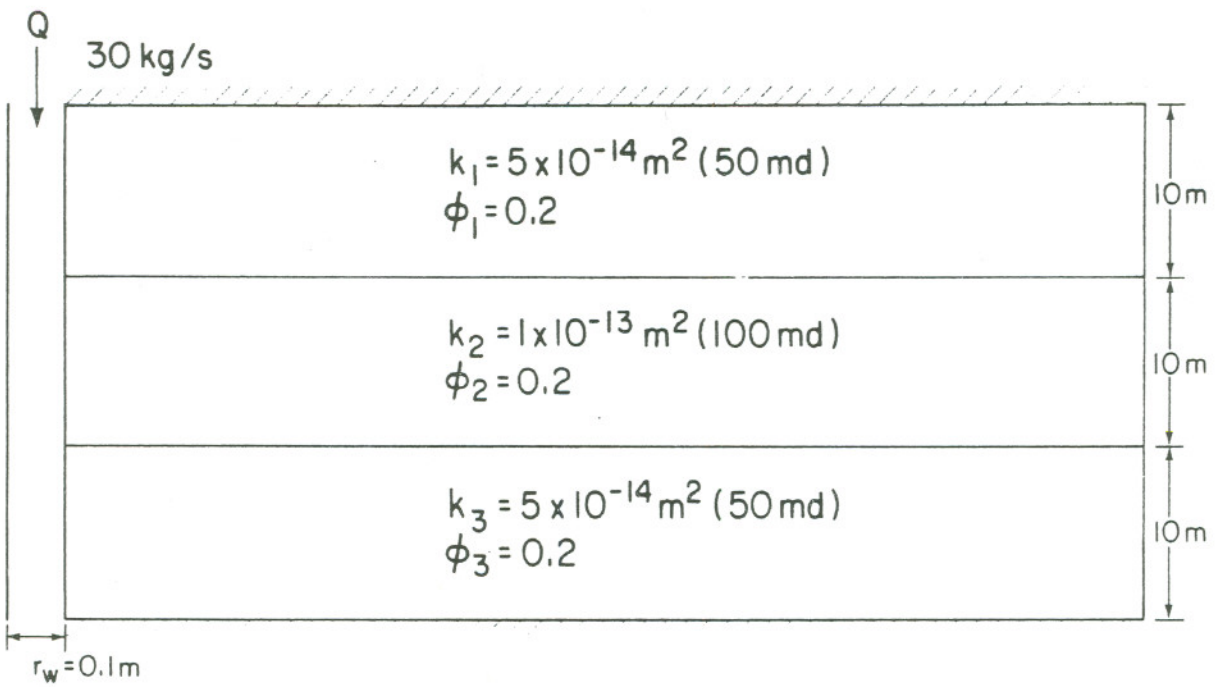


Figure 26. Schematic of the layered reservoir used in Example 5.

Pressure falloffs are simulated after three different periods of injection $10^4$, $2.5 \times 10^4$, and $10^5$ s (at a rate of 30 kg/s). Horner graphs of each falloff are shown in Figure 27. Note that by nondimensionalizing the data using $(t + \Delta t)/\Delta t$ the data fall on one curve. Each data set is typical of the two-fluid, composite reservoir behavior. Also note that the values of $p_{1s}$ are shown on the graph for each of the falloff tests.

The slope of the semi-log straight line, $m_o$, is used to calculate the "average" permeability ($\bar{k}$). The calculated value of $\bar{k}$, $6.7 \times 10^{-14}$ $m^2$ (6.7 md), is in excellent agreement with the correct value of $6.7 \times 10^{-14} m^2$. The apparent skin factors are calculated using Equation (57), if $\bar{k}$ is substituted for k. The calculated values of the apparent skin factors after $10^4$, $2.5 \times 10^4$, and $10^5$ s of injection are 9.7, 11.2 and 13.4, respectively. A plot of the apparent skin values vs. C is shown in Figure 28. Once again, the data fall on a straight line. The slope of the line is 3.7, which is close to the value of 3.6 computed using Equation (64). The line extrapolates to a value of $s_a = 0.2$ at the cumulative injection equal to $\pi r_w^2 h$. Therefore, $s_m$ is equal to -0.2 (calculated by Equations 66 and 36), which is consistent with the zero skin value used in the simulation.

In Figure 29, the simulated results of radial distance to the thermal front is shown for each of the three layers. Note that the front has extended farthest from the well in the most permeable layers. The radial distance to the front after each period of injection can be calculated from Equation (65). The respective values are 2.2 m, 3.5 m, and 7.1 m. Comparison between these values and those shown in Figure 29 indicates that the predicted values are midway between the distance to the front in the more

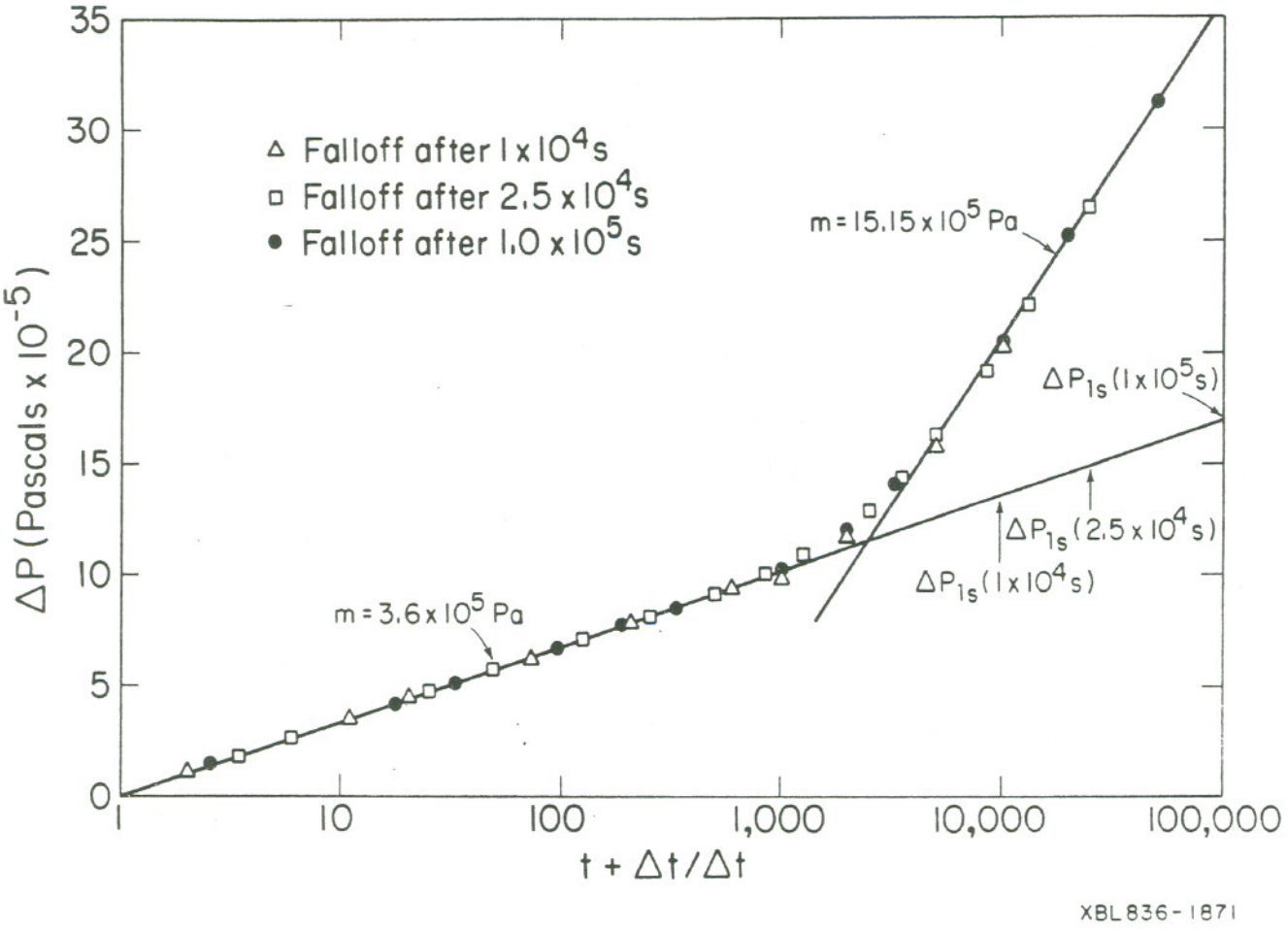


Figure 27. Pressure falloff data after $10^4$, $2.5 \times 10^4$ and $1 \times 10^5$ s of injection into a multilayered reservoir.

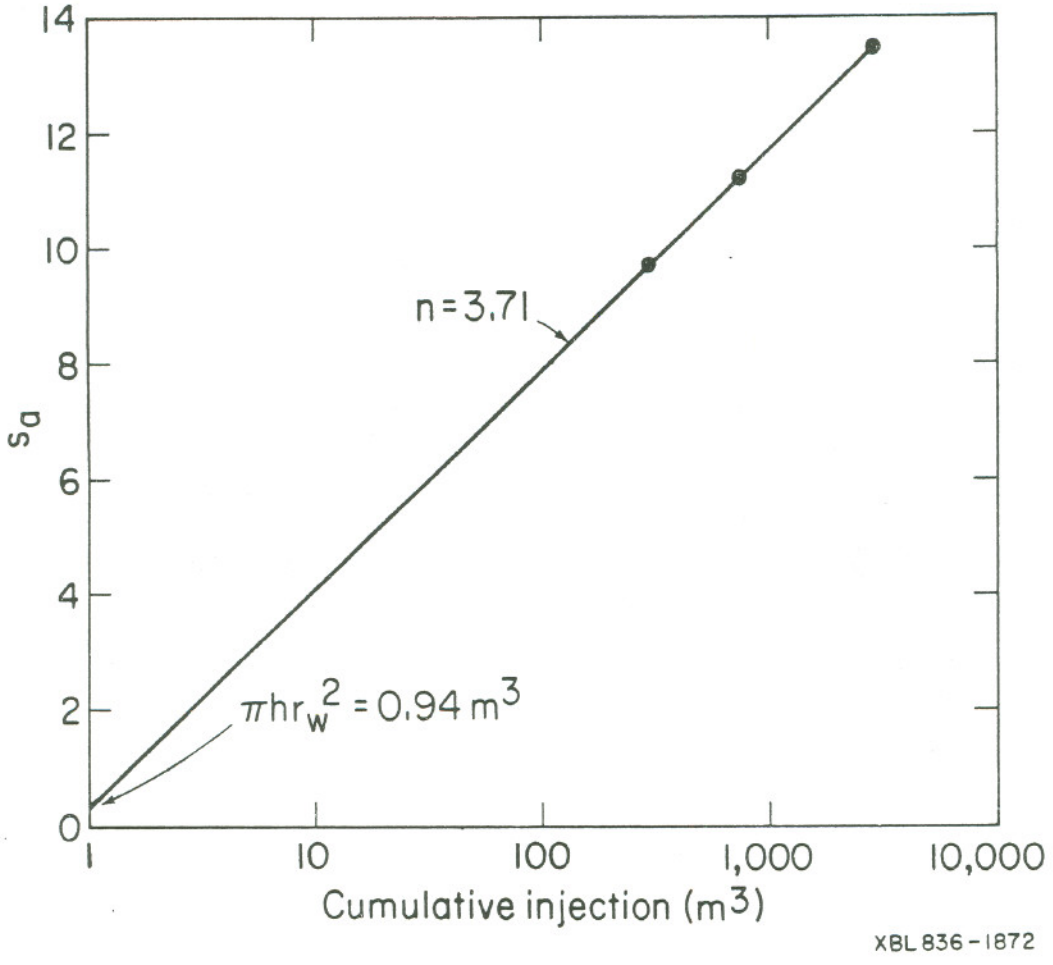


Figure 28. Apparent skin factors vs. cumulative injection for Example 6.

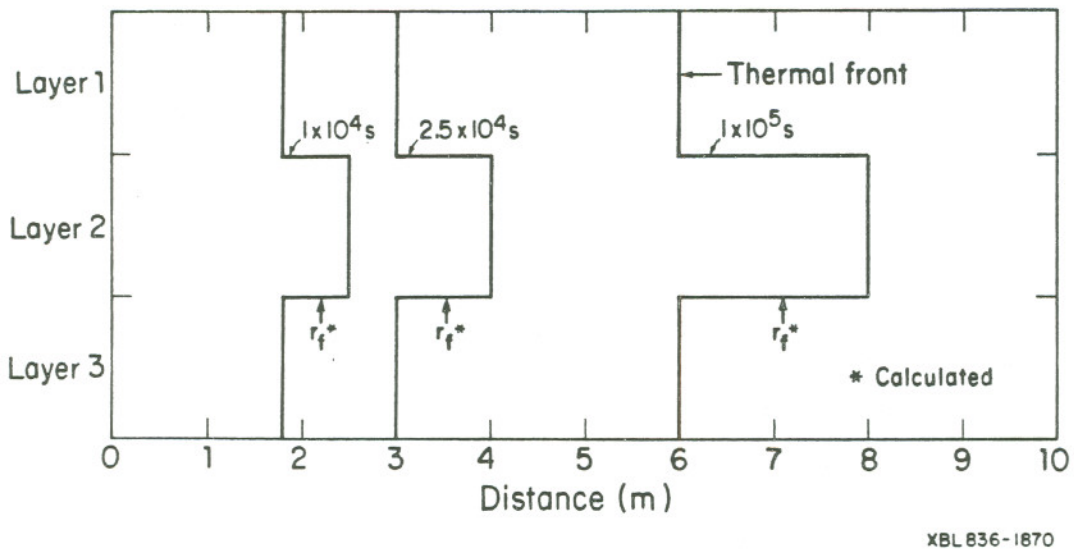


Figure 29. Distance to the thermal front after $10^4$, $2.5 \times 10^4$ and $10^5$ s of injection in a multilayered reservoir.

permeable layers and less permeable layer. This cannot be considered a rigorous analysis of front penetration in layered formations. It does, however, indicate that the small-scale heterogeneity prevalent in most formations will not significantly reduce the effectiveness of these methods of analysis.

Example 6. East Mesa Well 5-1: Pressure Buildup Analysis

The following data were obtained from an injection test in a geothermal reinjection well in the East Mesa geothermal field (McEdwards and Benson, 1978). Cold water (approximately 50°C) was injected into well 5-1 for four days, during this time downhole pressures were measured with silicon-oil-filled capillary tubing. The test consisted of several step-rates. The test segment discussed here comes from a buildup midway through the test. Table 14 summarizes the pertinent well/test data.

Knowing the cumulative volume of water injected prior to the test segment to be analyzed, the thickness of the reservoir, and the thermal properties of the reservoir rock, the penetration of the thermal front into the formation can be estimated (in standard oilfield units) from

$$r_f = 2.37 \sqrt{\frac{\rho_w c_w C}{\rho_a c_a \pi h}} \qquad (68)$$

Thus, $r_f$ = 12.5 ft for a cumulation injection of $2.3 \times 10^4$ STB. Wellbore storage effects are small because the well was completely filled with liquid water. However, the method used to measure the downhole pressure has a response time of approximately 20 minutes for transmitting large pressure changes (Miller and Haney, 1978). Therefore,

| | |
|---|---|
| Well radius ($r_w$) | 0.32 ft |
| Well depth | 6000 ft |
| Open interval | 4000-6000 ft |
| Injection interval (h) | 4000-4400 ft |
| Reservoir temperature | 150°C |
| Injection temperature (sandface) | 50°C |
| Rock type | Sandstone |
| Porosity ($\phi$) | 0.2 |
| Total compressibility ($c_t$) | $7.0 \times 10^{-6}$ $psi^{-1}$ |
| $B_w$ | 1.08 RB/STB |
| Flow rate (Q) - surface rate | $1.27 \times 10^4$ STB/D |
| Static pressure ($P_i$) | 135 psi* |
| Cumulative injection | $2.3 \times 10^4$ BBL |

*This is only a relative value because downhole pressures were measured with an oil-filled capillary tube.

Table 14. Injection test data summary: Example 6.

only data from 20 minutes onward are available for analysis. The drainage radius will exceed the size of the cold spot in (in field units)

$$t_f = 1189 \frac{\phi \mu_1 c_t}{k} r_f^2 \qquad (69)$$

For a 12.5 ft cold spot (k is estimated at 10 md), this occurs at approximately 50 s. The second change in slope, from hot to cold, occurs at (in field units)

$$t_o' = 4.28 \frac{\rho_a c_a}{\rho_w c_w} \frac{\pi h}{Q} r_f^2 \qquad (70)$$

or approximately 43 hours after the start of this test segment. Therefore, all of the pressure data between 50 s and 43 hours correspond to the fluid properties of the in situ reservoir fluids.

Figure 30 shows the plot of the downhole pressure vs. log (time). The semi-log straight line begins at approximately 20 minutes. The permeability-thickness can be calculated from (in field units)

$$kh = 162.6 \frac{Q B_w \mu_o}{m_o} \qquad (71)$$

Therefore, the permeability is approximately 20 md. The injection pressure at 1 hour is

$$p_{1hr} = 560 \text{ psi}$$

The apparent skin factor is evaluated as (in field units)

$$s_a = 1.151 \left( \frac{560-135}{48} - \log \frac{20}{(0.2)(0.18)(7\times10^{-6})(0.32)^2} + 3.2275 \right)$$

For this example

$$s_a = 3.7$$

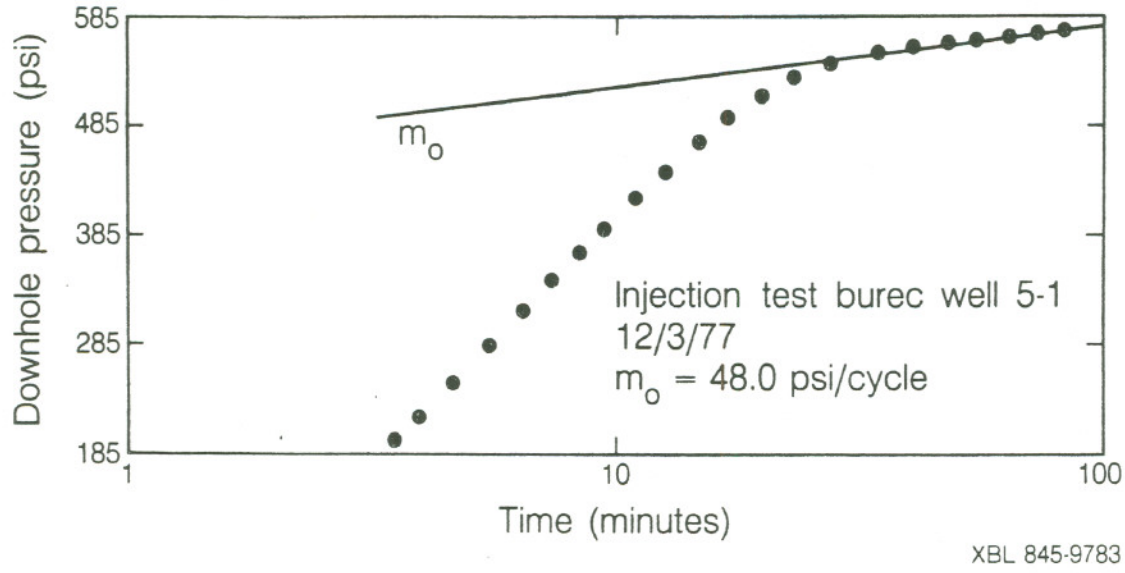


Figure 30. Pressure buildup data from East Mesa well 5-1.

The 12.5 ft cold spot creates a fluid skin factor of (calculated with Equation (24):

$$s_f = \left( \frac{.55}{.18} \frac{(57.4)}{(61.8)} - 1 \right) \ln \frac{12.5}{0.32} = 6.7$$

The apparent mechanical skin factor is calculated from Equation (55):

$$s_{ma} = 3.7 - 6.7 = -3.0$$

and the mechanical skin factor is calculated from Equation (38):

$$s_m = -3.0$$

In a previous analysis, in which the nonisothermal behavior was ignored, a skin value of +3.7 was calculated (McEdwards and Benson, 1978). The positive skin value was contrary to the evidence which suggested that the well had been hydraulically fractured inadvertently at an earlier data. The negative skin value calculated here suggests that a fracture intersects the well. This is consistent with the history of the well.

# CONCLUSIONS

The objective of this study was to develop procedures for analyzing nonisothermal injection test data during the early phases of injection. In particular, methods for determining the permeability-thickness of the formation, skin factor of the well and tracking the movement of the thermal front have been developed. The techniques developed for interpreting injection pressure transients are closely akin to conventional groundwater and petroleum techniques for evaluating these parameters.

The approach taken to the problem was to numerically simulate injection with a variety of temperatures, reservoir parameters and flowrates, in order to determine the characteristic responses due to nonisothermal injection. Two characteristic responses were identified: moving front dominated behavior and composite reservoir behavior. Analysis procedures for calculating the permeability-thickness of the formation and the skin factor of the well have been developed for each of these cases.

In order to interpret the composite reservoir behavior, a new concept has been developed; that of a "fluid skin factor", which accounts for the steady-state pressure buildup due to the region inside the thermal front. Based on this same concept, a procedure for tracking the movement of the thermal front has been established. The technique has the advantage over previous procedures in that it does not require the presence of pressure transients corresponding to the inner region to be apparent in the data. This allows front tracking to begin during the early phases of injection. Therefore, premature thermal break-

through can be identified early, and remedial measured be taken to prevent its occurrence.

The results obtained during this study also identify the dangers of not accounting the nonisothermal effects when analyzing injection test data. Both the permeability-thickness and skin factor of the well can be grossly miscalculated if the effects of the cold-region around the well are not taken into consideration.

REFERENCES

Allen, T. S., and Baza, J. R., 1980. The role of step-rate injectivity tests in liquid dominated highly fractured geothermal reservoirs. Presented at the 55th Annual Fall Technical Conference and Exhibition, Society of Petroleum Engineers of AIME, Dallas, TX, September 21-24, 1980, SPE-9275.

Avdonin, N. A., 1964. Some formulas for calculating the temperature field of a formation during thermal injection, Izv. Vysshikh Uchebn. Zavedenii, Nefti Gaz 7, No. 3, 37-41.

Benson, S. M. and Bodvarsson, G. S., 1982. Nonisothermal effects during injection and falloff tests. Presented at the 57th Annual Fall Technical Conference and Exhibition of the Society of Petroleum Engineers of AIME, New Orleans, Louisianna, September 27-29, 1982, SPE-11137.

Benson, S. M. and Bodvarsson, G. S., 1983. A pressure transient method for front tracking. Presented at the 58th Annual Fall Technical Conference and Exhibition, of the Society of Petroleum Engineers of AIME, San Francisco, California, October 5-8, 1983, SPE-12130.

Benson, S. M., 1983. Interpretation of nonisothermal step-rate injection tests. Proceedings, Eighth Workshop Geothermal Reservoir Engineering, Stanford University, Stanford, California, December 14-16, 1983, 103-109.

Bixel, H. C. and Van Poolen, H. K., 1967. Pressure drawdown and buildup in the presence of radial discontinuities. Society of Petroleum Engineers Journal (Sept. 1967), 301-309.

Bodvarsson, G., 1969. On the temperature of water flowing through fractures. Journal of Geophysical Research, v. 74, no. 8, 1987-1992.

Bodvarsson, G. S., and Tsang, C. F., 1980, Thermal effects in the analysis of fractured reservoirs. Proceedings, 3rd Invitational Well Testing Symposium Lawrence Berkeley Laboratory Report, LBL-12076, Berkeley, California, 110-119..

Bodvarsson, G. S., 1982, Mathematical modeling of the behavior of geothermal systems under exploitation. Ph.D. dissertation, University of California, Berkeley. Also, Lawrence Berkeley Laboratory Report, LBL-13937, Berkeley, California.

Bodvarsson, G. S., Benson, S. M., Sigurdsson, O., Halldorsson, G. K., and Stefansson, V., 1981. Analysis of well data from the Krafla Geothermal Field in Iceland. Proceedings, Seventh Workshop on Geothermal Reservoir Engineering, Stanford University, Stanford, California, December 15-17, 1981, 71-76.

Chen, H. and Brigham, W. E., 1974. Pressure buildup for a well with storage and skin in a closed square: Presented at the Society of Petroleum Engineers-AIME Annual California Regional Meeting, San Francisco, April 4-5, 1974, SPE-4890.

Doughty, C., Buscheck, T. A., and Tsang, C. F., 1983. Prediction and analysis of a field experiment on a multi-layered aquifer thermal energy storage system with strong buoyancy flow. Water Resources Research (Oct. 1983), Vol 19, No. 5, 1307-1315.

Duff, I. S., 1977, MA28 - A set of fortran subroutines for sparse unsymmetric linear equations: Harwell Report AERE-R 8730, Oxfordshire, Great Britain.

Earlougher, R. C., Kersh, K. M., and Ramey, H. J., 1973. Wellbore effects in injection well testing, Journal of Petroleum Technology (Nov. 1973), 1244-1250.

Earlougher, R. C. Jr., 1977. Advances in Well Test Analysis. Society of Petroleum Engineers, Monograph 5.

Edwards, A. L., 1972. TRUMP: A computer program for transient and steady-state temperature distribution in multidimensional systems. Lawrence Livermore Laboratory Report, UCRL-14754, Rev. 4.

Garg, S. K. and Pritchett, J. W., 1981. Cold water injection into two-phase geothermal reservoirs. Proceedings, 7th Workshop of Geothermal Reservoir Engineering, Stanford University, Stanford, California, December 15-17, 1981, 175-178.

Gobran, B. D., Brigham, W. E., and Sanyal, S. K., 1980. The temperature dependence of permeability. Geothermal Resources Council, TRANSACTIONS v. 4, p. 397-400.

Grant, M. A., Donaldson, I. G., and Bixey, P. F., 1983. Geothermal Reservoir Engineering. Academic Press, New York, New York.

Hawkins, M. F., 1956. A note on the skin effect. Trans. AIME (1956), V 207, 356-357.

Hazebroek, P., Rainbow, H., and Matthews, C. S., 1958. Pressure falloff in water injection wells. Trans., AIME (1958), v. 213, 250-260.

Hellstrom, G., Tsang, C. F., and Claessou, J., 1979. Heat storage in aquifers; buoyancy flow and thermal stratification problems. Lawrence Berkeley Laboratory Report, LBL-14246, Berkeley, California.

Horner, D. R., 1951. Pressure buildup in wells. Proceedings, Third World Petroleum Congress. The Hague, Sec. II, 503-523.

Howard, J., and others, 1978. Geothermal resource and reservoir investigations of the U.S. Bureau of Reclamation Leaseholds at East Mesa, Imperial Valley, California. Lawrence Berkeley Laboratory Report, LBL-7094, Berkeley, California.

Hurst, W., 1953. Establishment of the skin effect and its impediment to fluid flow into the wellbore. Petroleum Engineer (Oct. 1953), B6-B16.

Kazemi, H., 1966. Locating a burning front by pressure transient measurements. Journal of Petroleum Technology (Feb. 1966), 227-232.

Kazemi, H., Merrill, L. S., and Jargon, J. R., 1972. Problems in interpretation of pressure falloff tests in reservoirs with and without fluid banks. Journal of Petroleum Technology (Sept. 1972), 1147-1156.

Larkin, K. B., 1963. Solutions to the diffusion equation for a region bounded by a circular discontinuity. Society of Petroleum Engineers Journal (June 1963). 113-115.

Mangold, D. C., Tsang, C. F., Lippmann, M. J., and Witherspoon, P. A., 1980. A study of thermal effects in well test analysis. Journal of Petroleum Technology (June 1981), 1095-1105.

Matthews, C. S., and Russell, D. G. 1967. Pressure Buildup and Flow Tests in Wells. Society of Petroleum Engineers of AIME, monograph series, Vol. 1, Dallas, Texas.

McEdwards, D. G. and Benson, S. M., 1978. Results of two injection tests at the East Mesa KGRA. Proceedings, Second Invitational Well Testing Symposium, Lawrence Berkely Laboratory Report, LBL-8883, Berkeley, California, 34-48.

Merrill, L. S., Jr., Kazemi, H., and Gogarty, W. B., 1974. Pressure falloff analysis in reservoirs with fluid banks. Journal of Petroleum Technology (July, 1974), 809-818.

Miller, C. W., 1980. WELBORE user's manual, Lawrence Berkeley Laboratory, Report LBL-10910, Berkeley, California.

Miller, C. W. and Haney, J., 1978. Response of pressure changes in a fluid filled capillary tube. Proceedings, Second Invitational Well Testing Symposium, Lawrence Berkeley Laboratory Report, LBL-8883, Berkeley, California, 112-120.

Narasimhan, T.N., and Witherspoon, P.A., 1976. An integrated finite difference method for analyzing fluid flow in porous media. Water Resources Research, Vol.12, No.1, 57-64.

O'Sullivan, M. J. and Pruess, K. 1980. Analysis of injection testing of geothermal reservoirs. Transactions, Geothermal Resources Council, v. 4, 401-404.

Odeh, A. S., 1969. Flow test analysis for a well with radial discontinuity. Journal of Petroleum Technology (February, 1969), 207-210.

Ramey, H. J., 1970. Approximate solutions for unsteady liquid flow in a composite reservoir. Journal of Canadian Petroleum Technology (March, 1970), 32-37.

Saltaklaroglu, M. and Rodriguez, J. R., 1978. Injection testing in geothermal wells. Proceedings, Fourth Workshop on Geothermal Reservoir Engineering, Stanford University, Stanford, California, 176-187.

Satman, A., Eggenschwiller, M., Tang, R. W., and Ramey, H. J., Jr., 1980. An analytical study of transient flow in systems with radial discontinuities. Presented at the 55th Annual Fall Technical Conference and Exhibition of the Society of Petroleum Engineers, Dallas, Texas September 21-24, 1980 SPE-9399.

Sigurdsson, O., Bodvarsson, G. S., and Stefansson, V., 1983. Nonisothermal injectivity index can infer well productivity and reservoir transmissivity. Proceedings, Ninth Workshop on geothermal Reservoir Engineering, December 13-15, 1983, Stanford University, Stanford, California, 211-216.

Theis, C. V., 1935. The relationship between the lowering of piezometric surface and the rate and duration of discharge of wells using groundwater storage. Transactions, American Geophysical Union, 1935, V. 2, 519-524.

Tsang, Y. W. and Tsang, C. F., 1978. Analytic study of geothermal reservoir pressure response to cold water reinjection. Proceedings, 4th Workshop on Geothermal Reservoir Engineering, Stanford University, Stanford, California, December 13-15, 1978, 322-331.

Tsang, C. F., Zerzan, M., Bodvarsson, G. S., Lippmann, M., Mangold, D., Narisimhan, T. N., Pruess, K., and Schroeder, R.C., 1978. Numerical modeling studies in well test analysis. Proceedings, Second Invitational Well Testing Symposium, Lawrence Berkeley Laboratory Report, LBL-8883, Berkeley, California.

Van Everdingen, A. F., 1953. The skin effect and its influence on the productive capacity of a well. Transaction AIME (1953), v 198, 171-176.

Van Poollen, H. K., 1965. Transient tests find fire front in an in situ combustion project. Oil and Gas Journal (February 4, 1965), 78-80.

Wattenbarger, R. A., and Ramey, H. J., 1970. An investigation of wellbore storage and the skin effect in unsteady liquid flow. II. Finite difference treatment. Society of Petroleum Engineers Journal, 291-297, (Sept.1970).